Faculteit Industriële Ingenieurswetenschappen

master in de industriële wetenschappen: elektronica-ICT

Masterthesis

Testing and validating the lifetime of stretchable electronic circuits

Maarten Budenaers
Tom Stiers
Scriptie ingediend tot het behalen van de graad van master in de industriële wetenschappen: elektronica-ICT

PROMOTOR :
Prof. dr. ir. Wim DEFERME
Prof. dr. ir. Michael DAENEN

BEGELEIDER :
ing. Maximilian KRACK
ing. Lennert PURNAL

Gezamenlijke opleiding UHasselt en KU Leuven

Universiteit Hasselt | Campus Diepenbeek | Faculteit Industriële Ingenieurswetenschappen | Agoralaan Gebouw H - Gebouw B | BE 3590 Diepenbeek

Universiteit Hasselt | Campus Diepenbeek | Agoralaan Gebouw D | BE 3590 Diepenbeek
Universiteit Hasselt | Campus Hasselt | Martelarenlaan 42 | BE 3500 Hasselt

2022
2023

Faculteit Industriële Ingenieurswetenschappen

master in de industriële wetenschappen: elektronica-ICT

Masterthesis

Testing and validating the lifetime of stretchable electronic circuits

Maarten Budenaers
Tom Stiers
Scriptie ingediend tot het behalen van de graad van master in de industriële wetenschappen: elektronica-ICT

PROMOTOR :
Prof. dr. ir. Wim DEFERME
Prof. dr. ir. Michael DAENEN

BEGELEIDER :
ing. Maximilian KRACK
ing. Lennert PURNAL

UHASSELT KU LEUVEN

Foreword

This master's thesis "Testing and validating the lifetime of stretchable electronics" has been written as the final thesis for the master of electronics and ICT engineering technology program at UHasselt and KU Leuven.

We want to express our gratitude to our promoters Prof. dr. ir. Wim Deferme and Prof. dr. ir. Michaël Daenen. Furthermore, we want to thank our supervisors dr. Monika Rai, ing. Lennert Purnal, and ing. Maximilian Krack. We extend our gratitude to them for their guidance during our research, helping us with the production process, and for proofreading our master's thesis and poster. A special note of appreciation goes to ing. Lennert Purnal, whose advice on device and batch designs, guidance during device production, and provision of the initial versions of Arduino code and Labview code for the cycletesters were immensely valuable.

Furthermore, we want to thank Energyville for allowing us to use their damp heat climate chambers and in particular, Jan Mertens to assist us with the damp heat climate chambers. We want to thank ing. Gudrun Nowicki from Materials and Packaging Research & Services (MPR&S) as well for helping us with the QUV test.

Next, we want to thank Tom De Weyer from the Makerspace at PXL/UHasselt for providing assistance with the laser cutter and the 3D-printers.

Lastly, we wish to express our appreciation to all the researchers from the research group Functional Materials Engineering at imo-imomec for fostering a pleasant working environment in the lab, their insightful advice, and their generous assistance throughout our activities.

Table of contents

List of tables

List of figures

Glossary

Accelerated lifetime tests (ALTs)	A range of tests used to test a product by exposing it to conditions beyond its normal operating conditions in order to accelerate the aging process. These tests are used to estimate the product's lifespan.
Cycle	In the context of this study, the term refers to a stretching and relaxing motion of a silicone device by a cycletester.
Cycletester	An automated device used to apply stretching and relaxation to the silicone devices with controlled actions.
Device	The stretchable electronic circuits made in this research. This can be the stretchable wire or the stretchable LED strip.
Flexconnectors	The flexible PCBs used to connect the stretchable devices to an external circuit.
G-code	A programming language often used to program 3D printers.
Galinstan	An alloy composed of gallium, tin, and indium. It is used to make the stretchable conductive traces of the devices.
Spraycoater	A device used for the automatic spraying of a liquid.
Syringe pump	A device used to accurately control and deliver fluids from a syringe at a controlled rate.

Abstract (English)

Researchers at imo-imomec are using a novel technology consisting of a silicone encapsulation with galinstan traces and small rigid components to produce stretchable electronic devices. This study focuses on testing and validating the lifetime of these devices.

To obtain comparable results, two reference devices were designed: a device containing an LED, and a stretchable wire with contact points for four wire measurements. Subsequently, the devices were produced in batches and exposed to the following stress factors: temperature, humidity, UV radiation, and stretching in accelerated lifetime tests. The performance of the stretchable LED strip was assessed based on the functioning of the LED, while resistance measurements were the prominent parameter for the stretchable wires. During the exposure, both in situ and ex situ measurements and observations were performed.

The LED strips endure 859 cycles of 50% stretch on average. The manageable stretch is reduced by the damp heat test. Failures result from the silicone detachment from the LED which causes trace disconnection from the LED contacts. UV radiation increases silicone stiffness and extends the operation. The lifetime of the stretchable wires was significantly longer, as those devices lasted hundreds to thousands of cycles. Additionally, the resistance of the traces increased both during stretching and during exposure to increased temperature and humidity. However, UV radiation alone did not appear to have any direct effect on trace resistance.

Abstract (Nederlands)

Onderzoekers van imo-imomec gebruiken een nieuwe technologie die bestaat uit een siliconen encapsulatie met geleidende galinstanbanen en rigide componenten om rekbare elektronica te maken. Deze studie focust op het testen en valideren van de levensduur van deze elektronica.

Er zijn twee referentie-apparaten ontworpen: een apparaat dat een led bevat, en een rekbare draad zonder component. De apparaten zijn vervolgens in batches geproduceerd en blootgesteld aan de volgende stressfactoren: temperatuur, vochtigheid, UV-straling en uitrekking in versnelde levensduurtests. De prestaties van de rekbare ledstrips zijn onderzocht op basis van de werking van de led, terwijl weerstandsmetingen de belangrijkste parameter voor de rekbare draden zijn. Tijdens de blootstelling werden zowel in-situ- als ex-situmetingen en observaties verricht.

De rekbare ledstrips doorstaan gemiddeld 859 cycli van 50% rek. De handelbare rek wordt verminderd door de damp heat-test. Defecten ontstaan doordat de silicone los komt van de led, waardoor de banen contact verliezen met de led. UV-straling verhoogt de stijfheid en verlengt de werking van de led. De levensduur van de rekbare draden is aanzienlijk langer, aangezien ze honderden tot duizenden cycli overleven. De weerstand van de banen nam toe, zowel tijdens het uitrekken als tijdens de blootstelling aan verhoogde temperatuur en vochtigheid. UV-straling op zichzelf leek geen rechtstreeks effect te hebben op de weerstand van de banen.

1 Introduction

1.1 Context

Although flexible and stretchable electronics are a relatively recent technological advancement, their significance is rapidly increasing. Stretchable electronics have a wide range of application possibilities due to the fact that they can keep conducting current while being stretched, bent, twisted, compressed, or deformed into arbitrary shapes [1]. This unique ability can give them an advantage over rigid electronics. Additionally, a self-healing property can also be observed in some types of stretchable electronics [2].

Soft, flexible, and stretchable electronic devices open up new possibilities to develop and improve various kinds of applications. These applications can range from wearable devices to various healthcare applications [1][3][4], smart textiles [5], soft robotics [2][6], electronic skins [2] and many more. Currently, different types of stretchable electronics made of different materials and production techniques are used to make these applications such as using stretchable materials [7][8] or using rigid materials in combination with special structure designs [9].

Researchers from imo-imomec's Functional Materials Engineering (FME) expertise group and Hasselt University have developed a novel scalable DIY approach for the fabrication of soft stretchable electronics. The self-contained silicone devices with circuit traces are made out of liquid metal. The liquid metal used in this research is a gallium-based liquid metal named galinstan [8]. The main components of these devices are: silicone, galinstan, flexible PCBs, and small rigid electronic components.

This master's thesis will focus on testing and validating the lifetime of the stretchable electronic circuits. This study is part of a larger-scale project that seeks to identify the properties of the new technology with the goal of achieving improvements and eventually bringing these electronics to market.

1.2 Research problem

Since this type of stretchable electronics is a novel technology, the influence of various stress factors on the lifetime of these devices is not yet known. Therefore, the most influential stress factors need to be determined first. Additionally, the development of reliable and repeatable tests is necessary to subject the devices to these stress factors accurately. Conducting accelerated lifetime tests (ALTs) takes precedence in bringing this innovative technology to the market by subjecting the devices to an accelerated degradation process.

1.3 Research goal

This research has six subgoals. These subgoals will all contribute to the main goal of this research which is to investigate the influence of temperature, humidity, UV-radiation, and stretching on the life expectancy of these stretchable electronic devices. The first subgoal is to determine all the stress factors that influence the lifespan of these devices. After the determination of the stress factors, it is decided to focus on the influence of temperature, humidity, UV-radiation, and stretching. The second subgoal of the research is to develop, for each factor, a test procedure. These procedures will enable accurate measurements. The third objective is to develop a test setup for the stretch tests with the available cycle

testers. Furthermore, a program to control the cycle testers must be written. The fourth subgoal of the research is to identify possible improvements to the production process. These improvements will make the produced devices more reliable. The next subgoal is measuring the lifetime of the devices. Finally, the last subgoal is to identify all the failure mechanisms and propose solutions to lower the failure rate of the devices and increase the life expectancy. To conclude, all the previous mentioned subgoals contribute to the main goal of the research.

1.4 Work packages

This research mainly exists out of the designing, production, and testing of the devices. To accomplish this, the research is divided into five work packages. These work packages are:

- literature study,
- designing and production of the devices,
- environmental testing,
- stretch testing,
- data processing.

2 Literature study

The literature study presented in this chapter aims to provide an overview of the current state-of-the-art stretchable electronic devices, with a particular focus on liquid metal based stretchable devices, different ALTs, and the accompanying industry standards. Additionally, various applications of stretchable electronics and their advantages over conventional rigid devices will be discussed.

2.1 Materials

2.1.1 Silicone

This research uses two types of silicones: Dragon Skin 10 Fast and Dragon Skin FX-Pro. Dragon Skin 10 silicones can be used in diverse fields ranging from medical prosthetics and cushioning applications to a variety of industrial purposes due to their wide temperature range of -65°F to 450°F (-53°C to 232°C). It is available in Very Fast, Fast, Medium and Slow curing speed variants which have curing speeds of respectively 30 minutes, 75 minutes, 5 hours, and 7 hours [10].

Dragon Skin FX-Pro is mainly used for skin effects and makeup appliances. Furthermore, it needs 40 minutes to cure at room temperature (73°F/23°C). It is important not to cure it when the temperature is lower than 65°F/18°C [11].

Additionally, both silicone types have a skin safe certificate and thus do not cause skin irritation [10] [11].

Both Dragon Skin types consist of two parts: Part A and Part B that need to be mixed together. Before dispensing, Part A and Part B need to be stirred. A volume or weight ration of 1A:1B should be dispensed into the mixing container. When working with Dragon Skin 10, after the two parts are mixed, it is recommended to use a vacuum pump in order to remove the trapped air in the liquid silicone. The vacuum pump must be able to pull minimum 1 Bar [10][11].

TECHNICAL OVERVIEW

	Mixed Viscosity (ASTM D-2393)	Specific Gravity (g/cc) (ASTM D-1475)	Specific Volume (cu. in./lb.) (ASTM D-1475)	Pot Life (ASTM D-2471)	Cure Time	Shore A Hardness (ASTM D-2240)	Tensile Strength (ASTM D-412)	100% Modulus (ASTM D-412)	Elongation at Break % (ASTM D-412)	Die B Tear Strength (ASTM D-624)	Shrinkage (in./in.) (ASTM D-2566)
Dragon Skin™ 10 Very Fast	23,000 cps	1.07	25.8	4 min.	30 min.	10A	475 psi	22 psi	1000%	102 pli	< .001 in./in.
Dragon Skin™ 10 Fast	23,000 cps	1.07	25.8	8 min.	75 min.	10A	475 psi	22 psi	1000%	102 pli	< .001 in./in.
Dragon Skin™ 10 Medium	23,000 cps	1.07	25.8	20 min.	5 hours	10A	475 psi	22 psi	1000%	102 pli	< .001 in./in.
Dragon Skin™ 10 Slow	23,000 cps	1.07	25.8	45 min.	7 hours	10A	475 psi	22 psi	1000%	102 pli	< .001 in./in.
Dragon Skin™ 10 AF	23,000 cps	1.07	25.8	20 min.	5 hours	10A	475 psi	22 psi	1000%	102 pli	< .001 in./in.
Dragon Skin™ 15	21,000 cps	1.07	25.8	40 min.	7 hours	15A	537 psi	40 psi	771%	112 pli	< .001 in./in.
Dragon Skin™ 20	20,000 cps	1.08	25.6	25 min.	4 hours	20A	550 psi	49 psi	620%	120 pli	< .001 in./in.
Dragon Skin™ 30	20,000 cps	1.08	25.7	45 min.	16 hours	30A	500 psi	86 psi	364%	108 pli	< .001 in./in.

Mix Ratio: 1A:1B by volume or weight
Color: Translucent
Useful Temperature Range: -65°F to +450°F (-53°C to +232°C)
Dielectric Strength (ASTM D-149)***:*** >350 volts/mil

*All values measured after 7 days at 73°F/23°C

Figure 1: Properties of the different Dragon Skin 10, 15, 20, and 30 variants [10]

TECHNICAL OVERVIEW

Mix Ratio: 1A : 1B by weight or volume	
Mixed Viscosity, cps: 18,000	(ASTM D-2393)
Specific Gravity, g/cc: 1.062	(ASTM D-1475)
Specific Volume, cu. in./lb.: 25.0	(ASTM D-1475)
Pot Life: 12 minutes (73° F / 23°C)	(ASTM D-2471)
Cure time: 40 minutes (73° F / 23°C)	
Color: Translucent	
Shore A Hardness: 2	(ASTM D-2240)
Tensile Strength, psi: 288	(ASTM D-412)
100% Modulus, psi: 37.8	(ASTM D-412)
Elongation @ Break: 763%	(ASTM D-412)
Die B Tear Strength, pli: 61	(ASTM D-624)
Shrinkage, in./in.: <.001	(ASTM D-2566)

* All values measured after 7 days at 73°F / 23°C

Figure 2: properties of Dragon Skin FX-Pro [11]

Figure 1 and Figure 2 show the properties of the Dragon Skin 10 and Dragon Skin FX-Pro silicones. The four most important properties that will influence the lifetime of the silicones under stretch are: tensile strength, 100% modulus, elongation at break, and the tear strength. The tensile strength is a measure of how much force the silicone can handle before it breaks. 100% modulus gives the force needed to stretch the silicone for 100%. The elongation at break shows how much stretch the material can handle before it breaks. Finally, the tear strength shows how much force is required to tear the material.

Dragon Skin 10 Fast has a higher tensile strength (475 psi) , a lower 100% modulus (22 psi), a higher elongation at break (1000%), and a higher tear strength (102 pli) than Dragon Skin Fx-Pro. Dragon Skin Fx-Pro has a tensile strength of 288 psi, a 100% modulus of 37.8 psi, an elongation at break of 763%, and a tear strength of 61 pli [10][11]. This means that Dragon Skin 10 Fast is stronger, more flexible and more tear resistant than Dragon Skin FX-Pro. Furthermore, Dragon Skin FX-Pro has a higher 100% modulus which makes it stiffer than Dragon Skin 10 Fast.

2.1.2 Galinstan

Galinstan is an alloy composed of gallium, tin, and indium. Furthermore, it has the unique ability to behave as a metal, to conduct current, and to be in a liquid state at room temperature so that it can deform together with the silicone. More advantages of galinstan include its high conductivity (between 0.01 Ω/□ to 0.02 Ω/□) [8], high commercial availability, and its self-healing capabilities [8]. The main advantage of galinstan over mercury is the low toxicity [12]. Mercury is also liquid at room temperature but its toxicity limits its use in applications [13].

A gallium oxide layer forms on the surface of galinstan while in contact with oxygen. This oxide layer acts as a thin mechanical skin on the surface, enabling the liquid metal to sustain non-spherical structures [13]. To prevent the oxidation of galinstan, it can be kept in an inert environment such as argon or nitrogen [12] or it can be covered in an aqueous acid such as HCl [12][14] or in an aqueous base such as NaOH [14].

Furthermore, these devices can contain small rigid electronic components such as microcontrollers, sensors, power sources, and other small rigid components that are connected by the Galinstan traces [8]. Additionally, the galinstan traces can be connected to a flexible PCB which enables the stretchable devices to be connected to an external circuit. The production technique used in the paper allows for the production of vertical interconnect access (VIAs) in the devices. The possibility of using VIAs to make multi-layered devices together with the use of galinstan traces in combination with rigid electronic components facilitates the production of complex stretchable devices [8].

2.1.3 Flexconnectors

The PCBs used to connect these devices to an external circuit are flexible PCBs also called flexconnectors and are shown in Figure 3. These flexconnectors contain conducting traces that are protected by a polymer film. The flexconnectors can withstand temperatures ranging from -200°C to 400°C [15].

Figure 3: Flexconnector

2.2 Applications

This type of stretchable electronic devices can have a wide range of applications such as soft robotics [6], wearables devices [8], interactive tattoos [8], in textile embedded electronics [8], and stretchable circuits [8]. This chapter will describe some developed examples for every type of application.

2.2.1 Soft robotics

One example of an application made with these silicone-based stretchable devices is the soft gripper made by Heylands. This gripper uses a time-of-flight (TOF) sensor inside the device to measure the distance between the object and the gripper itself. The TOF sensor works by sending photons from its emitter. These photons reflect from the target object and are received by the receiver. This allows the TOF sensor to measure the distance to an object. As a result of the working principle of this type of sensor, the device needed to be designed so that no silicone is positioned in front of the sensor. Furthermore, the most significant advantage of this gripper is that it can deform into the shape of the object itself which gives it the soft property. Because of this, objects such as fruits or vegetables are not squished by the gripper [6]. Figure 4 shows the stretchable electronic device attached to the Festo Finray Finger.

Figure 4: Festo Finray finger with the stretchable device attached to it [6]

2.2.2 Wearable devices

Another example of an application made with this type of electronic devices is the stretchable wristband with integrated sensors for input, output, power and processing. Figure 5 shows the wristband. The wristband is designed as an interval timer for runners. One of the three modes: 3 min. running - 1 min. walking, 5 min. running - 5 min. walking, and 10 min. running - 5 min. walking can be selected with the integrated capacitive button. When this button is pressed for 2 seconds, the workout will start or stop. The user must walk when the LED is dimmed and run when the LED blinks. Furthermore, the wristband is controlled by the microcontroller ATtiny85-20SU, and powered by a replaceable coin cell battery [8].

Figure 5: Stretchable wristband with sensors for input and output, power and processing embedded [8]

2.2.3 Interactive tattoos

Figure 5 shows an interactive tattoo. This tattoo device is cured on the arm instead of wrapped around it like the wristband. As a result, the device will stretch and band together with the arm. The integrated strain sensor lights up LEDs when the wrist gets flexed [8].

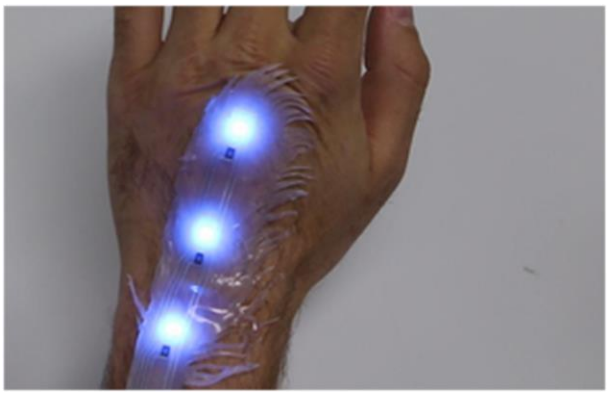

Figure 6: Stretchable tattoo with embedded strain gauge to track the bending of the arm [8]

2.2.4 In textile embedded electronics

Figure 7 shows a stretchable display integrated into a pillow. The display contains a coin cell battery, two 7-segment displays, and an Atmega328-AU. The clock in the pillow shows the current hour for 5 seconds when a strain sensor is pulled. The usage of soft silicone material eliminates potential discomfort for the sleeper [8].

Figure 7: Stretchable display [8]

2.2.5 Custom Stretchable circuits

The last example is a stretchable Arduino Uno development board. This Arduino uno integrates an Atmega328 microcontroller, and contains 3 circuit layers with 25 VIAs to interconnect the layers. Furthermore, the stretchable Arduino Uno contains all programmable GPIO pins and can be programmed via UART [8]. Figure 8 illustrates the stretchable Arduino Uno development board.

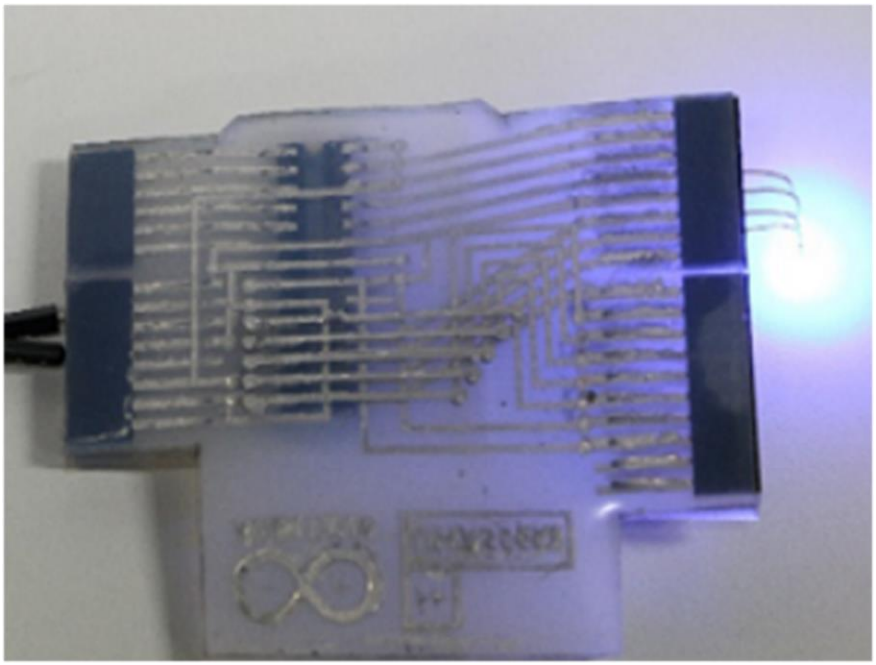

Figure 8: Stretchable Arduino Uno development board [8].

The production process that will be used in this research is based on the production process used by Vandervoort [15] which is based on the DIY production process invented by Nagels et al. [8].

2.3 Accelerated lifetime tests and industry standards

2.3.1 Rigid electronics

Before a new technology can be brought onto the market, its durability and reliability should be tested first. Herefore, ALTs can be used which will accelerate the degradation processes of the tested devices or components. Hereafter, the results from the ALTs can be converted into the expected lifetime for real-life applications.

ALTs often follow a certain industry standard. Multiple different industry standards exist for rigid electronics. MIL-STD-810, JEDEC JESD22, IEC 60068, and Telcordia GR-63 are some of the most used industry standards. The MIL-STD-810 standard is mostly used for electronic devices used in the military and other highly demanding electronics [16]. The JEDEC JESD22 standard is mostly used for electronic components. Telcordia GR-63 is a standard developed to test telecommunication equipment [17]. IEC standards are commonly used for general-purpose electronics.

2.3.2 Flexible electronics

IEC 60068-2 contains multiple different accelerated lifetime tests. Most of these tests can be used after adjusting some parameters to test the flexible electronics. However, this does not include ALTs to test the influence of stretching, bending, and twisting. Saleh et al. [21] reviewed multiple techniques to test the durability of flexible electronics while bending. These techniques include static, dynamic, push to flex, and roll to flex techniques. For these different techniques, some bending machines are presented and their advantages and disadvantages are discussed. Furthermore, Chow et al. [22] developed a testing device to in-situ monitor flexible electronics while they are being subjected to controlled twisting. Harris et al. [23] also developed bending, stretching, and twisting tests for flexible electronics. The influence of temperature, humidity, and UV-radiation can be tested in climate chambers. A climate chamber can stabilize the other factors when one of them is tested. As a result, the influence of the other factors on the device under test will be minimized.

2.3.3 Stretchable electronics

Currently, no industry standards exist for stretchable electronics. As a result, the main factors that influence these stretchable electronics should be determined first before new accelerated stress tests can be developed. The lifetime of the stretchable electronics is influenced by UV-radiation [18], temperature [19][21], humidity [20], vibration, and mechanical stresses like stretching, bending, and twisting. All these factors in combination with each other can be expected to interact with the stretchable electronic devices in real-life environments. Most of these factors also influence the lifetime of rigid electronics. As a result, the ALTs that will be used to test stretchable electronics can be based on the ALTs used to test rigid electronics. The expected applications of the stretchable devices are mostly general-purpose applications, as shown in chapter 2.2. Therefore, IEC seems to be the most promising industry standard on which to base the new ALTs on.

Furthermore, Vandervoort used a cycletester and four wire measurements to test the change in resistance while stretching the liquid metal-based stretchable electronic devices. Additionally, the self-heating properties of the devices as a result of the Joule effect were investigated. He concluded that the galinstan traces heat up 1°C for currents up to 100 mA with a ratio between the inside and outside temperature of 1.03. For currents equal to or greater than 1 A, the ratio between the outside and the inside temperature is 1.82 and the minimal cross-section of the galinstan traces must be 0.0117 mm^2 [15].

2.4 Damp heat test

One commonly used ALT is the damp heat test. Damp heat testing is a type of environmental test that is performed on electronic devices to investigate their ability to withstand increased temperature and humidity over a prolonged period of time. During this test, the electronic devices are placed in a climate chamber that is heated and humidified to a specific temperature and humidity level.

Damp heat testing involves several standards, and each standard has a different application for the test. IEC 60068-2-38, IEC 60068-2-78, and IEC 60068-2-30 are some of the most used damp heat industry standards. Commonly used damp heat tests include constant damp heat, cyclic damp heat, and composite temperature/humidity cyclic tests [24].

The constant damp heat test is often used to assess whether a product is suitable for use, storage, and transportation in environments with high humidity. The temperature, humidity percentage, and duration of the test can vary depending on the used industry standard. Cyclic damp heat testing is used to evaluate the suitability of products for use, transportation, and storage in conditions with high humidity that are accompanied by temperature changes. The bottom and upper temperature, the humidity percentage, the duration of one cycle, the total duration of the test, and the other parameters can again vary depending on the used industry standard. Figure 9 shows an example of a possible cyclic damp heat test cycle. The composite temperature/humidity cyclic test is meant to investigate the effect of frozen, trapped water in a device. With this test, the lower temperature limit lies below 0°C. The lower and upper temperature, the duration of one cycle, the number of cycles, and all the other parameters can again vary depending on the used industry standard. Figure 10 shows an example of a possible composite temperature/humidity cyclic test cycle [24].

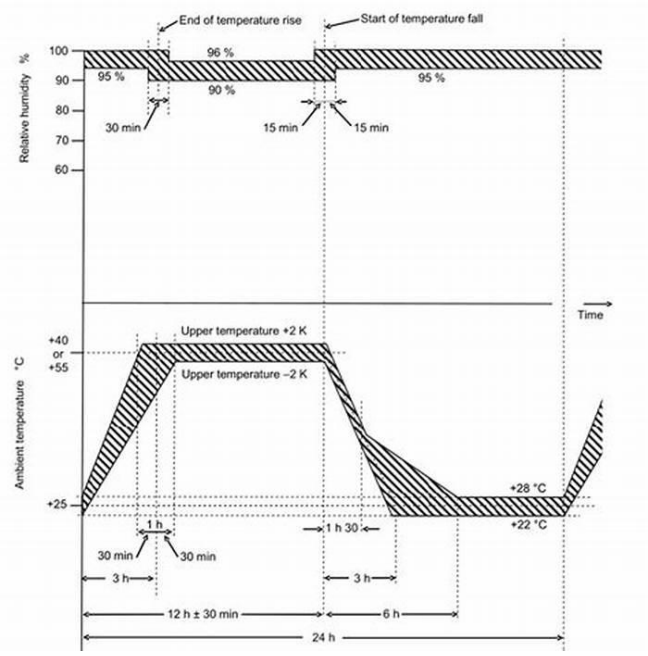

Figure 9: Example of a cyclic damp heat test cycle [24]

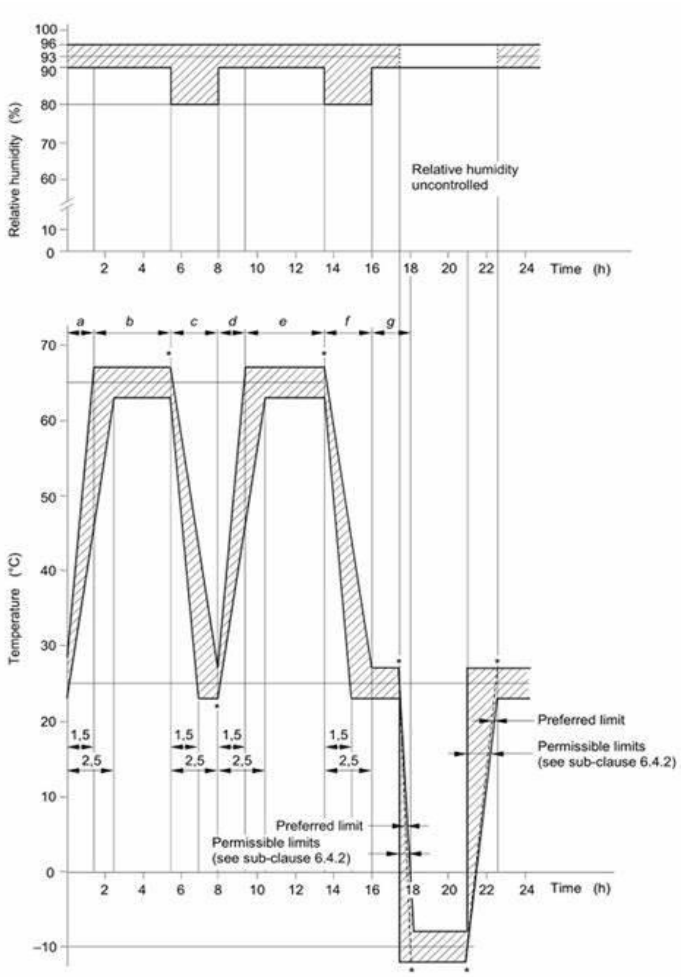

Figure 10: Example of a composite temperature/humidity cyclic test cycle [24]

2.5 QUV test

The stretchable devices have applications that could potentially expose them to environmental factors in the outside world. Those environmental factors not only include heat and humidity, but exposure to sunlight as well. The QUV tester employs fluorescent lamps to accurately replicate the detrimental effects of sunlight, specifically by simulating critical short-wave UV radiation. This simulation effectively reproduces various forms of physical damage, including but not limited to color alteration, loss of gloss, chalking, cracking, crazing, hazing, blistering, embrittlement, reduction in strength, and oxidation [25]. To test devices on their resilience to UV light, the QUV accelerated weathering tester of manufacturer Q-LAB at the Materials and Packaging Research & Services (MPR&S) was used.

The QUV accelerated weathering tester is capable of recreating an environment which reproduces the effects of sunlight, rain and dew [25]. Concretely, this means that devices in the chamber are exposed to multiple stress factors: UV light, heat, and humidity. Singling out only the UV stress factor is not possible with the QUV tester. However, due to the aim of this test being to gauge the resilience of the devices to the outside weather conditions, the test results will still produce valuable insights.

To ensure the exposures provided by the QUV tester are standardized, it is able to effectively replicate environments defined by different testing norms, including: ISO norms, DIN norms and IEC norms. Different norms describe standard practices for exposing various materials to environmental factors [26]. In the scope of this research, the ISO 4892-3 (DIN) norm was chosen as it provides guidelines for exposing plastic materials to fluorescent UV lamps to assess their durability. This standard specifies parameters such as irradiance levels, temperature, and humidity. Different methods are described in the ISO 4982-3 norm, in which some parameters can vary. Method C, as shown in Table 1, was applied in the tests conducted in the scope of this thesis, as it is considered the most detrimental. The most detrimental method was chosen due to limitations regarding the time frame available for the tests, which was approximately 4 weeks. As there were no similar environmental tests done previous to this research for reference, the objective was to expose the devices to a significantly high degree in order to cause differentiations with unexposed devices. In method C, UVB 313 lamps are used, which produce UV light with a wavelength of 310 nm which is shorter than those produced by the other lamps. Shorter wavelengths are generally considered more harmful due to the fact that they carry higher energy levels and can therefore cause significant damage to materials.

Table 1 describes the weathering cycle provided by method C, which lasts 12 hours and consists of two parts. The first part lasts 8 hours and consists of dry exposure to the UVB 313 lamps at a temperature of approximately 70 °C. In the second part, which lasts 4 hours, a condensation process is created, which mimics dew formation on the devices and exposes them to humidity [27].

Table 1: possible methods applicable by the QUV tester, based on the ISO 4892-3 norm

Method A: Artificial accelerated weathering with UVA-340 lamps				
Cycle No.	**Exposure period**	**Lamp type**	**Irradiance**	**Black-panel temperature**
1	8 h dry 4 h condensation	UVA-340 (type 1A)	0,76 $W \cdot m^{-2} \times nm^{-1}$ at 340 nm UV lamps off	60 °C ± 3 °C 50 °C ± 3 °C
2	8 h dry 0,25 h water spray 3,75 h condensation	UVA-340 (type 1A)	0,76 $W \cdot m^{-2} \times nm^{-1}$ at 340 nm UV lamps off UV lamps off	50 °C ± 3 °C Not controlled 50 °C ± 3 °C
3	5 h dry 1 h water spray	UVA-340 (type 1A)	0,83 $W \cdot m^{-2} \times nm^{-1}$ at 340 nm UV lamps off	50 °C ± 3 °C Not controlled
4	5 h dry 1 h water spray	UVA-340 (type 1A)	0,83 $W \cdot m^{-2} \cdot nm^{-1}$ at 340 nm UV lamps off	70 °C ± 3 °C Not controlled
Method B: Artificial accelerated weathering with UVA-351 lamps				
5	24 h dry (no moisture)	UVA-351 (type 1B)	0,76 $W \cdot m^{-2} \times nm^{-1}$ at 340 nm	50 °C ± 3 °C
Method C: Artificial accelerated weathering with UVB-313 lamps				
6	8 h dry 4 h condensation	UVB-313 (type 2)	0,48 $W \cdot m^{-2} \times nm^{-1}$ at 310 nm UV lamps off	70 °C ± 3 °C 50 °C ± 3 °C

NOTE 1 Higher-irradiance tests may be conducted if agreed upon by all interested parties. When high-irradiance conditions are used, lamp life may be significantly shortened.

NOTE 2 The ±3 °C variation shown for the black-panel temperature is the allowable fluctuation of the indicated black-panel temperature around the given black-panel temperature set point under equilibrium conditions. This does not mean that the set point can vary by ±3 °C from the given value.

NOTE 3 Black-panel temperature during the water spray cycle is not controlled but should not exceed 30 °C. Spray water temperature might have a significant effect on the test result.

3 Designs

3.1 Component design

3.1.1 Objective

Most applications made with this technology include one or more rigid electronic components. Therefore it is important not only to investigate the degradation of the galinstan traces themselves but also the contact points between the galinstan traces and the rigid components. This is the goal of the component device. The component in this device is a WS2812B LED. Therefore, the component device will be called a stretchable LED strip in this paper. A LED has been chosen because the functionality of an LED can be easily observed. Furthermore, the flat contacts of the LED makes it ideal to include in these stretchable devices. The functionality of the LED can be observed by measuring the current or by visually confirming if the LED lights up.

3.1.2 Prototype

After the devices were designed two prototypes were made. These prototypes were made to test the functionality of the design itself and to test the compatibility of the designs with the cycletesters. The prototypes were produced with individual molds and not with batch production. Furthermore, no stencil was used to produce the prototypes in contrast to the devices that will be tested. Instead of using a stencil that contains the traces outlines cut-outs, the laser cutter was used to cut-out the traces outlines from the vinyl.

Figure 11 and figure 12 show the made prototypes. The length of the smaller rectangular shaped silicone between the two flexconnectors is 3 cm. Both the height of the top and bottom layer of silicone was 2 mm. The LED has a height of 1.57 ± 0.05 mm, this results in a silicone layer of 0.43 ± 0.05 mm on top of the LED and a silicone layer of 2 mm below the LED. Furthermore, the wider parts of the device, where the flexconnectors are located, are made longer than necessary in order to prevent the liquid metal traces from being pressed on when being placed in the cycletesters.

The LEDs have a Vdd (power supply), data out, Vss (ground), and data in pins. Figure 13 shows the pin configuration of the LED. The galinstan traces are designed to connect each pin of the LED to two connections of a flexconnector in order to build in redundancy at the flexconnectors. Figure 11 also shows the design of the traces.

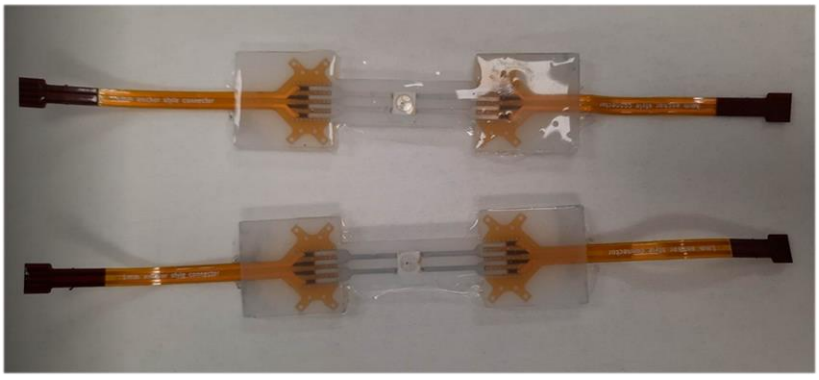

Figure 11: Top view of the stretchable LED strip prototypes

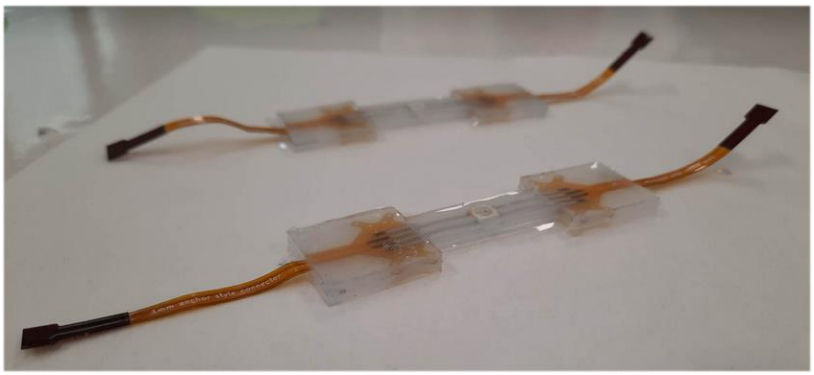

Figure 12: Side view of the stretchable LED strip prototypes

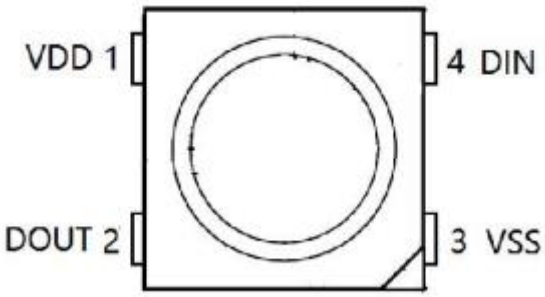

Figure 13: Pin configuration of the WS2812B LED [30]

3.1.3 Alterations

The prototypes contained two problems that needed to be solved. First, when placing the prototypes into the cycletesters, it was discovered that the rectangular shape of the wider parts of the devices did not fit into the cycletesters' device holders. To solve this problem for the prototypes, the corners of the devices were cut off and silicone was cut off from between the flexconnectors. Furthermore, the designs of the devices and the molds were adjusted to include this adjustment into the designs themself. Figure 14 shows the shape of the device holders, Figure 15 the final shape of the devices, and Figure 16 shows how a device will be positioned in the device holders.

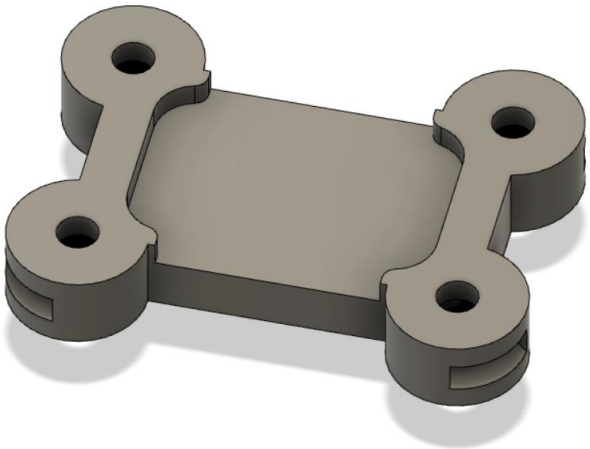

Figure 14: Shape of the device holder

Figure 15: Final shape of the devices

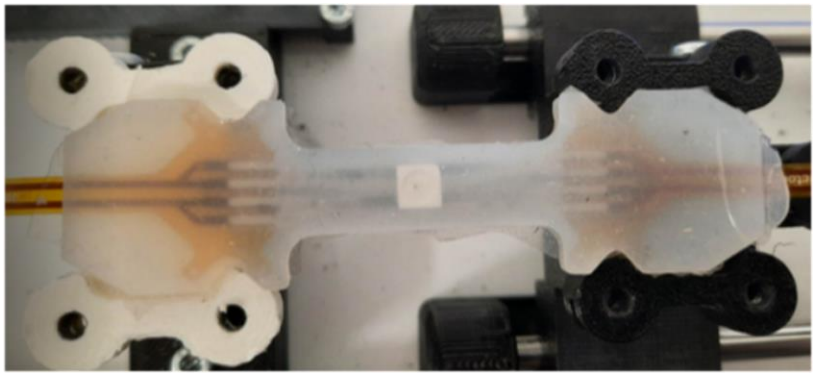

Figure 16: Device positioned on the device holders

The second problem relates to the height of the prototype. The silicone layer on top of the LED was too thin to withstand the stretch caused by the cycletesters. This caused the silicone to rupture around the LED when being stretched for 150%. Figure 17 shows a ruptured prototype. When the silicone is ruptured, the galinstan traces can become exposed. This causes the traces to lose contact with the LED contacts. Furthermore, this will also speed up the oxidation of the galinstan traces since the traces are now exposed to more oxygen. Lastly, the risk of galinstan contamination increases since the galinstan can now come out of the silicone encapsulation. To solve this issue, the top mold will be heightened from 2 mm to 3 mm this will allow for a silicone layer of 1.43 ± 0.05 mm to form on top of the LED. Furthermore, the bottom mold will be lowered to 1 mm this will ensure that the total height of the silicone device stays the same while lowering the position of the LED at the same time.

Figure 17: Ruptured prototype being stretched

Lastly, a third alteration was made to possibly extend the lifespan of the silicone. The diameter of the curve between the smaller and wider parts of the device was increased in order to get a smoother transition between the two parts. This will decrease the chances of ruptures occurring in these places. The diameter was extended to 3 mm.

3.1.4 Measurements

Both prototypes functioned after production. However, no reliable measurements were made due to the rupture of the silicone in both devices after stretching.

3.1.5 Final design

To conclude, the final design will have a total height of 4 mm. The top silicone layer will be 3 mm high and the bottom silicone layer will be 1 mm high. This will result in a silicone layer of 1.43 ± 0.05 mm on top of the LED and a silicone layer of 1 mm below the LED. Furthermore, the design of the devices itself is changed to ensure that the devices fitt between the 3D-printed screw hole outlines of the device holders of the cycletesters. The design of the galinstan traces themself were not altered. The small alterations to the design will result in better results. Figure 18 shows the final design of the stretchable LED strip.

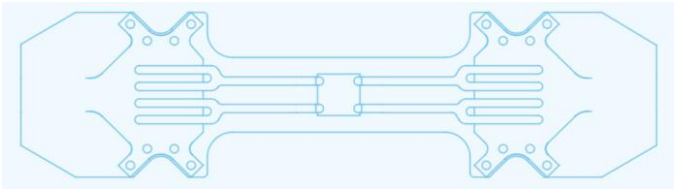

Figure 18: Final design of the stretchable LED strip

3.2 Stretchable wire design

3.2.1 Objective

For evaluating the lifetime of silicone devices, the degrading of the liquid metal traces is a significant factor. The degrading of these traces will affect the overall workings of any device made with the novel technology. The degradation causes the resistance of the traces to increase, subsequently the current must also increase in order to keep the current-supply to any components within the device constant. Increased heat dissipation within the traces follows, possibly accelerating the degradation process even further. Therefore, trace degradation must be researched and evaluated thoroughly if future devices with one or multiple components are to be manufactured that comply with certain norms.

Single-trace monitoring

To evaluate trace degradation resistance is measured using the four wire technique. However, since the connection with a trace is not made within the device, other resistances have the possibility to interfere with the measurement. These other resistances are the resistance of the flexconnector and its contact with the liquid metal traces. Copper traces run within the flexconnector between the cable contacts on one side to the liquid metal contacts on the other side, as seen on Figure 19.

Figure 19: Flexconnector

To eliminate both the resistance of the copper traces and the contact resistance between the flexconnector and the liquid metal traces a four wire setup needed to be realized within the device itself. A four wire setup within a device can be made by arranging the liquid metal traces in such a way that the to-be-measured trace has four connections to the outside. As can be seen in figure 20, those four connections can be realized by other traces themselves. Two of the four connections are used during a four wire measurement to inject a current through the to-be-measured trace. When the current is injected, a voltage drop will occur over the to-be-measured trace. That voltage drop will subsequently be measured through the other two connections.

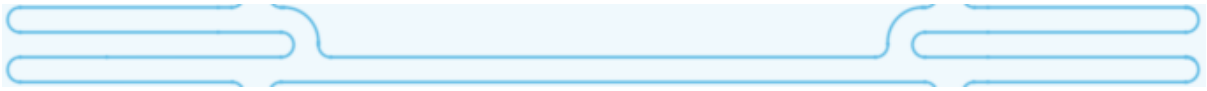

Figure 20: The 4 connections necessary for four wire measurement.

Figure 21 shows that 8 connections can be made via the 2 flexconnectors, of which 4 are redundant. The redundant connections are foreseen as a backup: if a contact between a liquid metal trace and the flexconnector should fail, there is an extra contact that can replace it.

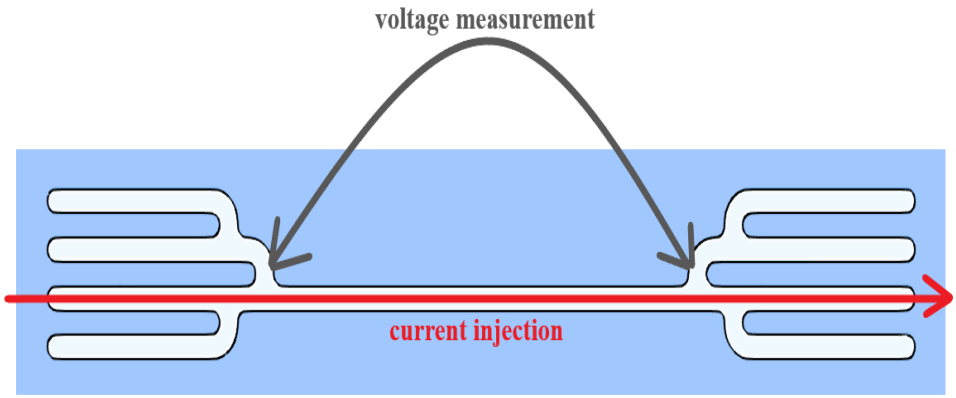

Figure 21: The 8 connections to the measured trace and principle of four wire resistance measurement

3.2.2 Prototype

Due to the fundamental nature of this research, simplicity was a major parameter for the device design. Figure 22 shows the prototype device after production. As mentioned in paragraph Y, the goal of the prototype device was determining the compatibility of the design with the cycletester. Stretching was a stress factor that all devices using the design would be exposed to. Devices need to be clamped between two 3D-printed parts in the cycletester during stretch testing. To minimize strain on the devices following this clamping, the silicone ends were reshaped to better fit the clamps.

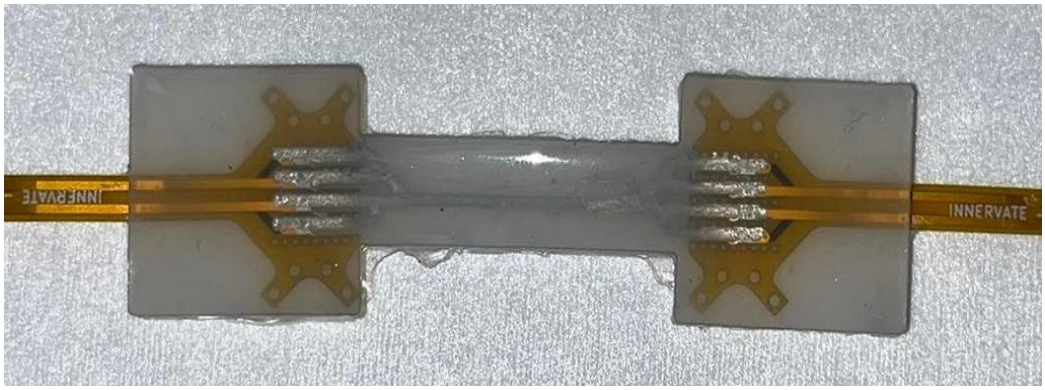

Figure 22: stretchable wire prototype devices after production

On Figure 23, the adjusted reshaped device can be seen, which is similar to the stretchable LED strip. The reshaped device was made by cutting away excess silicone around the flexconnector, using a scalpel.

Figure 23: Adjusted stretchable wire

3.2.3 Encountered issues

Figure 24 shows a close up of the contact between the liquid metal traces and the flexconnector in the stretchable wire prototype. The liquid metal traces are noticeably misaligned with the contact pads of the flexconnector. However, no short circuit is made and no contact between the two is completely cut off. Due to the nature of the measurements done on the stretchable wire, which are resistance measurements of a part of the trace in the middle of the device, there was no effect of the misalignment on the measurements. The misalignment is a direct consequence of the usage of vinyl for determining the shape of the liquid metal traces, which is an inherently inaccurate method.

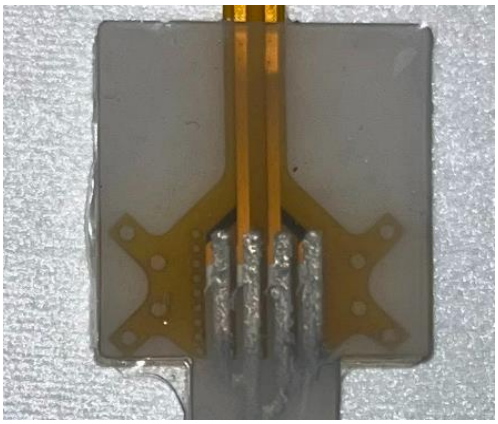

Figure 24: Misalignment of the liquid metal traces and the flexconnector

3.2.4 Measurements

Resistance variation during stretched state

There is a period of continuously increasing resistance after a device is stretched. The resistance increase starts off at a significant rate before settling at a certain value.

The resistances of two of the prototypes without component were measured after they were stretched for the third time. Figure 25 shows the resistance of both devices as a function of the time they were held in the stretched position. The dimensions of the prototype design ensure a stretch of 150%, elongating the devices' stretched area to 3 times their original length.

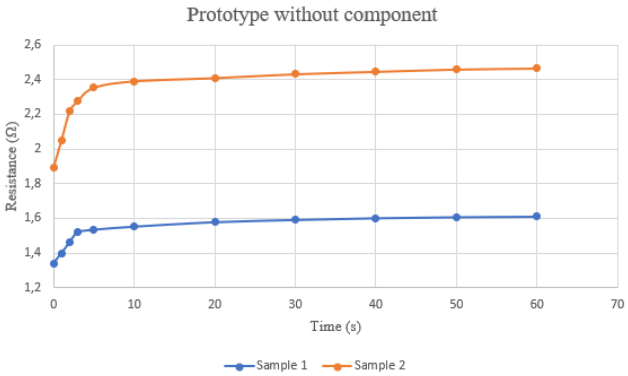

Figure 25: Static stretch resistance of the prototype devices

The majority of the resistance increase occurred within 5 minutes of the stretching of the device. Figure 25 shows this phenomenon. After the initial significant resistance increase, a period of less rapid increase follows. Measurements were stopped after 1 hour, at which point the resistance increase had slowed down to 0.17 mΩ/s for device 1 and 0.12 mΩ/s for device 2.

The magnitude of the resistance increase after stretching was noticeably smaller as the number of stretch cycles executed on the devices went up.

Multiple explanations as to why the resistance increases after stretching are possible: the flowing of the liquid metal, the silicone settling or the four wire current heating up the trace or the most viable. The four wire current being the cause was ruled out by executing brief measurements, which lasted no more than 5 seconds, every 10 minutes instead of continuously. However, this resulted in the exact same resistance increase, ruling out the four wire current as a viable explanation. This implies that it must be the silicone settlement or a liquid metal flow that causes the resistance increase. Both are viable explanations as they potentially affect the geometrical properties of the trace, such as the cross section.

Resistance variation during stretch cycling

Repeated stretching of a device causes resistance changes in its traces. To evaluate this change, a cycletester was used to stretch the device and the resistance was measured multiple times after a certain amount of stretches. Since the resistance is different for the stretched and relaxed state, both the stretched and relaxed trace resistance was measured each time.

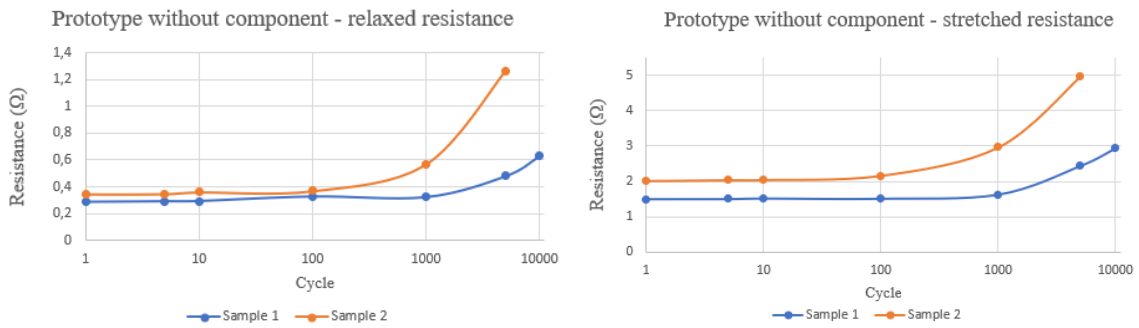

Figure 26: Resistance as a function of the number of cycles the devices were stretched.

Figure 26 shows the trace resistances of devices 1 and 2 as a function of the number of cycles when the devices were in a relaxed and stretched state, respectively. The resistance of device 1 is in both the relaxed and stretched state slightly higher than that of device 2. This difference grows larger as the number of times the device is stretched increases.

Anomalies during stretch cycling

Since the testing process was still being tested for optimal execution within the scope of this thesis, two changes were made during testing.
The second change was the stretching speed, which was altered from 2.18 to 1.45 seconds per stretch after 1000 stretches. The speed alteration was made for the purpose of shortening testing time, as the number of available cycletesters was a limiting factor in the research described later in this paper.
It must be noted that the servomotor of the cycletester of device 2 shocked significantly from 3000 to 5007 cycles, before its complete failure at the 5008th cycle. Figure 26 shows the resistance of both devices diverging significantly after 1000 cycles, which could have been due to the severe shocking of device 2. However, the diverging appears to start at a few hundred cycles, making more similar tests required for pinpointing the exact cause.

Periods of standstill

During stretch testing, three periods of standstill existed. The first period was between the 1000th and 1001st cycle and lasted for 2 days. The second period was between the 5008th and 5009th cycle and lasted for 2 hours. The last period was only undergone by device 1 and was between the 10,000th and 10,001st cycle for 3 days. After each period of standstill, the resistance in both the relaxed and stretched state were measured.

The 2-day period was caused by the fact that the cycletester were not deemed stable enough at the moment testing started to let them run without supervision. Thus, during the 2-day period supervision of the cyclic testing was not possible, the cycletesters were stopped. Prior to the 2-day standstill period, the resistances were measured, as 1000th stretch cycles had been executed. After the 2-day period, the resistance of device 1 had risen from 0.323 Ω to 1.279 Ω in the relaxed state, and from 1.632 Ω to 2.774 in the stretched state. During the same period, the resistance of device 2 had risen from 0.568 Ω to 1.836 Ω in the relaxed state, and from 2.965 Ω to 5.702 Ω in the stretched state. A clear trend of rising resistance could be observed after a 2-day period of standstill. When cyclic testing continued, the resistance again dropped to the original values measured prior to the standstill between the 100th and 120th cycle.

The 2-hour standstill period occurred due to the breakdown of the servo motor in the cycletester for device 2 in the 5008th cycle. Before device 2 could be moved to another cycletester, 2 hours passed. During these 2 hours, the cyclic testing of both device 1 and device 2 was stopped to increase the comparability of their results. Despite the standstill not being planned, the resistances of both devices were measured just 8 cycles prior, rationalizing another measurement after the 2-hour period for comparison.
After the 2-hour period, the resistance of device 1 had risen from 0.481 Ω to 0.518 Ω in the relaxed state, and from 2.440 Ω to 2.540 Ω in the stretched state. During the same period, the resistance of device 2 had decreased from 1.261 Ω to 1.139 Ω in the relaxed state, and from 4.960 Ω to 4.470 Ω in the stretched state. There is no clear trend in resistance values after the 2-hour standstill, apart from their deviation from the value measured prior to it.

Lastly, stretch cycling of device 1 was continued beyond 10 000 cycles after a 3-day standstill period. Device 2 was not measurable due to a severe rupture before. After the 3-day period, the resistance of device 1 had decreased from 0.632 Ω to 0.558 Ω in the relaxed state, and from 2.938 Ω to 2.683 Ω in the stretched state.

Considering all standstill periods, no clear up- or downward trend was observed. However, the resistance change was significant.

Measurement conclusions

The objective of the measurements was to select relevant phenomena which were to be researched on the more statistically relevant batches described in paragraph 3.3. The resistance variation as a function of time and the resistance variation after stretch cycling were significant and will thus be researched further. The results from the prototypes will, unlike the results from the batch devices, not be used statistically in the final conclusions. The reason for this is the testing conditions which were not stable, as the testing process itself was being fine-tuned.

3.2.5 Final design

Figure 27 shows the final stretchable wire design, with all its components. The outer shape on Figure 27, determines the silicone shape of the device. Within this shape, the tracks for the four wire resistance measurements and the flexconnectors are illustrated as well.

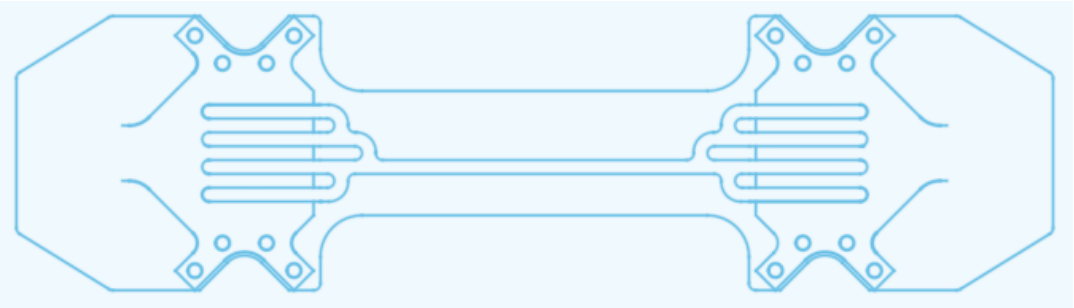

Figure 27: Final stretchable wire design

3.3 Batch design

A batch design was used to reduce variation of different variables during the production process. The batch production approach offers a consistent way of producing uniform devices. Both the batch design for the stretchable LED strips and the four wire devices design are designed to produce 12 devices simultaneously. Figure 28 shows the batch design for the stretchable LED strips. The small circles in the design are screw holes that make it possible to attach the bottom plate to the molds with screws. The purpose of the rectangles in the middle of the design is to make it possible to bring the tails of the flexconnectors from between the mold and the base plate outside.

3.3.1 Stretchable LED strip

The devices made with this batch design are numbered starting from the top left corner and going to the bottom right corner. Figure 28 also shows the numbering. During the galinstan spraying process, the batch has been placed with the top side of the batch, as shown in figure 28, at the rear of the spray coater. Furthermore, the devices will be named starting with a 'B' followed by a number that indicates the batch number which will be followed by an 'S' and the sample number (e.g. B1S1 indicates that the device was made in the first batch on position 1 of the batch). By using this naming system, the possible influence of the position of the device during the production process can be taken into account when measuring the lifetime.

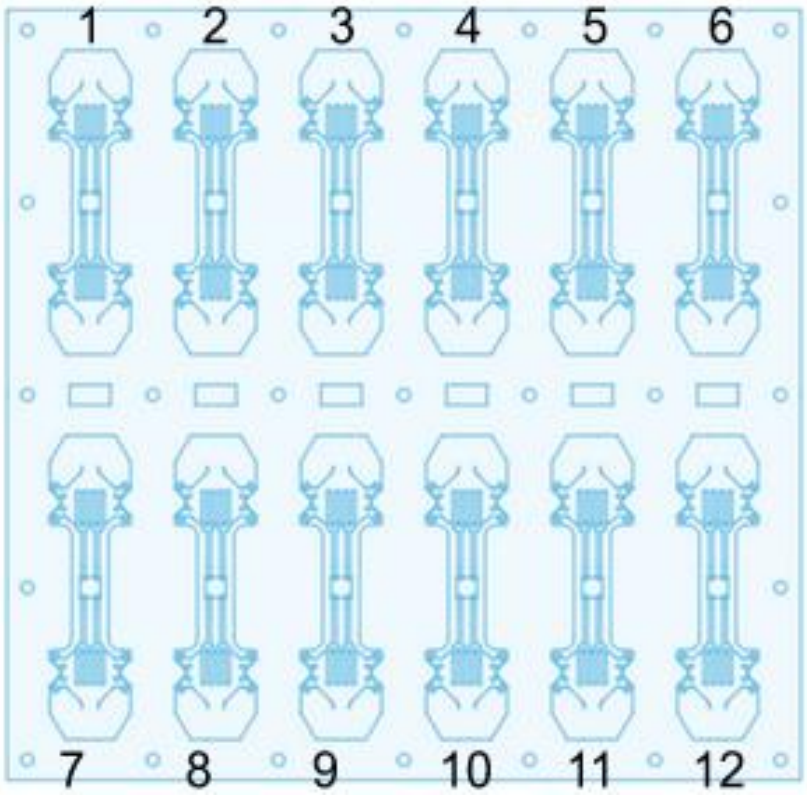

Figure 28: Stretchable LED strip batch design

3.3.2 Stretchable wire design

In accordance with the logic of the stretchable LED strip batch design, devices of the stretchable wire batch design will be numbered from the top left to the bottom right. Positioning under the galistan spraying mechanism was similar to that described in paragraph 3.3.1 as well. Figure 29 shows the batch design with design aspects: the device shape that determines the shape of the mold, the liquid metal tracks which determine the shape of the stencil, and the outlining of the position the flexconnector will have within the devices, necessary for their aligned placement on the vinyl sheet as described in Chapter 4, 'Production Process'.

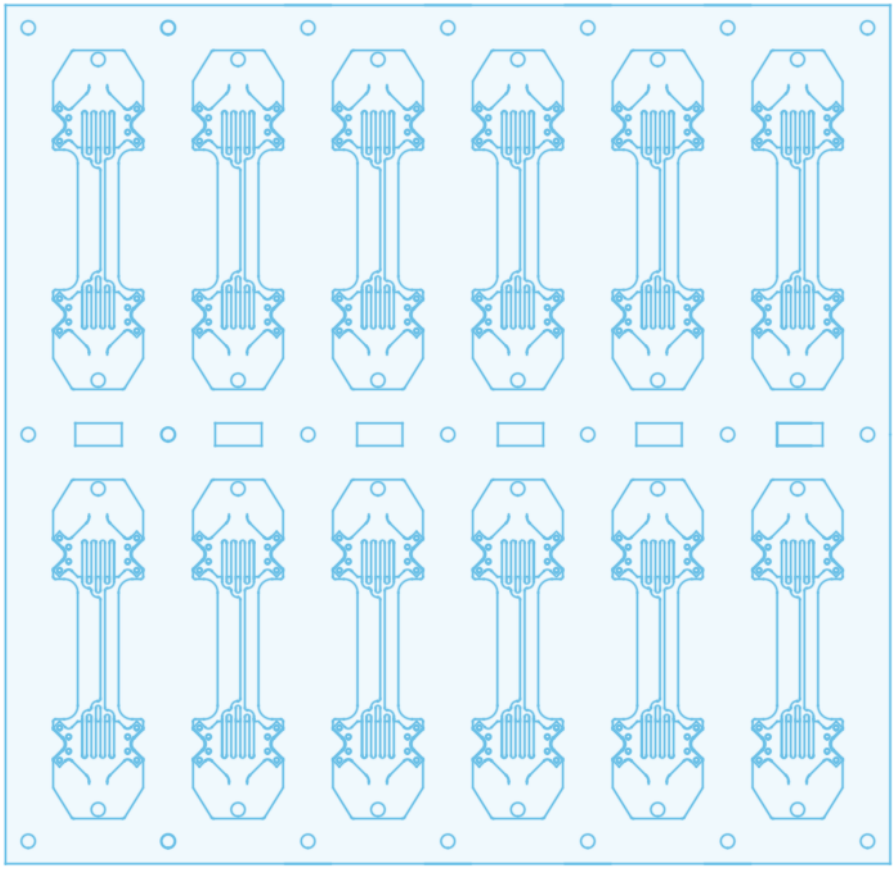

Figure 29: Stretchable wire batch design

4 Production Process

This chapter will describe the production process of the devices. A step-by-step description of the production process is included in Appendix A.

4.1 Materials

The following equipment and materials are needed to produce the stretchable devices:

Plexi sheet The plexi sheets will be used to laser cut the molds out of. The plexi sheets used will have a height of 1.5 mm, 2 mm and 3 mm.

Vinyl The vinyl will be engraved by the laser cutter. Furthermore, the sticky side of the vinyl will be placed upwards and will keep the placed components in their correct position.

Trotec Speedy100R This laser cutter has a 30 W CO_2 laser [29]. It was used to laser cut the molds and base plate from the plexi sheets. Furthermore, it was used to engrave the vinyl with the outlines of the components. Figure 30 shows the laser cutter.

Figure 30: Trotec Speedy 100R laser cutter

Oven An oven is needed to needed to dry the prewetted flexconnectors and other components.

Primer The primer is used in order to improve the adhesion between the silicone and the rigid components. It will be sprayed on the rigid components under a fume hood. Figure 31 shows a bottle with primer that can be attached to an airbrush so that it can be sprayed.

Figure 31: Bottle with primer

Dragon Skin The silicone used for the devices is Dragon Skin 10 Fast and Dragon Skin FX-Pro from Smooth-On. This type of silicone is skin safe which makes it suitable for these kinds of devices. Furthermore, it consists of a Part A and a Part B that should be mixed together. Figure 32 shows the silicone used, the yellow bottle contains Part A and the blue bottle contains Part B.

Figure 32: Dragon Skin silicone

DAC 150 SP This speedmixer is used to mix the two parts (Part A and Part B) in order to create the Dragon Skin 10 silicone. Figure 33 shows the speedmixer.

Figure 33: DAC 150 SP speedmixer

Galinstan The liquid metal used to make the traces in the devices is an alloy composed of gallium, tin, and indium called galinstan.

Syringe pump and spray coater Both the syringe pump and the spray coater were developed in earlier research at imo-imomec. The syringe is filled with liquid metal which will be provided to the spray coater. The menu on the screen of the syringe pump allows for the setting of some settings. The spray coater is a converted Tronxy X5SA 3D-printer. The spray coater has a special nozzle to spray the liquid metal. Furthermore, the spray coater is connected to the N_2 gas supply from the fume hood. Figure 34 shows the syringe pump connected to the spray coater. G-code is used to program the path that the nozzle will follow. The used G-code can be found in Appendix B.

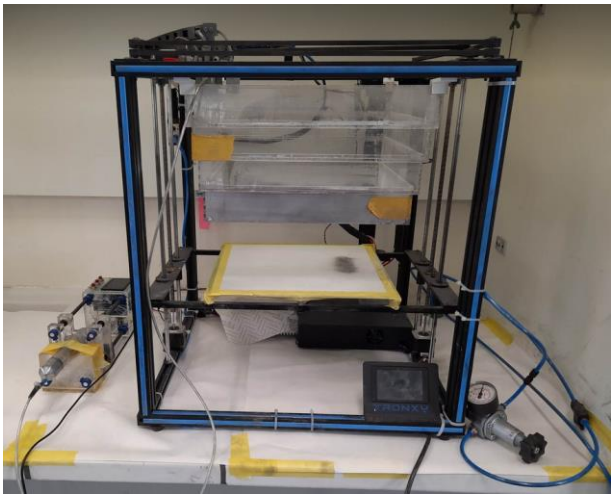

Figure 34: Syringe pump and spray coater

Stencil The metal stencils contain the outlines of the galinstan traces.

WS2812B Digitale 5050 RGB LED This LED has flat contacts which are ideal to integrate with the liquid metal traces. Figure 35 shows the top and bottom view of this type of LED. Furthermore, the flat and small size of the LED makes it ideal to integrate in the stretchable devices. The WS2812B LED can easily be powered by 5V. Furthermore, libraries exist to control these LEDs with an Arduino [28].

Figure 35: WS2812B LED [28]

4.2 Method

The production process can be split up in eight main steps. Each step will be discussed in this chapter. The method described in this chapter will be the method used to produce the stretchable LED strips. The method for producing the stretchable wire devices is similar with the exception of the steps involving the LED component.

4.2.1 Designing and production of the molds

The first step of the production process is to design the devices and molds in a software program. A suitable program to design the molds and devices is Fusion 360. Other programs with the same functionality can also be used. The made design can then be exported into Inkscape software in order to remove possible double lines. Hereafter, the designed molds and the base plate can be cutted out from the plexi sheets with the laser cutter. The removal of double lines is important when using the laser cutter. The laser in the laser cutter during the engraving phase has the suitable power and speed configuration so that the vinyl will only be engraved and not cutted. Double lines will force the laser to engrave one line multiple times which will result in a cut instead of an engraving.

4.2.2 Engraving

The next step is the engraving step. In this step, the vinyl must be taped to the base plate with the sticky side upwards as can be seen in figure 36. Hereafter, the base plate with the vinyl must be placed in the laser cutter and be engraved with the outlines of the components and the flexconnectors. Figure 36.b shows the base plate with the vinyl taped to it in the laser cutter.

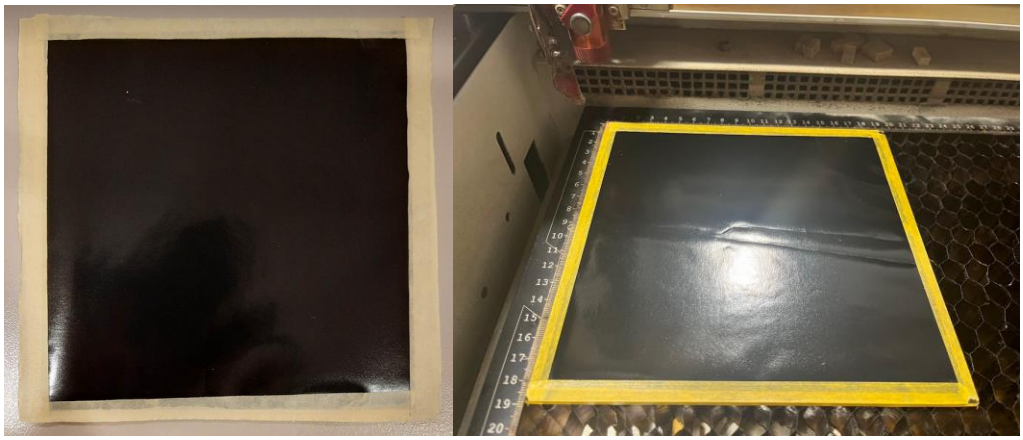

Figure 36.a: Vinyl taped to the base plate, Figure 36.b: base plate with the vinyl in the laser

.

4.2.3 Prewetting

To achieve optimal adhesion between the liquid metal and the components, a prewetting procedure needs to be conducted. During this step, a thin layer of liquid metal will be deposited on the contacts of all components and will be put in an oven set to 60°C. The components will stay in the oven to dry for a minimum of 10 minutes. Figure 37 and 38 shows a flexconnector respectively before and after the prewetting process. The brown-coloured copper contacts, visible on figure 37, will be covered with a thin layer of silver coloured liquid metal which can be seen on figure 38. The prewetting process should be performed within a fume hood.

Figure 37: Flexconnector before the prewetting process

Figure 38: Flexconnector after the prewetting process

4.2.4 Primer spraying

The fourth step is to spray primer on all the components. The primer must be sprayed on the opposite side of the side with the contacts to prevent interference with them. The purpose of the primer is to increase the adhesion between the components and the silicone. The procedure must be performed within a fume hood. The flexconnectors can be taped to a sheet of paper as can be seen in Figure 39, the LEDs can be placed in a container to prevent them from flying away when sprayed on as can be seen in Figure 40. To spray the primer, the bottle with the primer can be attached to an airbrush. Move slowly from left to right and from right to left over the connectors and LEDs to spray the primer.

Figure 39: Flexconnectors positioned to apply primer

Figure 40: LEDs positioned to apply primer

4.2.5 Placement of the components

The next step is to place the components on the engraved vinyl. The components should be placed exactly within the engraved outlines to make sure that the components and the liquid metal traces will be properly aligned. Misalignment can result in failed devices.

4.2.6 Silicone pouring (first layer)

The following step is to place the top mold and to pour the silicone in the mold. Figure 41 shows the top mold placed on the base plate with the components placed on the vinyl. Dragon Skin silicone consists of two liquids, liquid A and B, that need to be combined. The ratio of liquid A and B should be 1:1 and should be mixed with the speed mixer. Hereafter, the silicone can be poured on the mold. The excess of silicone on the mold must be scraped off slowly in order to get a smooth and flat silicone layer. When the silicone will be scraped too fast, it will pull away more silicone than intended creating devices that are thinner than intended. Finally, the silicone must cure.

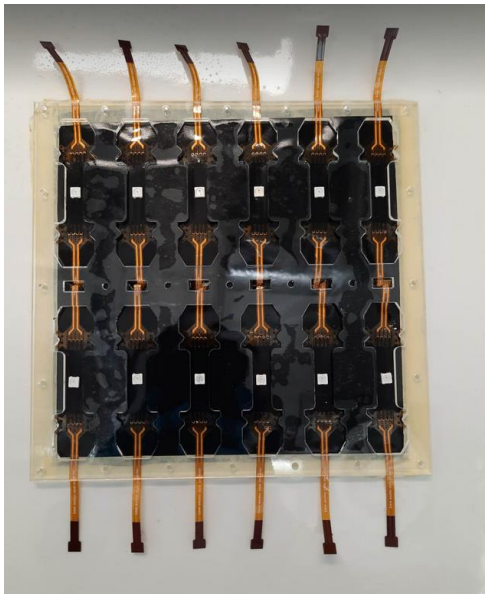

Figure 41: Top mold placed on the base plate

4.2.7 Liquid metal spraying

After the silicone is cured, the bottom plate must be removed and the vinyl must be carefully ripped off. This will expose the contacts of the components. The next step is to place the stencil on the devices. Now, only the outlines of the liquid metal traces on the silicone are visible. After attaching the stencil with tape or screws, the topmold with the stencil can be placed on the platform of the spray coater. The code in the spray coater can be executed without spraying the liquid metal to confirm the correct position. Once the correct position has been achieved the N_2 gas supply can be set to 3.5 bar, the syringe pump can be activated and the code can be executed by the spray coater to spray the liquid metal. Figure 42 shows the sprayed devices. Hereafter, the stencil can be removed and cleaned to remove the liquid metal.

Figure 42: Sprayed devices

4.2.8 Silicone pouring (second layer)

Finally, the second layer of silicone must be poured. First, the bottom mold should be attached to the top mold. Next, the preferred amount of silicone should be made by mixing liquid A and B. After mixing, the silicone can be poured on the mold and the excess of silicone can be scraped off again. When the silicone has cured, the devices can be removed from the molds and the excess of silicone can be cut off from the devices.

5 Environmental testing

5.1 Damp heat testing

The damp heat test used in this research is a constant damp heat test. The temperature will be set to 85°C and the relative humidity level to 85%. Both the temperature and the humidity level will stay constant during the test. In order to execute the damp heat test a Weiss SB 22/160/80 climate chamber was used for the first four batches. The devices from the fifth batch used an Espec ESL-2CW climate chamber to execute the damp heat test. The usage of the two different climate chambers does not have a significant impact on the damp heat test itself due to the similar characteristics of the two climate chambers. The Weiss climate chamber has a temperature range of -40°C to 180°C and a relative humidity range of 10% to 98%. The Espec climate chamber has a temperature range of -35°C to 150°C and also a relative humidity range of 10% to 98%. The test chamber itself of the Weiss climate chamber has a dimension of 67.0 cm x 54.0 cm x 39.0 cm. The test chamber of the Espec climate chamber has a dimension of 50.8 cm x 60.96 cm x 76.2 cm. The fan at the back of the climate chambers ensures an equal temperature and relative humidity level across the chamber. Therefore, the position of the devices inside the chamber does not influence the results. The damp heat test will run for approximately three weeks for the stretchable LED strips and four weeks for the stretchable wire devices. Because both climate chambers are set to the constant temperature and relative humidity level constantly, the three and four weeks can only be approximated. Every week, the devices will be taken out of the climate chamber to be tested. These tests include four wire resistance measurements for the stretchable wire devices and current measurements and a visual inspection of the functionality of the LED for the stretchable LED strips. After these tests, the devices will be placed back in the climate chamber to continue the damp heat test. Figure 43 shows devices placed in the Weiss SB 22/160/80 climate chamber.

Figure 43: Devices placed in the Weiss SB 22/160/80 climate chamber

5.1.1 Approach stretchable LED strips

In comparison to the stretchable wire devices, the stretchable LED strips were exposed for three weeks instead of four weeks. This adjustment was made due to time constraints resulting from the need to produce additional batches due to the high failure rate observed in the first two batches.. The devices from batch 1, 2, and 3 were exposed for 166 hours in the first week, 184 hours during the second week, and 164 hours during the third week. This adds up to a total exposure time of 514 hours or 21.42 days. The devices from batch 4 were exposed for 184 hours during the first week, 164 hours during the second week, and 163 hours during the third week. This adds up to a total exposure time of 511 hours or 21.29 days. The devices of the fifth batch were exposed for 166 hours during the first week, 148 hours during the second week, and 167 hours during the third week. This adds up to a total exposure time of 481 hours or 20.04 days.

5.1.2 Approach stretchable wires

All stretchable wire devices were exposed for 166 hours during the first week, 184 hours during the second week, 164 hours during the third week, and 163 hours during the fourth week. This adds up to a total exposure time of 677 hours or 28.21 days.

5.2 QUV All Weathering testing

For exposing the devices to UV radiation, the QUV Accelerated Weathering Tester from manufacturer Q-LAB (shown in Figure 44) was used. Intrinsically, this weathering tester not only exposes experimental specimens to UV light, but to heat and humidity as well. This defines the QUV test as an instrument for testing the resistance of specimens to a combination of multiple stress factors.

Figure 44: QUV all weathering tester

Within the QUV tester, the stretchable devices were mounted near vertically on a metal plate, using metal tape, as seen on Figure 45. Metal tape was used as it had proven resilient to losing its adhesive properties due to heat and humidity during previous testing in the scope of research at the Materials and Packaging Research and Material (MPR&S) research group.

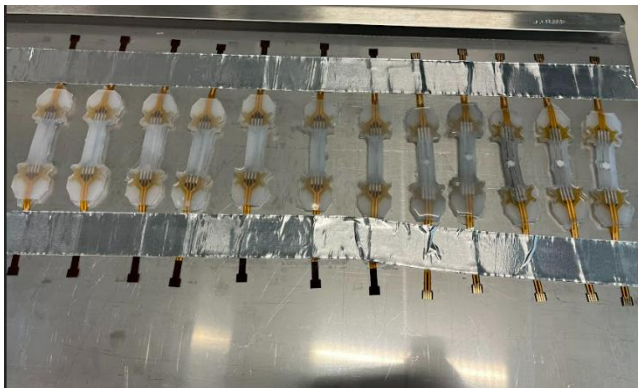

Figure 45: Devices as attached in the QUV chamber using metal tape

The QUV testing conditions can be altered depending on the needs of specific experiments. Factors such as dry exposure, condensation exposure, and UV exposure can be set. In the scope of this research, the ISO 4892-3 normwas used. Table 1 shows different methods, as defined by the ISO 4892-3 norm, that are frequently used by the MPR&S research group.

5.2.1 Approach stretchable LED strips

The devices subjected to the QUV test were tested for 504 hours in total which is equivalent to three weeks. After every week of testing, the devices were taken out of the QUV tester to perform current measurements on and to evaluate the functionality. After this, the devices were placed back into the QUV tester.

5.2.2 Approach stretchable wires

In total, seven stretchable wire devices were exposed to environmental stress factors using the QUV tester: batch 1 device 2 and 4, and batch 2 device 2, 4, 6, 8 and 10. These devices were all exposed for 672 hours, which translates to 4 weeks. Every week the devices were taken out for approximately 2 hours, for observations and to be tested on their functionality.

6 Stretch testing

6.1 Objective

During stretch testing of the devices, different stages of degradation will presumably arise. Degradation monitoring was realized through measurements and visual inspection. Both in-situ and ex-situ measurements and inspections will be performed during the span of the stretch strain experiments. The visual inspections will consist of photographs taken during the tests and between tests, and high-magnification images taken between tests.
Using the in-situ photographs, different stages of degradation could be monitored by visually confirming the functionality of the device or demonstrating the emergence of ruptures in the materials. The ex-situ high-magnification images could more accurately shed light on degradation mechanisms by demonstrating the physical nuances in the devices at certain intervals after a number of cycles.

6.2 Setup

6.2.1 Cycletesters

The cycleters used to stretch the devices were previously designed at imo-imomec. Figure 46 shows a cycletester. All cycletesters are controlled by an Arduino Mega, attached within its frame. This arduino Mega is connected to a driver which controls a stepper motor used for driving the mechanism that stretches the devices.

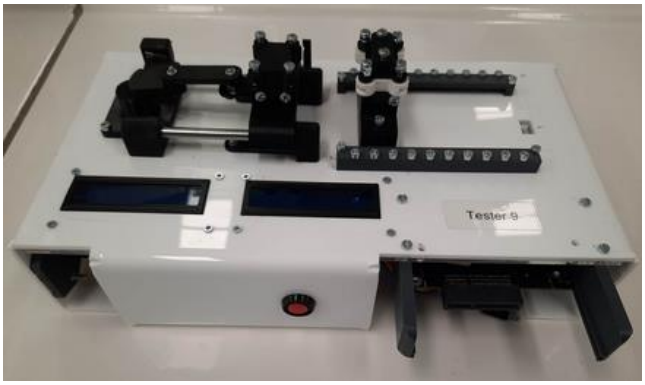

Figure 46: Cycletester

6.2.2 Camera

The camera used in the setup is a Nedis USB webcam. This webcam can be connected to the computer with a USB cable and can be used in the Labview program via the Vision Acquisition function.

6.2.3 Multimeter

The HP 33401A digital multimeter (Figure 47) is used to execute the resistance and current measurements. This digital multimeter has been chosen because of its possibility to take accurate current measurements as well as four wire measurements. Furthermore, it has the ability to be connected to a PC. These abilities make it suitable to use for this setup.

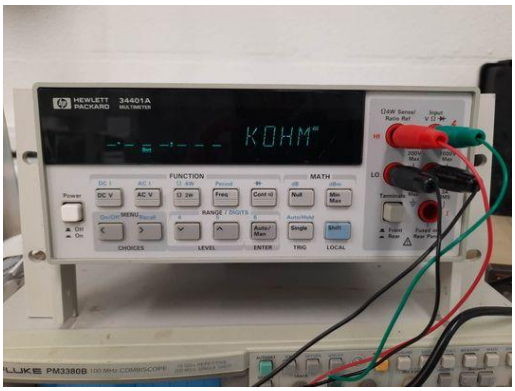

Figure 47: HP 34401A multimeter

6.2.4 PC (control unit)

A PC is used to run the Labview program. The PC is connected via USB to the multimeter, multiplexer, the four cycletesters' Arduinos, and the USB webcam. Furthermore, to test the stretchable LED strips, the PC is also connected to a separate Arduino Uno that will control the LEDs. This means that seven or eighth USB ports, depending on the device, are needed for this setup.

6.2.5 Power supply

A PC power supply from the manufacturer Ewent is used to power the cycletesters. At 12 V, the power supply can deliver 30 A, which is more than sufficient for the cycletesters. Figure 48 shows the power supply used in the setup. It was modified to hold 2 bolts which are used to mount it on the bottom of the cycletester setup.

Figure 48: Ewent power supply

6.2.6 Multiplexer

A multiplexer is used to acquire measurements from multiple devices using a single multimeter.

6.2.7 Microscope

An Andonstar microscope is used to make high-magnified images of the traces of the devices. Figure 49 shows the Andonstar microscope. To make the images, an LED hand lamp is used to light up the back of the devices in order to increase the contrast and thus the visibility of the traces. The microscope images were all taken as ex-situ observations, for taking an image devices had to be taken out of the cycletester setup.

Figure 49: Andonstar microscope

6.2.8 Full cycletester setup

Figure 50 shows the full cycletester setup. The camera is situated in the middle above the cycletesters so that all four cycletesters can be photographed at the same time. The cycle testers are kept in place with corner joints. The power supply and the multiplexer are not visible on the image, as they are mounted on the bottom of the MDF plate on which the cycletesters are mounted.

Figure 50: Full cycletester setup

6.3 Test Approaches

6.3.1 Approach stretchable LED strip

The stretch test for the stretchable LED strips followed the following approach. Before the cycle testers can start running, some steps need to be completed. First, the LEDs in the devices need to be turned on. The accompanying Arduino code can be found in Appendix C. This code will be uploaded to a separate Arduino Uno. Next, the Arduino Megas controlling the cycle testers needed to be programmed. This program can be found in Appendix D.

This code controls the stepper motor of the cycletester and interacts with the Labview program. The code will receive the number of steps that need to be performed from the Labview program. The Arduino code divides this number by the number of steps the stepper motor required to perform a 50% cycle. This will result in the number of cycles that needs to be executed. Each cycle consists of activating the stepper motor to execute a 50% stretch and returning to its original position. When all the requested cycles are completed, the code sends the message "FIN\r\n" back to the Labview program via the serial port, indicating the test's conclusion.

The Labview code can be found in Appendix E. Figure E.1 shows the front panel of the Cycletester_synchronous.vi. This front panel contains multiple settings that need to be set before the test can start. In the "DMM port" input the USB port of the digital multimeter needs to be selected. Furthermore, the USB port of the connected multiplexer and the USB port of every connected cycletester must be selected. Next, the number of cycles between each measurement, the number of cycles between taking images, and the total numbers of cycles need to be entered. Finally, the type of measurement and the file path to the file where the measurements will be stored must be selected. The auto range must stay enabled.

The current is measured every cycle both stretched and unstretched. The images will be taken every 10 cycles. This will also be done both stretched and unstretched. After 100 cycles the test will be stopped for the first time and the devices will be taken out of the device holders. Hereafter, the high-magnification images will be taken from the devices' traces. Next, the devices will be placed back onto the cycletesters and the stretch tests will continue until the devices are stretched for 500 cycles in total. This will again be followed by the removal of the devices from the cycletesters and the subsequential taking of the high-magnification images. From now on, the devices will be tested for 500 cycles after which the high-magnification images will be taken. This will be repeated until the devices fail permanently.

After the devices have failed working. Some of the devices will be subjected to a 150% stretch test in order to investigate the influence of the damp heat and QUV test on the lifetime of the silicone. During these tests the current will not be measured. However, every 15 cycles, an image will be taken to allow for an accurate determination of the lifetime of the silicone.

6.3.2 Approach stretchable wire

The stretchable wire devices were tested according to a different strategy. They were to be stretch tested until they no longer function, while performing both in- and ex-situ measurements and observations. In situ measurements and observations consisted of resistance measurements of the relaxed and stretched state, and of images taken by the camera mounted above the cycletester setup. The ex situ measurements

and observations consisted of static stretch tests (as described in paragraph 7.2.4) and high zoom images with backlighting taken with an andonstar digital microscope.

Inevitably, the ex situ measurements interfered with the in situ measurements, as the device would have to be taken out of the clamps of the cycletester and put back in each time. Thus, the ex situ measurements and observations were limited to a minimal amount. They were done at logarithmic intervals at: 100, 500, 1000, 5000 and 10000 stretch cycles. Not all devices retained functionality for 10000 cycles, thus those devices had no measurements and observations performed after their point of failure.

During stretch testing, the frequency of images taken was minimized as well. This is due to the influence of the time it takes to take and save an image on the measurements. When there are no images taken, the cycletesters run continuously, stopping only one at a time, to take relatively short measurements. When one cycletester is stopped, the others always keep running due to precision timing of the process as a whole. However, when an image is taken, the timing no longer functions, as an image necessitates the standstill of a device for over 10 seconds. This standstill distorts the timed process, and since static stretch tests pointed out that the standstill of a device affects its resistance in time (paragraph 7.2.4), the measurements taken after a standstill cannot be compared with those taken directly at the moment of stretching or relaxing. Therefore, the images were only taken every 100 cycles, to limit the number of measurements that would be affected. The results in paragraph 7.2.5 confirm the existence of deviating values around every multiple of 100 cycles where an image was taken.

The in situ resistance measurements were performed every 5 cycles for the first 1000 cycles, and every 10 cycles after that point.

7 Results

7.1 Stretchable LED strip results

7.1.1 Production results

Tables 2, 3, 4, 5, and 6 show the results of the batch production of the stretchable LED strips. The devices from batch 1 and 2 were manufactured with the Dragon Skin FX-Pro silicone and with a galinstan spray rate of 0.7 ml/mm. The devices from batch 3 were mistakenly produced with Dragon Skinn Ecoflex silicone and with a galinstan spray rate of 1.2 ml/mm. Furthermore, the devices from batch 4 and 5 were made with the Dragon Skin 10 Fast silicone and with a galinstan spray rate of 1.2 ml/mm. Only ten devices were produced in batch 5. The first column of each table illustrates the name of the device, the second column shows if the LED functioned after production, and the last column shows a description of possible flaws in the silicone. All these devices were produced following the batch production process. Note that the devices from the third batch all have thinner silicone layers than the expected height.

Table 2: Production results for batch 1

Device	Functional	Anomalies
B1S1	Yes	air bubble next to the LED
B1S2	No	air bubble next to the LED
B1S3	No	air bubble next to the LED
B1S4	No	air bubble next to the LED
B1S5	No	air bubble next to the LED
B1S6	Yes	air bubble next to the LED
B1S7	Yes	
B1S8	No	
B1S9	No	
B1S10	No	air bubble next to the LED
B1S11	No	LED sticks partially out of the silicone
B1S12	Yes	

Table 3: Production results for batch 2

Device	Functional	Anomalies
B2S1	No	air bubble next to the LED
B2S2	Yes	air bubble next to the LED
B2S3	Yes	air bubble next to the LED
B2S4	Yes	air bubble next to the LED
B2S5	No	
B2S6	No	air bubble next to the LED
B2S7	No	
B2S8	Yes	
B2S9	No	
B2S10	No	
B2S11	No	
B2S12	No	

Table 4: Production results for batch 3

Device	Functional	Anomalies
B3S1	No	thin layer of silicone
B3S2	No	thin layer of silicone
B3S3	No	thin layer of silicone
B3S4	Yes	thin layer of silicone
B3S5	Yes	thin layer of silicone
B3S6	Yes	thin layer of silicone
B3S7	Yes	thin layer of silicone
B3S8	Yes	thin layer of silicone
B3S9	Yes	thin layer of silicone
B3S10	Yes	thin layer of silicone
B3S11	No	thin layer of silicone
B3S12	Yes	thin layer of silicone

Table 5: Production results for batch 4

Device	Functional	Anomalies
B4S1	Yes	
B4S2	Yes	
B4S3	Yes	
B4S4	Yes	
B4S5	Yes	air bubble next to the LED
B4S6	Yes	air bubble next to the LED
B4S7	Yes	
B4S8	No	
B4S9	Yes	
B4S10	Yes	
B4S11	Yes	
B4S12	No	

Table 6: Production results for batch 5

Device	Functional	Anomalies
B5S1	Yes	
B5S2	No	air bubble next to the LED
B5S3	/	/
B5S4	Yes	air bubble next to the LED
B5S5	No	air bubble next to the LED
B5S6	Yes	air bubble next to the LED
B5S7	Yes	
B5S8	Yes	

B5S9	/	/
B5S10	No	
B5S11	Yes	
B5S12	Yes	

Table 7 shows the division of the devices over the different tests. The division is made based on the state of the silicone and the measured current after production. By dividing it in this way, it can be ensured that the high-quality devices of each batch are divided between the tests. This will ensure that all tests have high-quality devices. The devices from batch one are divided between the QUV test followed by the stretch test and only the stretch test. The devices from batch two are divided between the damp heat test followed by the stretch test and only the stretch test. These two divisions were made because only four devices from each batch functioned. As a result, dividing these devices over the tree tests will result in measurements that are less reliable since they can not be verified by measurements from devices from the same batch.

Table 7: Division of the produced devices over the different tests

Only stretch test	**Damp heat followed by stretch test**	**QUV test followed by stretch test**
B1S7	B2S3	B1S1
B1S12	B2S8	B1S6
B2S2	B3S5	B3S6
B2S4	B3S9	B3S8
B3S4	B3S12	B3S10
B3S7	B4S3	B4S1
B4S2	B4S7	B4S4
B4S5	B4S11	B4S10
B4S6	B5S1	B5S6
B4S9	B5S7	B5S11
B5S4		
B5S8		
B5S12		

The devices that are not going to be subjected to the QUV test or damp heat test will stay in the lab at imo-imomec during the three weeks when the two environmental tests are running. The lab has an average temperature of 20°C to 21°C.

During the first three weeks after the production, current measurements were taken to investigate the change in current. Figure 51 shows the measured current after every week of the three unexposed devices of batch five. The graph indicates that there are no significant changes in the current of these devices during these three weeks.

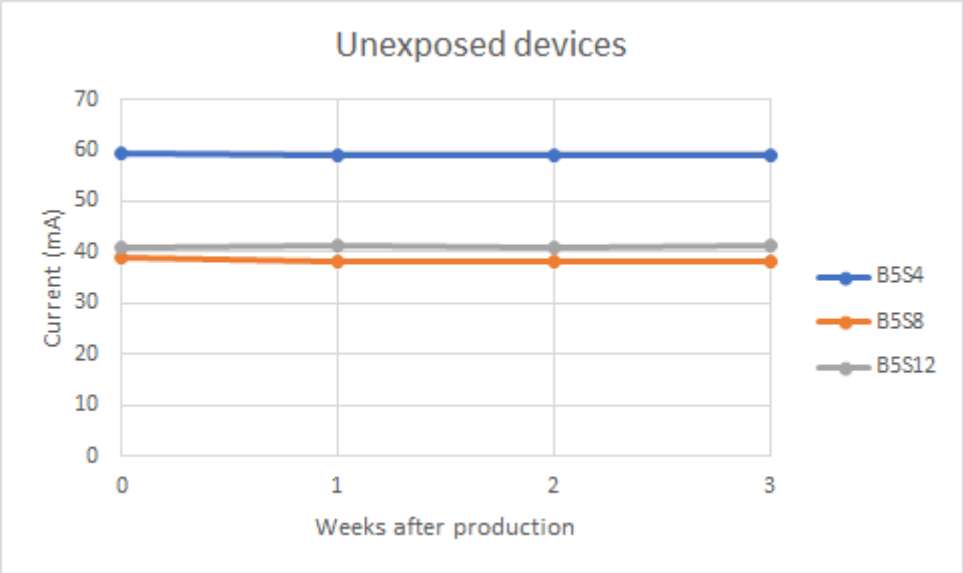

Figure 51: Change in current of B5S4, B5S8, and B5S12

7.1.2 Damp heat test results

Figure 52 shows two devices three weeks after production. The top device has undergone the damp heat test for three weeks, the bottom device has not been used in any environmental test. It can be observed that the silicone of the device has been discolored by the damp heat test. Furthermore, the silicone of that device has also become stiffer. The discoloration and stiffening of the silicone was observed in all the devices that were subjected to the damp heat test.

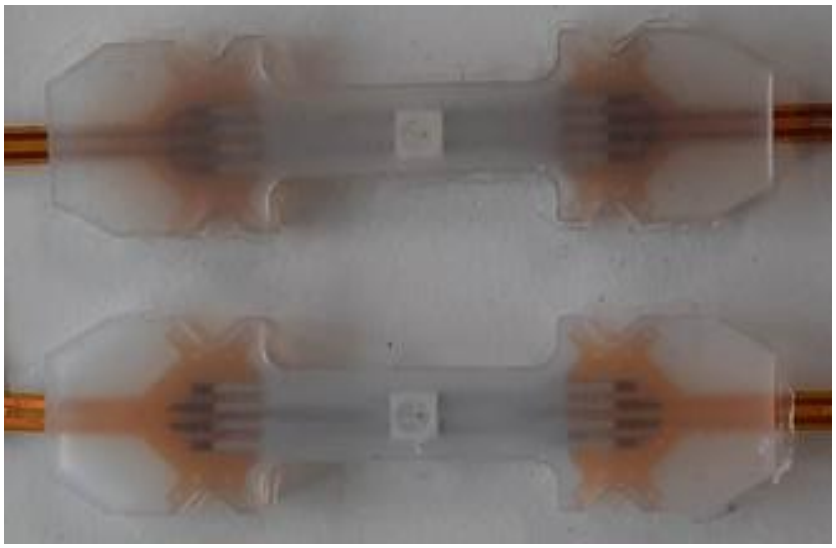

Figure 52: Top device underwent three weeks of damp heat testing; bottom device was not used in an environmental test

To test the influence of the damp heat test on the LEDs, two in silicone encapsulated and two separate LEDs were subjected to the damp heat test. The two encapsulated LEDs were recovered from the silicone after the three weeks of subjection. All four LEDs still functioned and no visual changes to the LEDs themself or to the LEDs characteristics were observed. Figure 53 shows the four LEDs after three weeks of damp heat testing. This means that possible changes in the measured current cannot be attributed to the LEDs.

Figure 53: The four LEDs after three weeks of damp heat testing

After the third week (514 hours) of damp heat testing, the devices from batch two and three stopped functioning. The LED of the devices did not light up anymore. The previously mentioned test indicates that the LEDs themself are not damaged by the damp heat test. As a result, this could indicate that the high temperature and humidity level during the damp heat test increased the moisture ingress of the devices. This increased moisture ingress caused the galinstan traces to oxidate. The oxide layer could have decreased the adhesion between the galinstan and the copper LED contacts. However, more research is needed to investigate this hypothesis.

The current measurements taken during the damp heat test are shown in figure 54 . The devices tested are B5S1 and B5S7. B5S1 failed to work after three weeks of damp heat testing. Furthermore, the measured current through B5S7 lowered significantly between the second and third week. This indicates that the increased temperature and humidity level the devices encountered during the damp heat test influences the contact points between the LEDs and the traces and the traces themself.

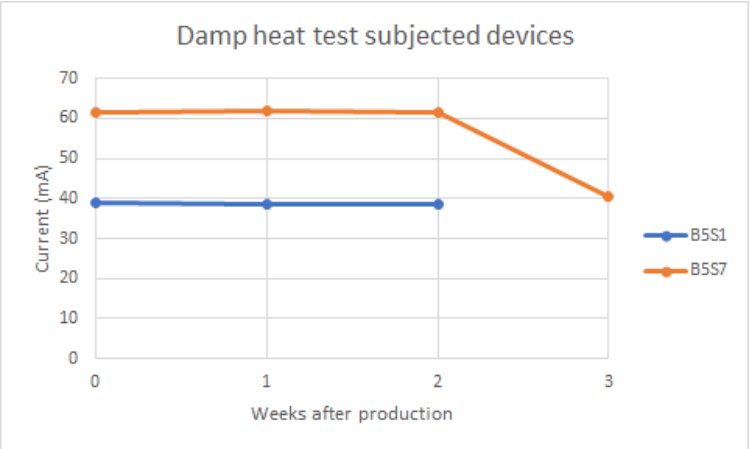

Figure 54: Change in current of B5S1 and B5S7 during the damp heat test

7.1.3 QUV test results

Similar to the damp heat subjected devices, the QUV subjected devices show a yellowish discoloration of the silicone.
To investigate the influence of the QUV test on the LEDs, two LEDs encapsulated in silicone and two separate LEDs were subjected to the QUV test. The two encapsulated LEDs were recovered from the silicone after the three weeks of subjection. Furthermore, all four LEDs still functioned and no visual changes to the LEDs themself or to the LEDs characteristics were observed. Figure 55 shows the four LEDs after three weeks of QUV testing.

Figure 55: The four LEDs after three weeks of QUV testing

The results of the current measurements of the devices used for the QUV testing are shown in figure 56. The graph shows that the current of the devices stays constant during the three weeks of QUV testing. The graph shows the results for devices B5S6 and B5S11.

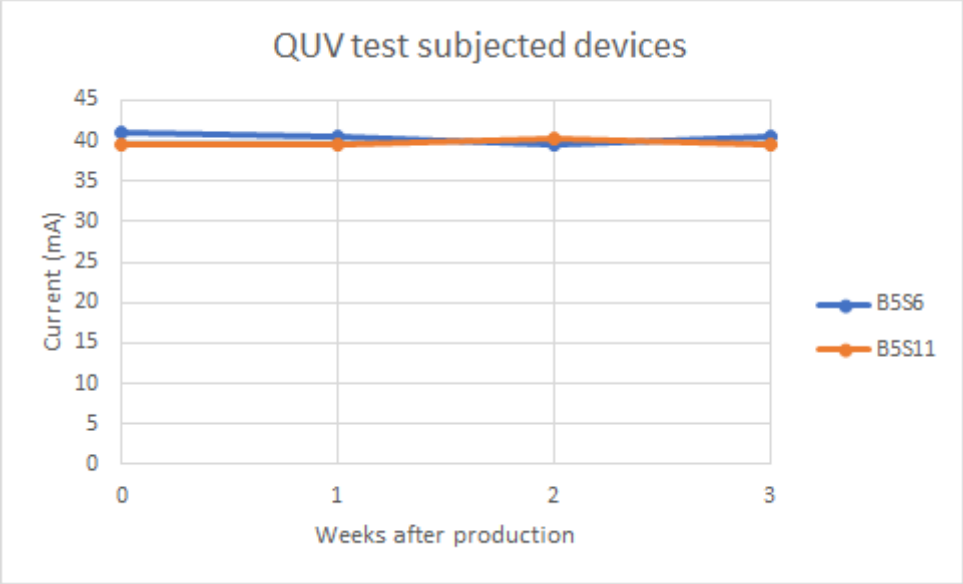

Figure 56: Change in current of B5S4, B5S8, and B5S12 during the damp heat test

7.1.3 Stretch test results

Not exposed to environmental stress factors

The individual graphs from every tested device can be found in Appendix H. Device B4S6 did not function anymore after the three weeks.

Figures 57 and 58 show the stretch test results for devices B2S2, B2S4, and B1S12. However, due to visibility constraints, the results for device B1S7 were not included in these figures. These devices were not subjected to one of the environmental tests. The devices were stretched for 50%.

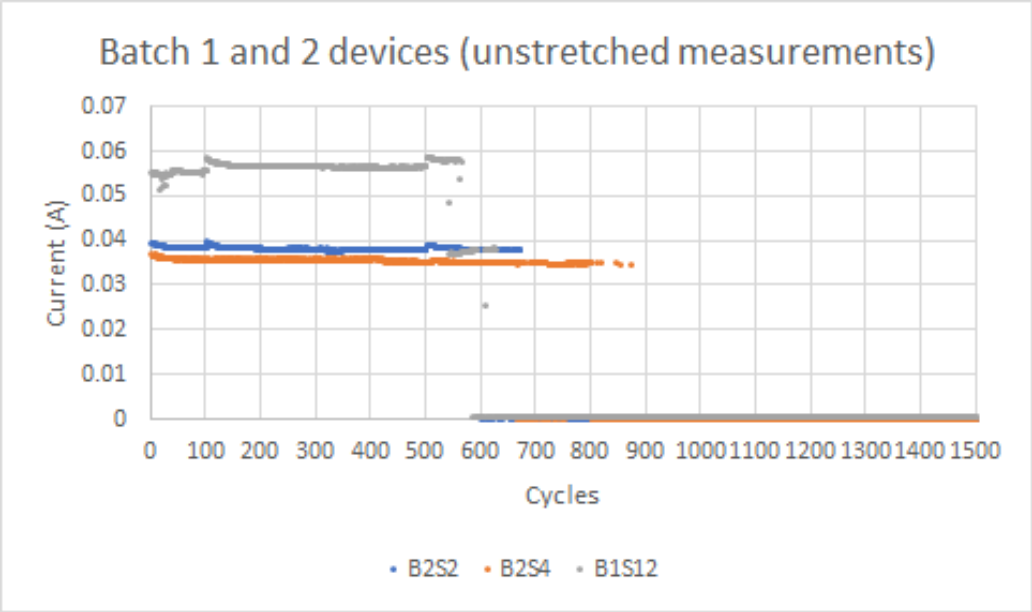

Figure 57: Current (unstretched) in function of the number of cycles for B1S12, B2S2, and B2S4

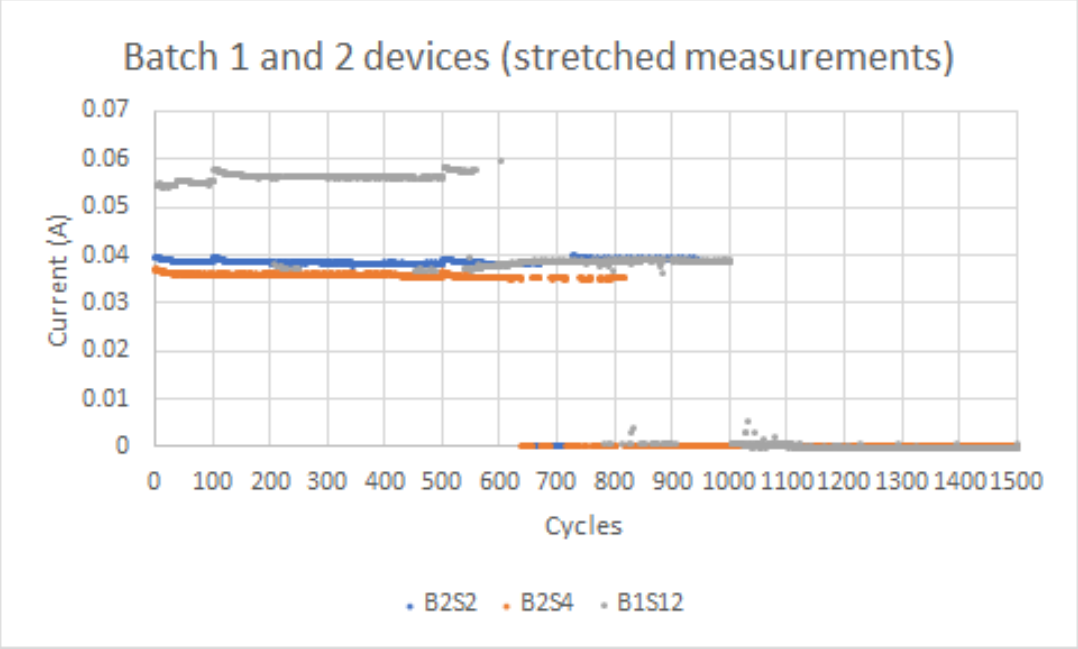

Figure 58: Current (stretched) in function of the number of cycles for, B1S12, B2S2, and B2S4

The results show three distinct phases in the lifetime of the devices. In the first phase, the devices keep functioning permanently. In the second phase of the lifetime, the devices show intermittent failures, followed by recoveries. This behavior illustrates the self-healing capabilities of the devices. Finally, the third phase marks the definite failure of the devices without the possibility of recovering. Furthermore, the graphs from the devices from batch one show two distinct current levels. The LEDs function on both current levels. However, the devices from the other batches do not repeat this behavior, indicating that this behavior can be the result of the production process. In general, the measured current has two levels. The top level is the current when the LED is on, this level is mostly situated around 40 mA. The bottom level is the measured current when the LED is off, this level is 0 mA.

Device B1S7 started to fail when stretched after 126 cycles and when unstretched after 144 cycles. It permanently failed when stretched after 516 cycles and when unstretched after 619 cycles. Device B1S12 experienced its first unstretched failure at cycle 583 and permanent failure at cycle 625. It also failed when stretched for the first time at cycle 778 and permanently after 1006 cycles. Device B2S2 started to fail when unstretched after 600 cycles and permanently failed after 671 cycles. Stretched, it started to fail after 643 cycles and permanently failed at cycle 946. Device B2S4 began to fail when stretched after 639 cycles and permanently failed after 817 cycles. Additionally, it started to fail when unstretched after 666 cycles and permanently failed in the unstretched state at cycle 873.

Figures 59 and 60 show the stretch test results for devices B4S2, B4S5, and B4S9. Figure 61 and 62 illustrates the stretch test results for devices B5S4, B5S8, and B5S12. These devices were not subjected to one of the environmental tests.

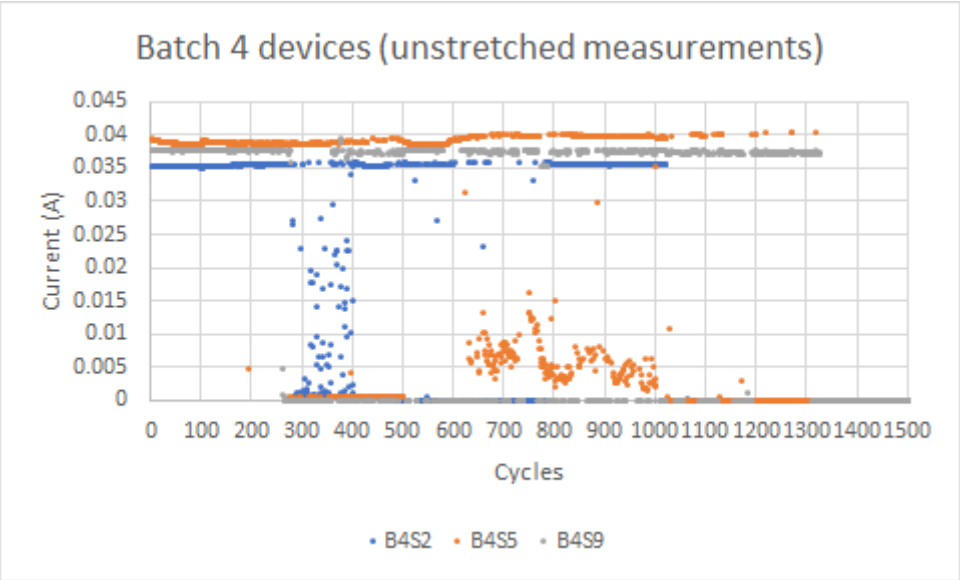

Figure 59: Current (unstretched) in function of the number of cycles for B4S2, B4S5, and B4S9

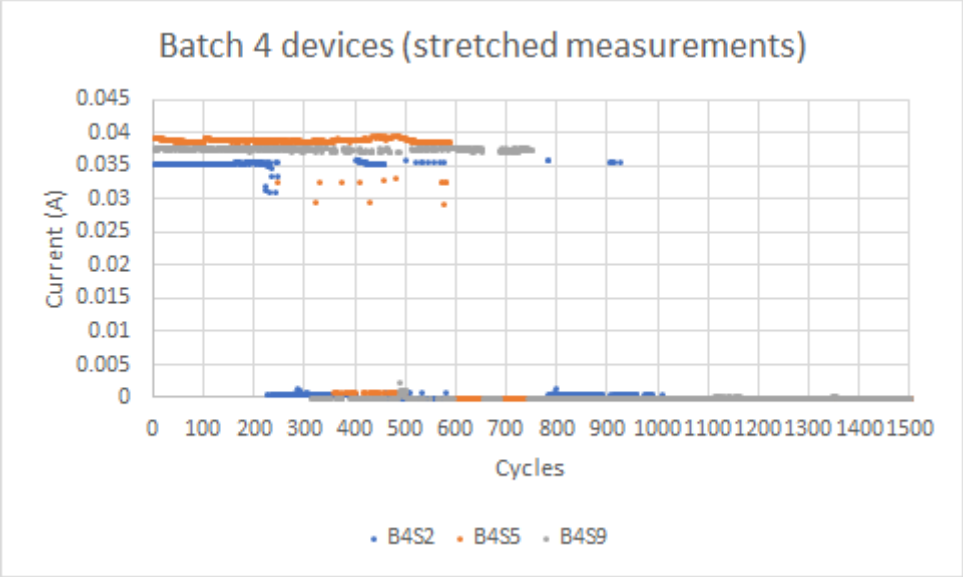

Figure 60: Current (stretched) in function of the number of cycles for B4S2, B4S5, and B4S9

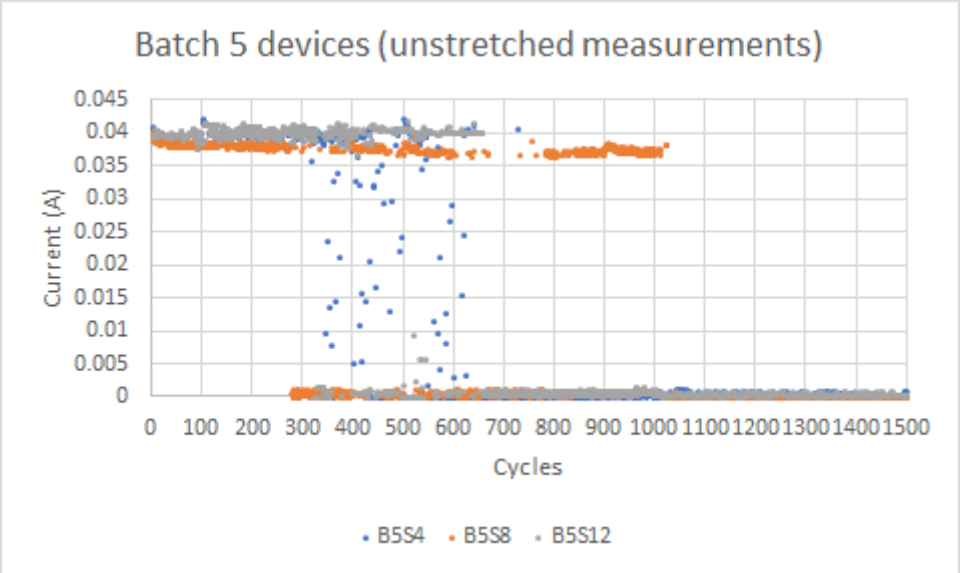

Figure 61: Current (unstretched) in function of the number of cycles for B5S4, B5S8, and B5S12

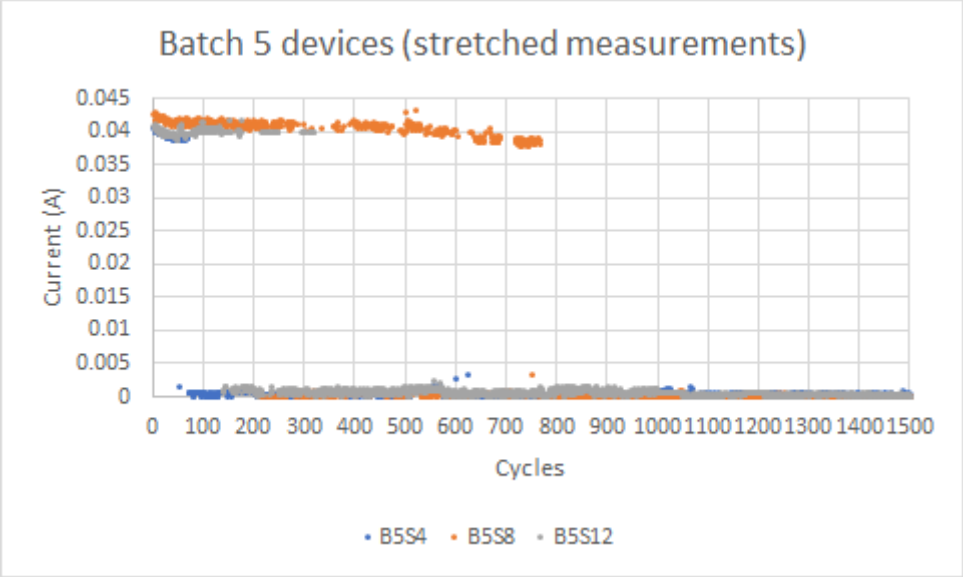

Figure 62: Current (stretched) in function of the number of cycles for B5S4, B5S8, and B5S12

The previously observed three phases in the lifetime of a device can also be observed in the devices made in batch four and five. Furthermore, devices B4S2, B4S5, and B5S4 show current measurements situated between the top and bottom level when being unstretched. This can have been caused by the flowing of the galinstan of the traces. During these intermediate values, the LED will not light up.

Device B4S2 experiences its first failure when stretched after 226 cycles and when unstretched after 281 cycles. Moreover, it permanently fails in the stretched state after 926 cycles and in the unstretched state after 1020 cycles. In the case of device B4S5, the first failure occurs when the device is stretched after 242 cycles and when unstretched after 273 cycles. It permanently fails in the stretched state after 586 cycles and in the unstretched state after 1318 cycles. Device B4S9 starts to fail when stretched after 313 cycles and when unstretched after 260 cycles. The device permanently fails in the stretched state after 751 cycles and in the unstretched state after 1324 cycles. Device B5S4 starts to fail when unstretched after 318 cycles and permanently fails after 726 cycles. Additionally, it fails when stretched after 52 cycles and permanently after 106 cycles. For device B5S8, the first failure occurs in the unstretched state at cycle 281 and permanently at cycle 1020. It fails in the stretched state at cycle 212 and permanently after 765 cycles. Lastly, device B5S12 fails for the first time when unstretched after 319 cycles and permanently fails after 655 cycles. It fails for the first time when stretched after 138 cycles and permanently after 313 cycles.

Figures 63 and 64 show the stretch test results for devices B3S4 and B3S7. These devices were not subjected to one of the environmental tests.

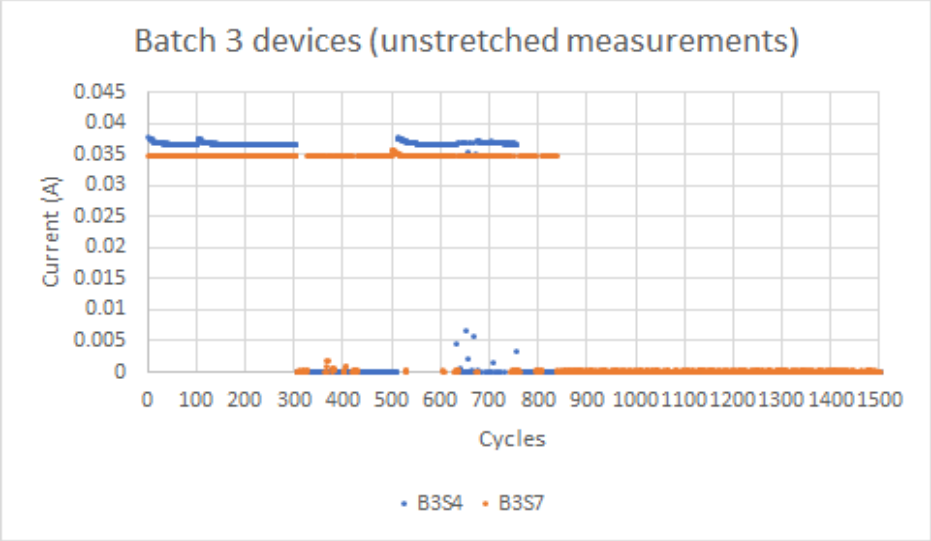

Figure 63: Current (unstretched) in function of the number of cycles for B3S4 and B3S7

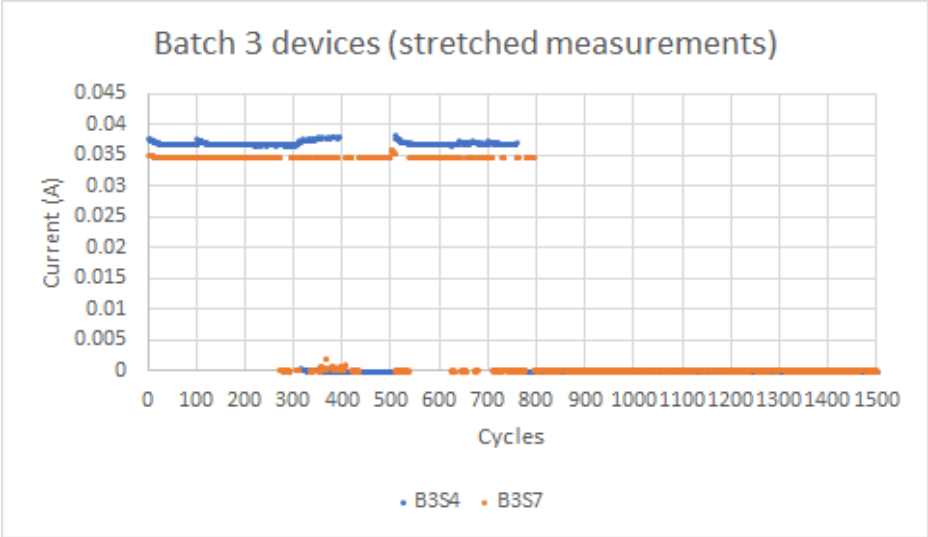

Figure 64: Current (stretched) in function of the number of cycles for B3S4 and B3S7

The same three phases in the lifetime of the devices can also be observed in the devices from batch three.
For device B3S4, the first failure occurs when it is unstretched after 304 cycles, and it permanently fails in the unstretched state after 753 cycles. Additionally, it fails for the first time when stretched after 317 cycles and permanently when stretched after 759 cycles. Device B3S7 fails for the first time when unstretched after 307 cycles, and it permanently fails in the unstretched state after 832 cycles. Furthermore, it fails for the first time when stretched after 273 cycles and permanently when stretched after 793 cycles.

The silicone of device B3S11 has ruptured during the first 100 cycles. Therefore, no graphs have been made for this device. The rupture is the result of the thinner silicone layer which was too thin to withstand the stretching cycles. Figure 65 shows the rupture in the silicone of device B3S11.

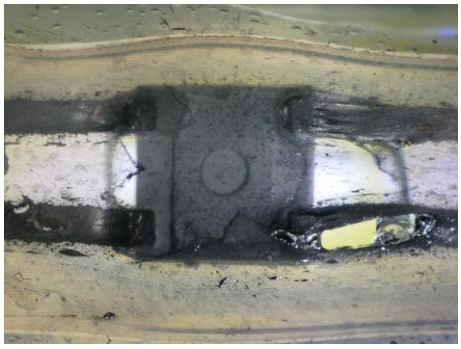

Figure 65: Rupture in the silicone of device B3S11

Figure 66 shows a bar chart that illustrates the average cycles before first and permanent failure of the non-exposed devices. The bar chart shows that the first failure occurs on average on cycle 359 unstretched and cycle 332 stretched. Furthermore, the devices fail permanently unstretched after 865 cycles and stretched after 695 cycles.

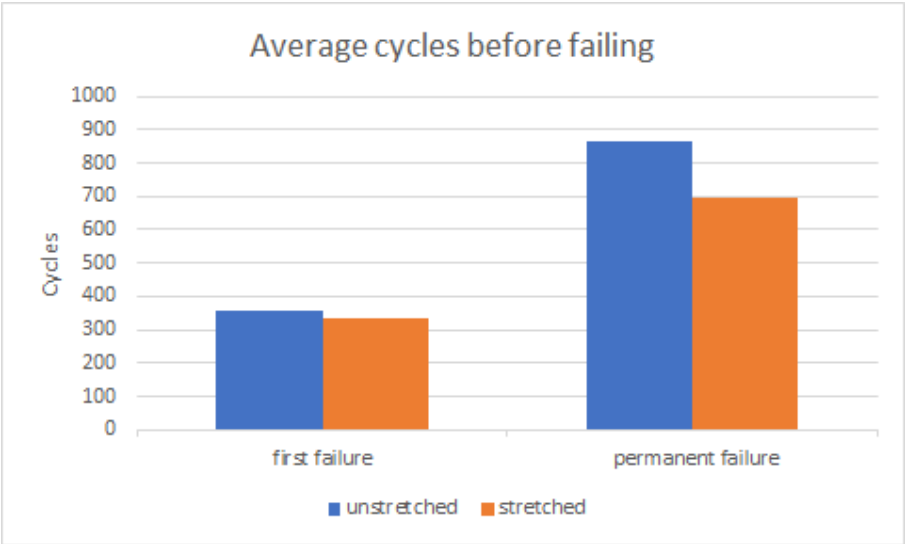

Figure 66: Bar chart depicting the average number of cycles survived by non-exposed devices

Exposed to damp heat

The devices from all batches that were subjected to the damp heat test could no longer withstand a stretch of 50%. The galinstan traces stopped making contact with the LED contacts when the devices were stretched for 50%. The lowering of the stretch capabilities of the devices could have been caused by the increased amount of galinstan oxidation caused by the increased temperature and humidity level. The oxide layer could have decreased the adhesion between the galinstan and the copper LED contacts. However, more research is needed to investigate this hypothesis.

Exposed to UV

Devices B1S1, B3S6, and B4S10 failed to work after one cycle. Therefore, no graphs are made for these devices.

Figures 67 and 68 show the stretch test results for device B1S6. This device was first subjected to the QUV test.

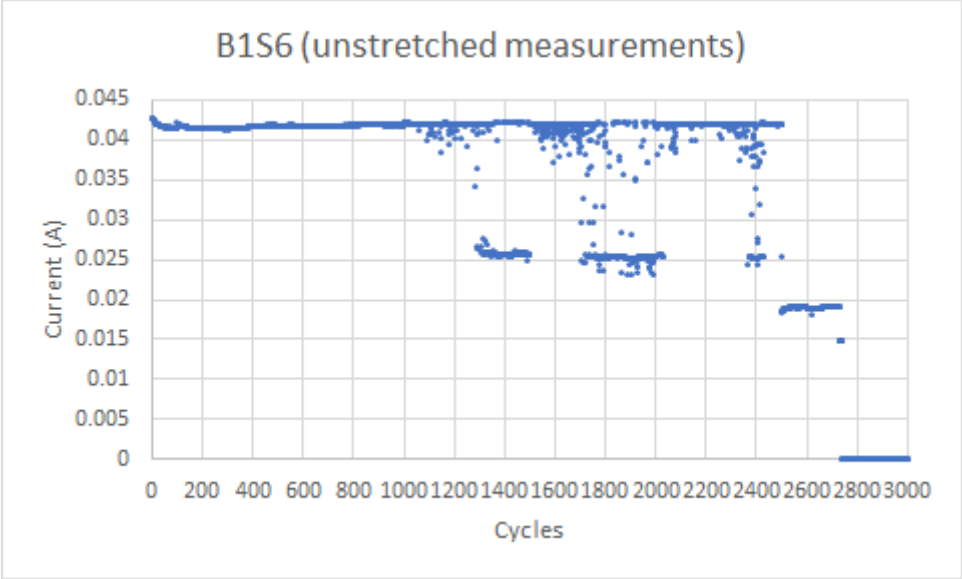

Figure 67: Current (unstretched) in function of the number of cycles for B1S6

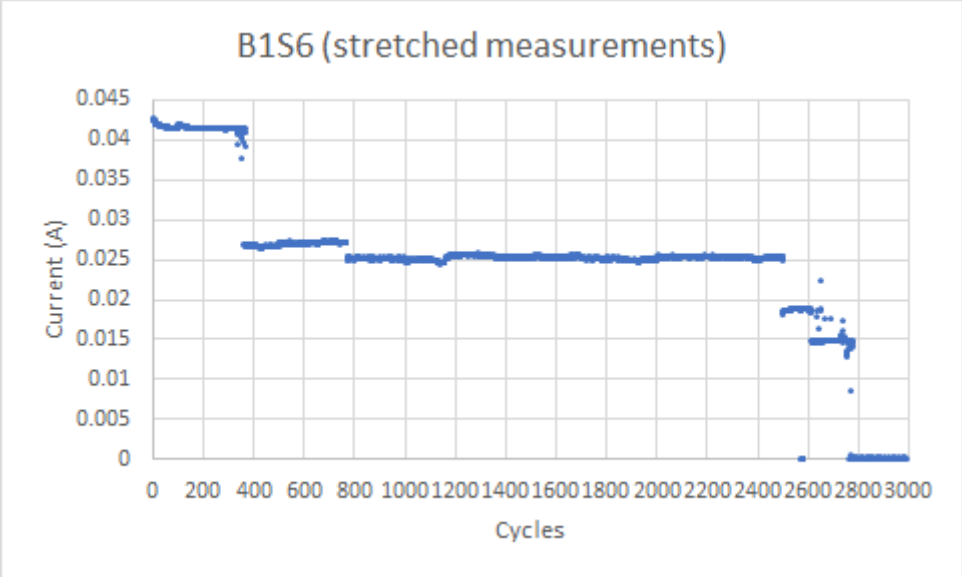

Figure 68: Current (stretched) in function of the number of cycles for B1S6

The graphs shown in figures 67 and 68 obtained from device B1S6 show an additional current level, measuring approximately 0.25 A. Under this current level, the LED's brightness is reduced and there may be a shift in the emitted light color. This behavior can be attributed to an increase in resistance. The increased resistance causes a decrease in the current passing through the LED, resulting in a lower brightness or color shift. Comparable deviations in other rigid electronic components can lead to complete malfunctioning. Consequently, this LED malfunction will be classified as a failure. Figure 69.a shows the normal functionality of the device. The LED shows the expected color output and brightness. Figure 69.b shows a decrease in the LED's brightness. The light emitted by the LED appears less bright compared to the functionality depicted in figure 69.a. Furthermore, figure 69.c illustrates a color shift in the LED's light. With this in consideration, it can be concluded that device B1S6 fails unstretched for the first time after 1284 cycles and permanently unstretched after 2494 cycles. Furthermore, device B1S6 fails stretched for the first time after 356 cycles and permanently after 370 cycles.

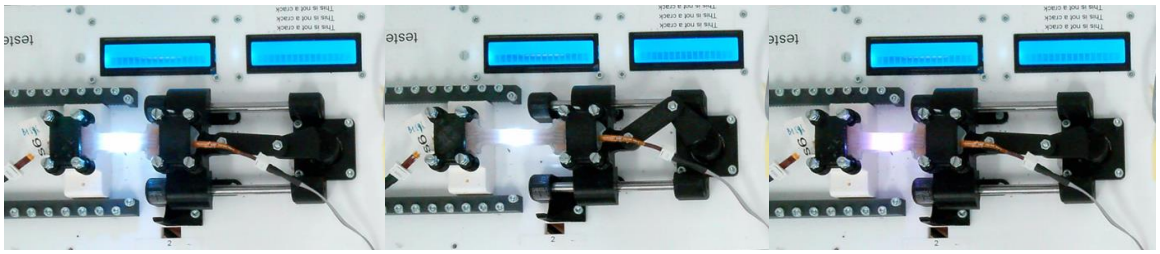

Figure 69.a: Normal brightness of the LED of device B1S6, Figure 87.b: dimmed brightness of the LED of device B1S6, Figure 87.c: color shift of the light of the LED of device B1S6

Figures 70 and 71 show the stretch test results for devices B4S1 and B4S4. Furthermore, Figures 72 and 73 show the stretch test results for devices B5S6 and B5S11. All these devices were first subjected to the QUV test.

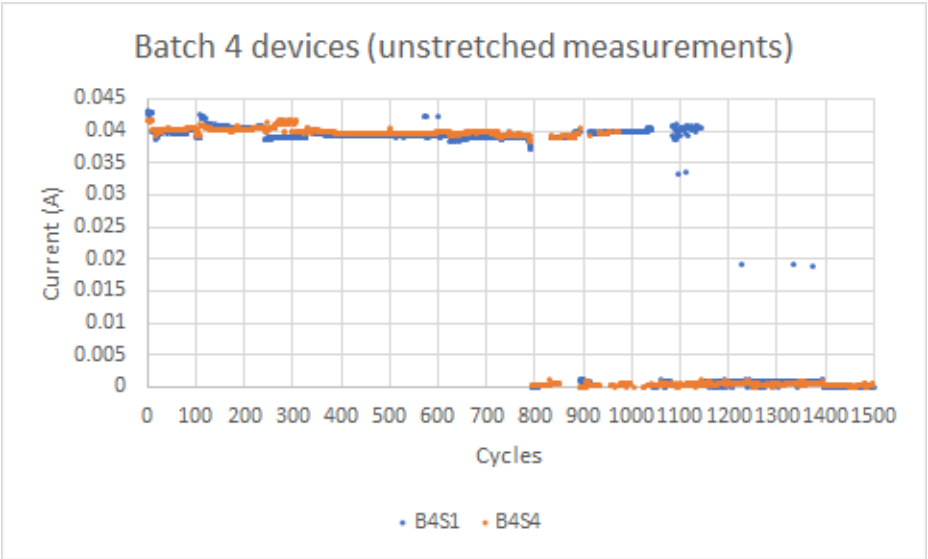

Figure 70: Current (unstretched) in function of the number of cycles for B4S1 and B4S4

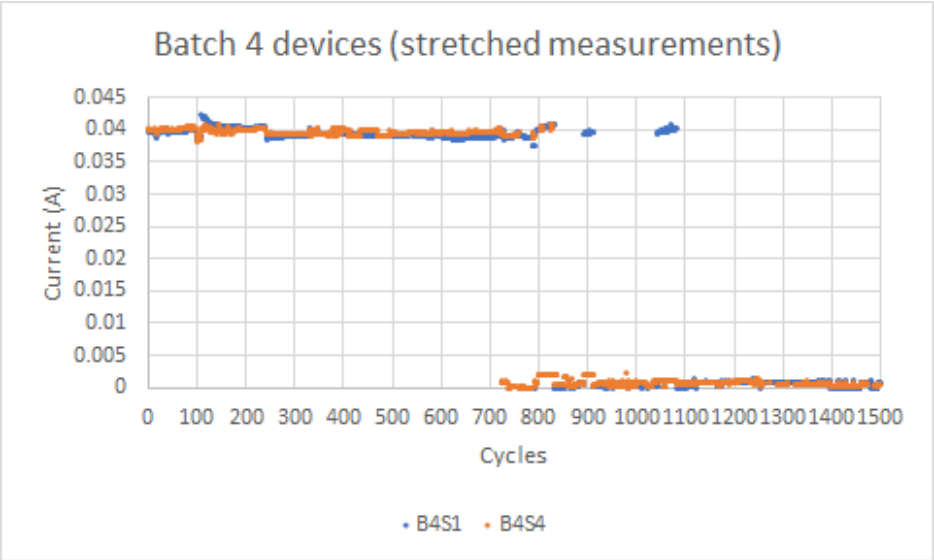

Figure 71: Current (stretched) in function of the number of cycles for B4S1 and B4S4

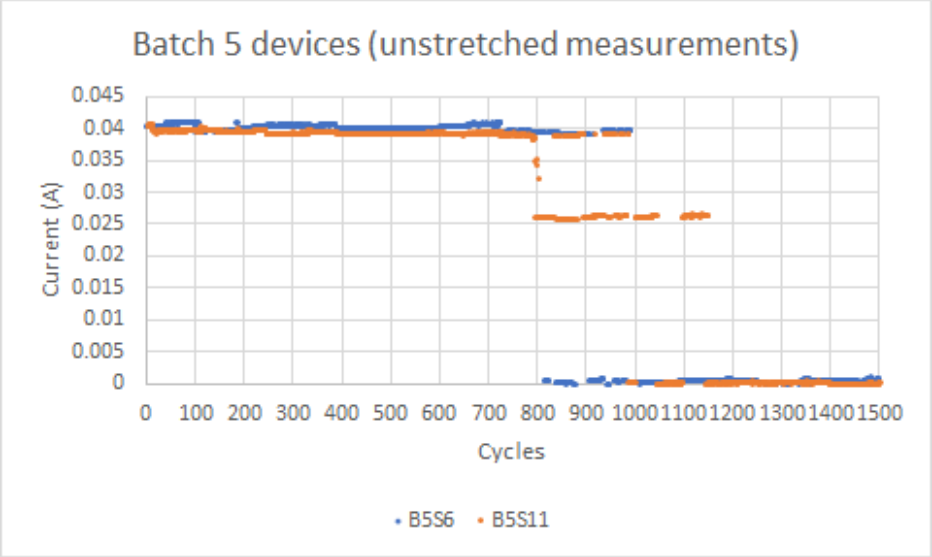

Figure 72: Current (unstretched) in function of the number of cycles for B5S6 and B5S11

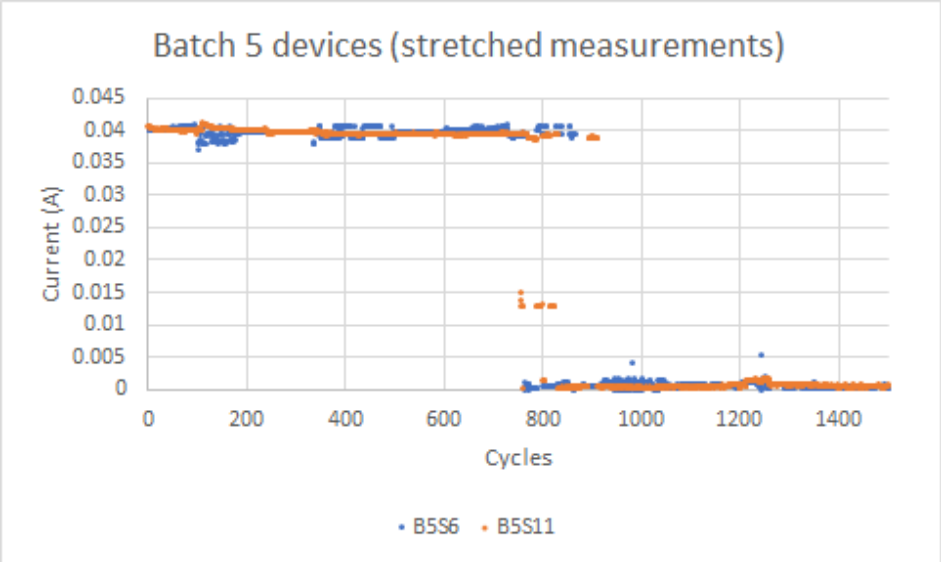

Figure 73: Current (stretched) in function of the number of cycles for B5S6 and B5S11

Device B4S1 experienced its initial failure in the unstretched state after 796 cycles, followed by a permanent failure occurring after 1139 cycles. When stretched, the device exhibited its first failure after 792 cycles, with a permanent failure observed after 1079 cycles. For Device B4S4, the device failed for the first time in the unstretched state after 814 cycles, and its permanent failure transpired after 972 cycles. Additionally, when stretched, the device encountered its initial failure after 723 cycles, followed by a permanent failure after 825 cycles. Device B5S6 demonstrated its first failure in the unstretched state after 815 cycles, followed by a permanent failure occurring after 990 cycles. In the stretched state, the device failed for the first time after 761 cycles, and its permanent failure was observed after 866 cycles. In the case of device B5S11, the device experienced its initial failure in the unstretched state after 794 cycles, and its permanent failure occurred after 986 cycles. When stretched, the device exhibited its first failure after 755 cycles, and permanent failure after 908 cycles.

Figures 74 and 75 illustrate the stretch results for devices B3S8 and B3S10. The current of device B3S8 is measured for 2000 cycles, while the measurements of device B3S10 are taken up to 1500 cycles.

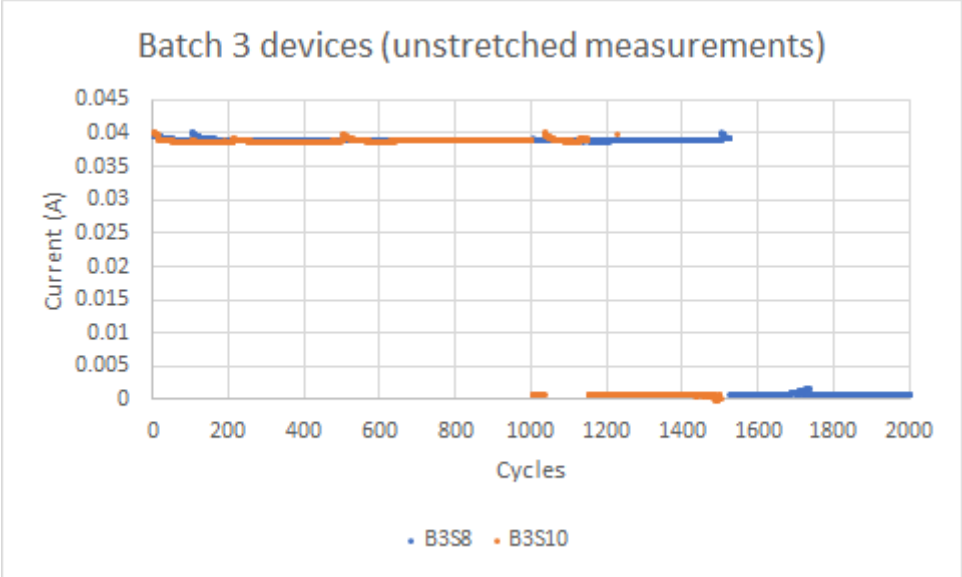

Figure 74: Current (unstretched) in function of the number of cycles for B3S8 and B3S10

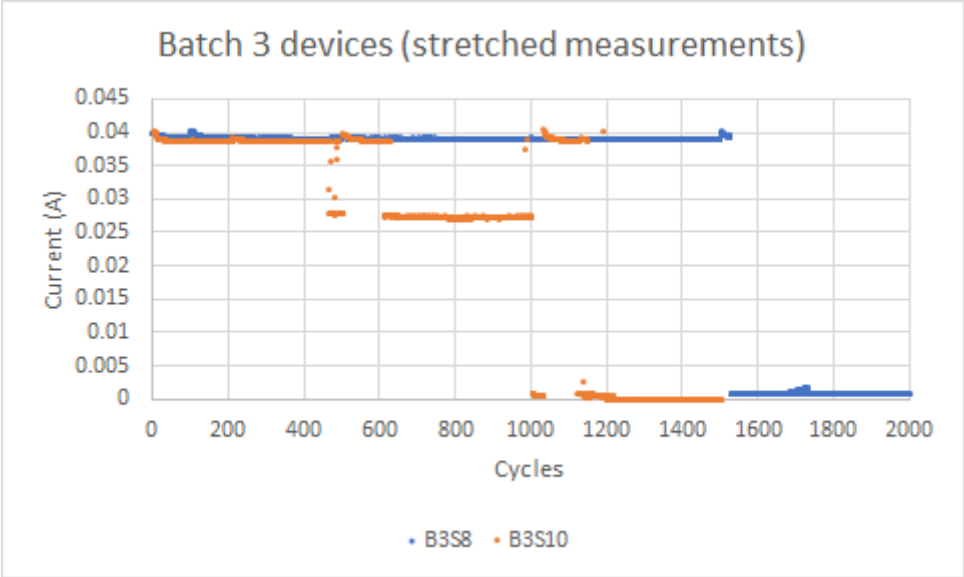

Figure 75: Current (stretched) in function of the number of cycles for B3S8 and B3S10

The graphs from device B3S8 show that the device failed unstretched for the first time after 1506 and permanently after 1521 cycles. Furthermore, it failed stretched after 1505 cycles and failed permanently at cycle 1526. The graphs from device B3S10 show that it failed stretched for the first time after 465 cycles of stretch and permanently after 1191 cycles. Additionally, the device failed unstretched for the first time after 989 cycles and permanently after 1226 cycles.

Figure 76 shows the bar chart that illustrates the average cycles before first and permanent failure of the devices that were subjected to the QUV test. The bar chart shows that the first failure occurs on average on cycle 999 unstretched and cycle 765 stretched. Furthermore, the devices fail permanently unstretched after 1333 cycles and stretched after 966 cycles.

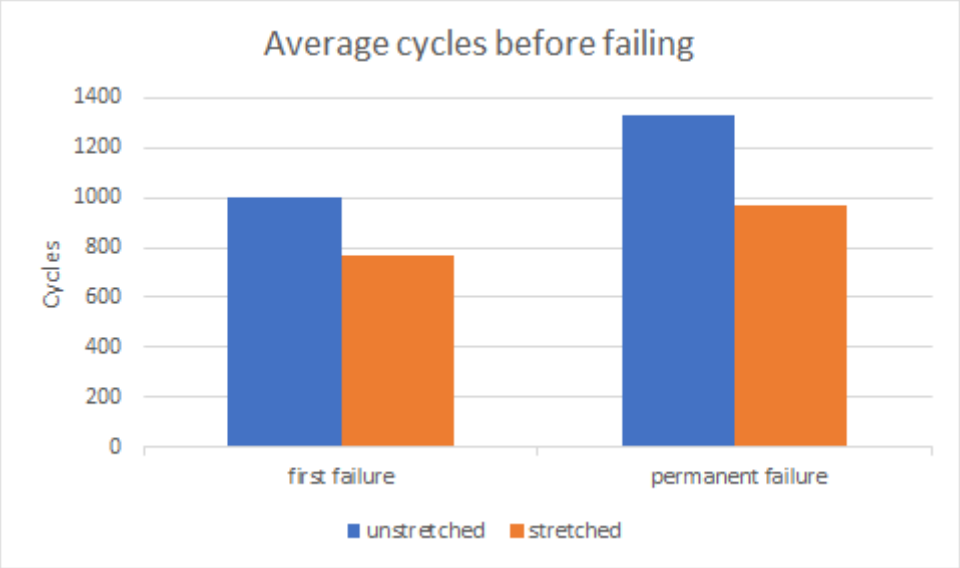

Figure 76: Bar chart depicting the average number of cycles survived by the to the QUV test subjected devices

In contrast to expectations, the UV-exposed devices show a prolonged lifespan compared to the unexposed devices, which initially seems counterintuitive given that the QUV test aims to simulate accelerated aging and environmental degradation. However, this unexpected result can be attributed to an increase in the stiffness of the silicone material. Consequently, the silicone demonstrates reduced flexibility compared to its original state. Notably, the primary failure mechanism observed in these devices involves the detachment of the silicone around the LED, allowing the galinstan to flow into the created gap. The increased stiffness of the silicone provides greater resistance to deformation, reducing the likelihood of the silicone detaching or loosening around the LED, which will result in a prolonged lifetime.

7.1.4 150% stretch test

All the devices listed in this chapter have completed 1500 cycles of 50% stretch before being subjected to the 150% stretch test.

Exposed to damp heat

The silicone of device B4S3 ruptured after 2848 stretching cycles around the transition zone between the smaller and the wider part of the device. Furthermore, the silicone of device B4S7 ruptured around the LED when stretched for 150% during 3305 cycles. The different positions of the rupture could indicate that the silicone layer around the LED of device B4S7 was thinner than that of device B4S3 as a result of the production process. Figure 77 illustrates the rupture of device B4S7 around the LED. Figure 78 shows the rupture of device B4S3. Device eight from batch two survived 2320 cycles. The rupture occurred in the transition zone between the smaller and wider parts of the device.

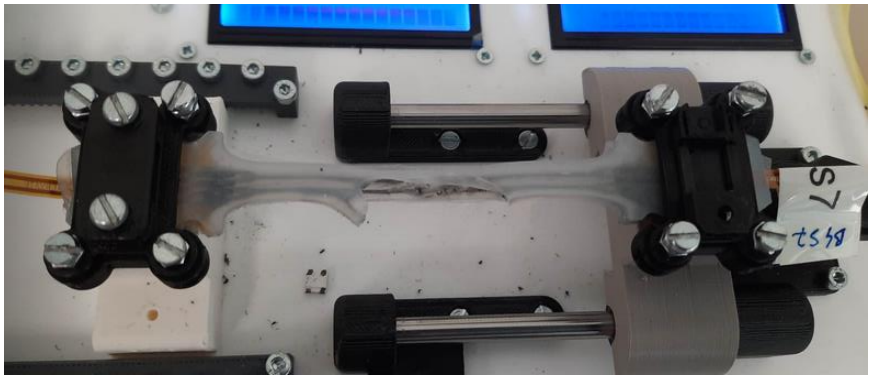

Figure 77: Rupture in the silicone of device B4S7 that underwent the damp heat test

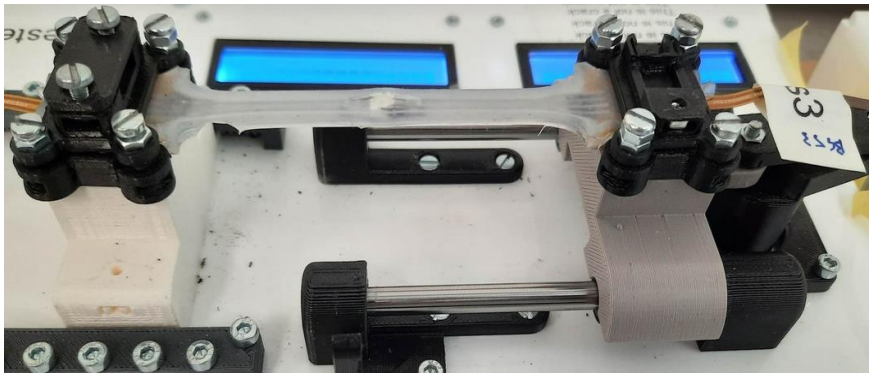

Figure 78: Rupture in the silicone of device B4S3 that underwent the damp heat test

Exposed to UV

Device one from batch four that was stretched for 150% during the stretch tests failed after 845 cycles of stretching. Additionally, device B4S10 ruptured in the same area as device B4S1 after 1544 cycles. Furthermore, the two front side legs of the silicone of one of its flexconnectors cut through the silicone of device B4S10. Figure 81 shows this. This could have prolonged the lifespan of the silicone of the device since the stretchable part of the device is now longer. However, this also causes the traces near the flexconnector to deform which will lower the total lifespan of the device. The silicone of device one from batch one that also was stretched for 150% failed after 490 cycles. This is significantly less than the devices that were not exposed to the UV-radiation. This indicates that the UV-radiation significantly reduces the lifespan of the silicone itself. Figures 97 and 98 show the rupture of the silicone of devices B4S1 and B1S1 respectively. Both devices ruptured at the same place. Redesigning these specific parts can potentially expand the lifespan of the silicone.

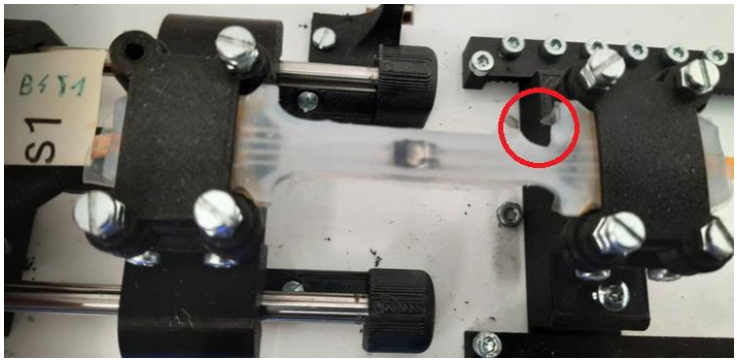

Figure 79: Rupture in the silicone of device B4S1 that underwent the QUV test

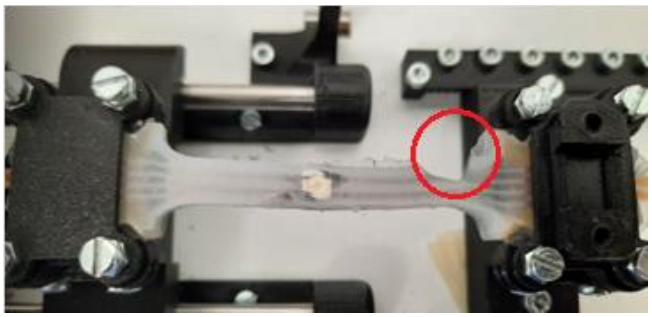

Figure 80: Rupture in the silicone of device B1S1 that underwent the QUV test

Figure 81: Front side leges of the flexconnector sticking out of the silicone of device B4S10

Not exposed to environmental stress factors

During the production of device B2S2, two legs of the flexconnector were not properly attached to the vinyl. This resulted in the two legs of the flexconnector sticking up a little in the silicone. After 2320 cycles of 150% stretching, the legs of the flexconnector stuck out of the silicone. Therefore, it is important during the production process to make sure that all the legs of the flexconnector are perfectly positioned horizontally which prevent them from cutting the silicone. Furthermore, this means that the flexconnectors can also cut the internal silicone of the devices during stretching. Figure 82 shows the device. Additionally, the two front side legs of the flexconnector caused further complications, cutting their way out of the silicone. This allowed the silicone and the galinstan traces to deform around the flexconnector.

Figure 82: Two flexconnector legs sticking out of the silicone of device B2S2

Device B4S5 survived 2864 stretch cycles of 150%. The silicone of this device ruptured around the LED. Figure 83 shows the rupture. This type of failure can be mitigated by thickening the silicone layer around the LED.

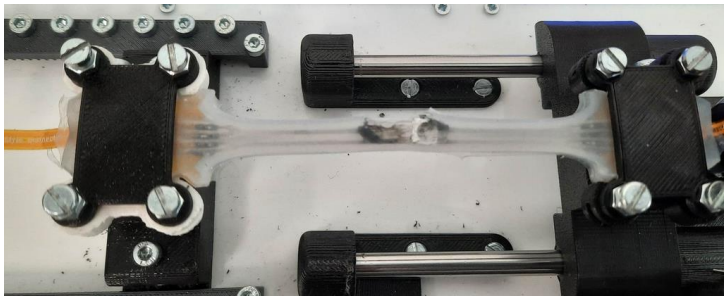

Figure 83: Rupture in the silicone of device B4S5 that did not underwent an environmental test

7.1.5 Failure mechanisms

Silicone detachment from the LED

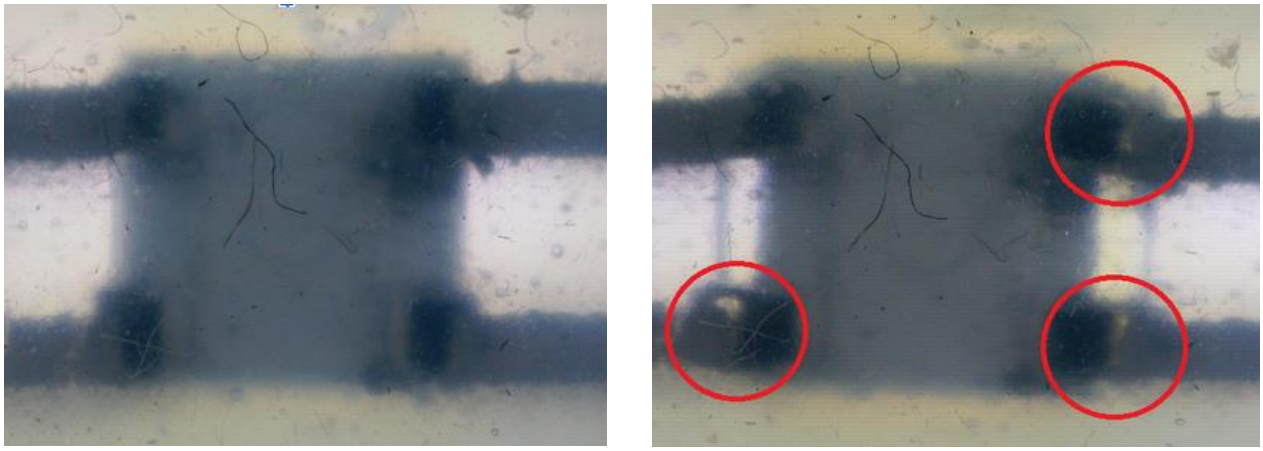

Figure 84.a: LED and attached traces of the B4S5 device while being unstretched, Figure 102.b: LED and attached traces of the B4S5 device while being stretched for 50%

Figure 84.a shows the LED and attached galinstan traces of the B4S5 device while being unstretched. Figure 84.b shows the LED and traces of the B4S5 device while being stretched. Both images were taken after 1500 stretching cycles of 50% stretch. Figure 84.b shows that three traces are getting detached from the LED contacts when being stretched for 50% after 1500 cycles. Furthermore, it can be noticed from figure 84.b that the silicone gets detached from the LED when stretched. This behavior can also be observed in the other devices.

Figure 85 shows the top view of the encapsulated LED of the B4S5 device. It can be noted that some black coloured stripes appear on top of the LED. Furthermore, the small triangle of the LED has completely been colored black. This phenomenon is the result of the galinstan being pushed upwards by the continuously stretching and relaxing of the device. When the silicone gets detached from the LED during stretching, some galinstan can move into the gap. Now, if the device gets relaxed again, the silicone will push the galinstan against the LED. If this process gets repeated for multiple cycles,

some galinstan can end up on top and on the side of the LED. This process lowers the amount of galinstan situated in the traces, especially near the LED contacts. As a result, the traces will break faster, closely to the LED contacts. This has also been observed in multiple devices.

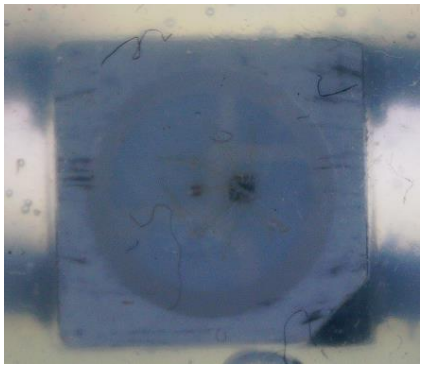

Figure 85: Top view of the LED of the B4S5 device after 500 cycles

Ruptures

During the 150% stretch test, it can be noticed that most devices ruptured around the LED or in the transition zone between the smaller middle part and one of the wider parts. Thickening the silicone layer around the LED will prolong the lifetime of the devices. Increasing the diameter of the curve between the smaller and wider parts of the device, so that the transition between the two parts is smoother, will reduce ruptures in this transition zone from occurring. These two alterations can prolong the lifespan of the silicone of the devices. To conclude, it can be noted that the QUV test significantly lowers the lifespan of the silicone itself.

Cutting in the silicone by the flexconnectors

During the 150% stretch tests, it was observed in multiple devices that the legs of the flexconnectors can cause cuts in the surrounding silicone. In certain instances, these cuts can result in the legs sticking out of the silicone. Such cuts have the potential to allow galinstan to escape from the devices. Moreover, internal cuts in the silicone can create the possibility of short circuits if the galinstan from two traces flows into each other around the flexconnector.

7.2 Stretchable wire results

7.2.1 Production results

Following the methodology of the batch production, all devices were inventorized and key parameters and defects were logged. Three batches were made in total. Due to the unprecedented novelty of the batch production, a test batch was made first to evaluate the feasibility of the process. However, none of four devices produced in this batch exhibited properties which would inhibit testing according to the strategies discussed in this thesis. Therefore, those devices were included in further research as fully-fledged testing specimens, and fell under batch 1. Two more batches were produced consequently, referred to as batch 2 and batch 3, each containing 12 devices. All relevant properties and anomalies were logged and explained more in detail in the following paragraphs.

Batch 1

Table 8 shows the device number, and its corresponding initial resistance which was measured before exposure to any stressfactor. Column 3 contains the stressfactor to which each device was exposed. Distribution of all devices between the stress factors was made based on the initial resistance, in order to evenly divide them. Devices of batch 1 were either exposed solely to stretch testing or to both UV and stretch testing. The exposure to the latter was done sequentially, first exposing the devices to UV light after which all devices were studied and measured, then the devices were stretched tested as well. From this batch, one device will not be exposed to any stress factor in order to compare the evolution of the devices' properties to the ones that were.

Table 8: Batch 1 devices

Device number	Initial resistance	Stress factor(s)
1	0.313	None
2	0.258	UV, stretch
3	0.268	Stretch
4	0.204	UV, stretch

Batch 2

As can be seen in table 9, more variances exists between different devices in terms of initial resistance. To achieve maximal comparability, devices from the entire resistance range will be divided between the possible stress factor exposures. Secondly, the device number plays an important role in the division as well. Devices from different positions within the mold have to be represented in all the stress factor tests, to minimize the influence of production flaws.

Table 9: Batch 2 devices

Device number	Initial resistance	Stress factor(s)
1	0.390	stretch
2	0.923	UV, stretch
3	1.884	stretch
4	0.526	UV, stretch
5	0.353	stretch
6	0.380	UV, stretch
7	0.324	none
8	0.313	UV, stretch
9	0.526	none
10	0.212	UV, stretch

11	0.427	stretch
12	0.428	stretch

Batch 3

Parallel to the methodology for the division of devices between the stress factors used for batch 1 and batch 3, devices from batch 2 were also divided as seen in table 10.

Table 10: Batch 3 devices.

Device number	**Initial resistance**	**Stress factor(s)**
1	0.917	none
2	0.503	Damp heat, stretch
3	0.633	Stretch
4	0.357	Damp heat, stretch
5	0.426	none
6	1.760	Stretch
7	1.186	Damp heat, stretch
8	2.240	Damp heat, stretch
9	2.684	Stretch
10	0.666	Damp heat, stretch
11	0.310	stretch
12	0.557	stretch

7.2.2 Damp heat test results

The evolution in resistance of devices from batch 3 during the 672 hours of damp heat exposure is shown in Figure 86. There are five data points per device plotted on the graph, the first one is the initial resistance, measured after production of the devices, the last four are from the ex-situ measurements taken at regular intervals during exposure.

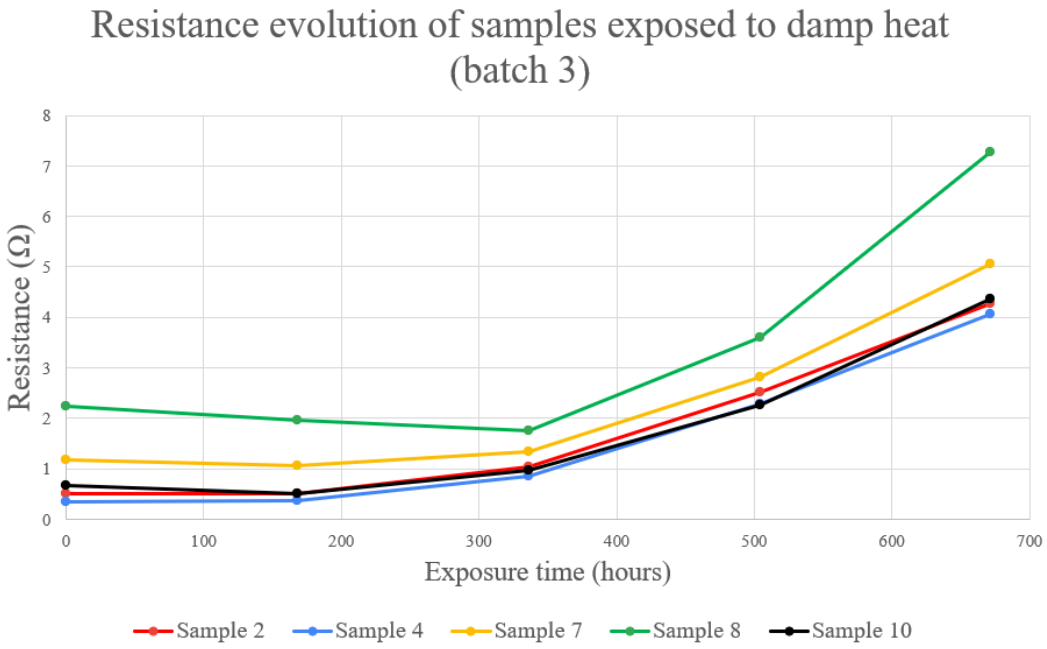

Figure 86: Resistance evolution of devices from batch 3 which were exposed to damp heat

The first 170 hours of exposure the resistance of all devices remains relatively constant. For most devices, this period is followed by a slight resistance increase towards 340 hours of exposure. Exclusively device 2 has undergone a slight resistance decrease in this period. However, given the relatively low variance in all devices during the first 340 hours, the anomaly of device 2 can likely be attributed to factors not related to the exposure to damp heat.

Between 340 and 670 hours of exposure a significant resistance increase was observed in all devices, including device 2 which exhibited anomalous behavior previous to 340 hours of exposure.

7.2.3 QUV test results

The resistance of all devices that underwent QUV testing are plotted on figure 87, analogous to the damp heat results under paragraph 7.2.2. QUV results differ drastically from damp heat results, as there is no clear deviation of resistance from the initial value. However, as will be discussed in paragraph 7.2.5, the combination of this test followed by stretch testing did significantly affect the devices.

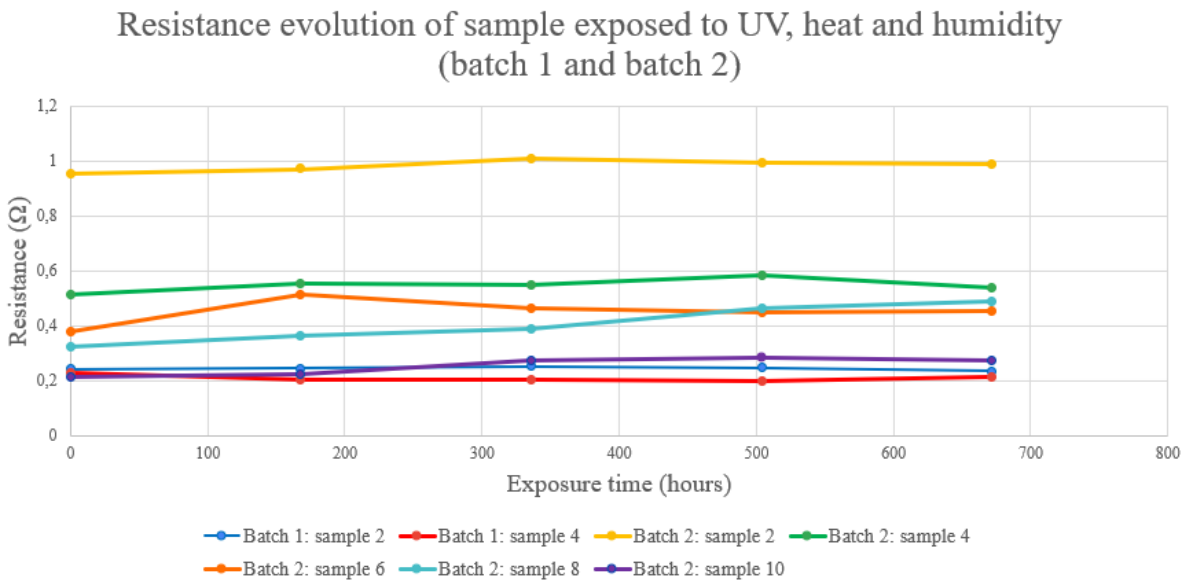

Figure 87: Resistance evolution of devices from batch 1 and 2 which were exposed to UV, heat and humidity

7.2.4 Static stretch test results

When a device is stretched and held in this state, there is a certain period starting at the moment of stretching, during which the resistance of the device increases. Presumably this is caused by a relatively small flow of liquid metal within its trace in combination with the silicone that is still settling in the new stretched state. In applications where a device is stretched continuously, this increase in resistance is relevant as it will affect currents within the device in deviating ways at different points in time.

Not exposed to environmental stress factors

Figures 88, 89 and 90 demonstrate the static stretch resistance of the device after production and, in case the specific device was still functional at this point, after 1000 cycles. Figure 88 and 89 show the static stretch resistances of devices from batch 1 and 2, of which the resistance all stopped rising significantly after 10 minutes. The measurements continued to 100 minutes, to remain consistent between all devices from all batches, however these measurements are not included in Figure 88 and 89 as they provide no added value due to them reaching a state of equilibrium.

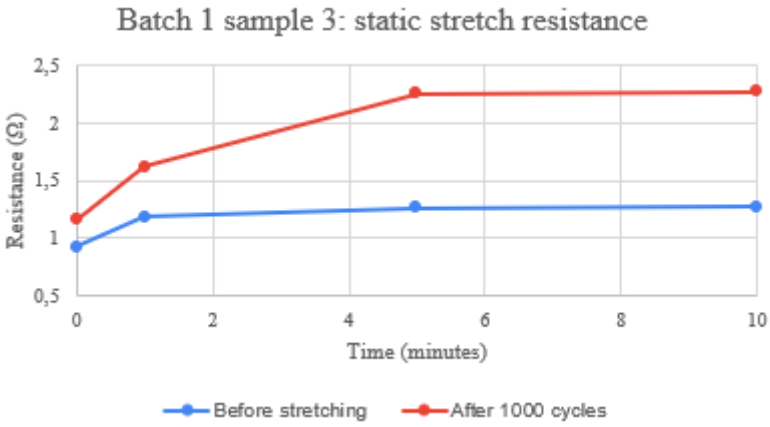

Figure 88: Static stretch resistance of device from batch 1 which was not exposed to environmental stress factors

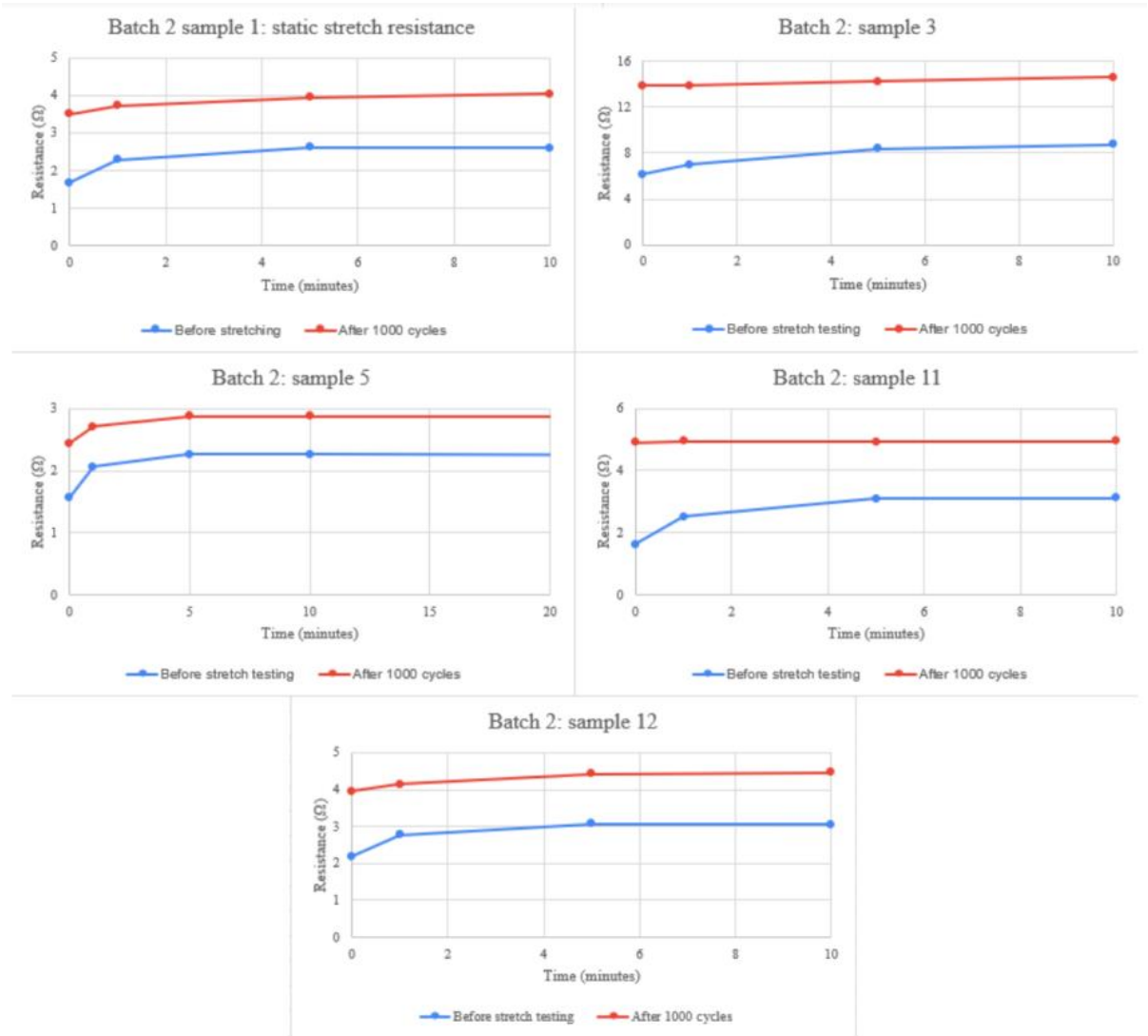

Figure 89: Static stretch resistance devices from batch 2 which were not exposed to environmental stress factors

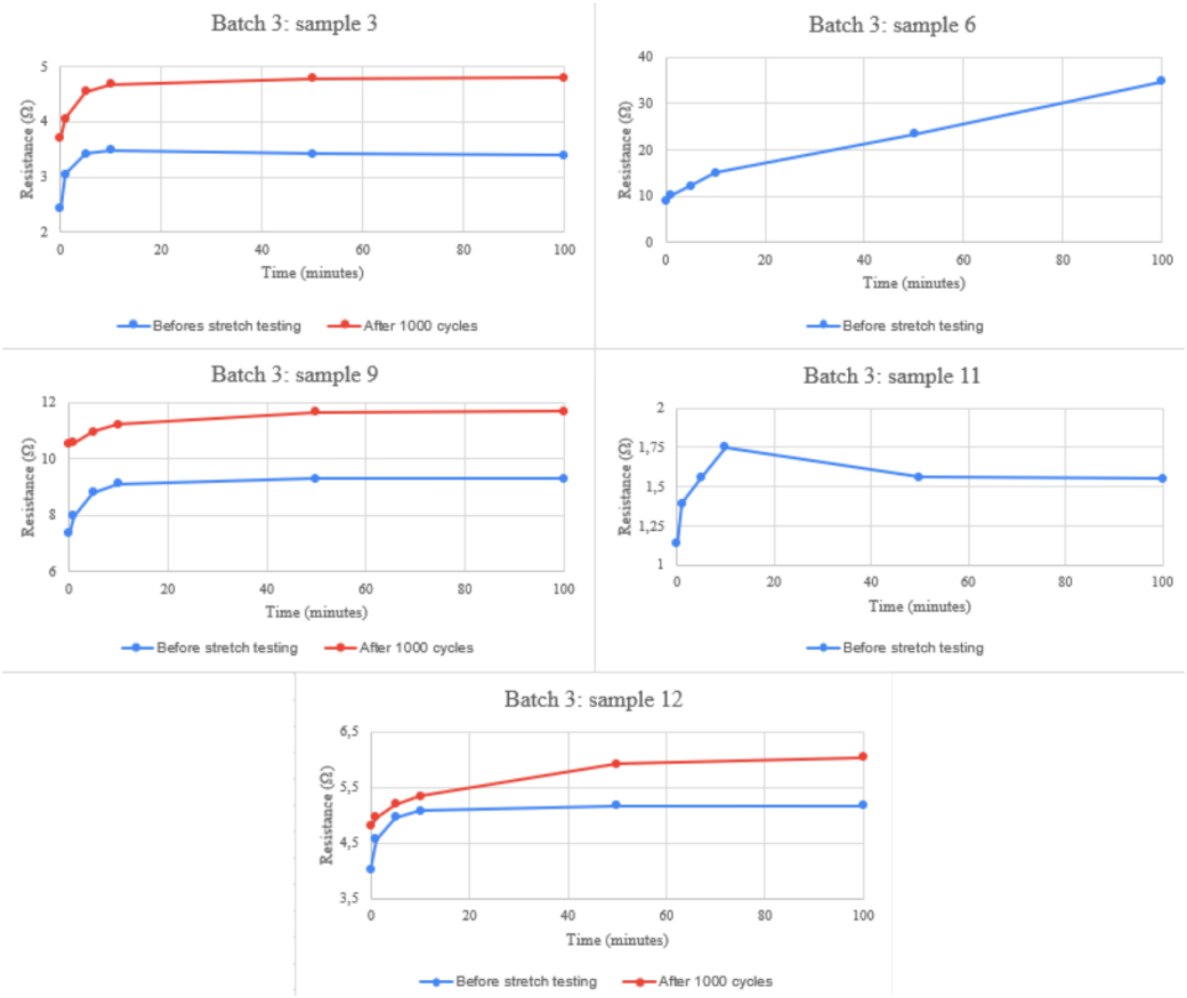

Figure 90: Static stretch resistance devices from batch 3 which were not exposed to environmental stress factors

Exposed to damp heat

From batch 3, only one device remained functioning immediately after stretching, device 10. All other devices failed within seconds of their first stretch, indicating that the devices had been significantly affected by the exposure to damp heat. Device 10 of batch 3 was the only device that retained some functionality, for approximately 10 minutes the resistance rose from 9 ohms to 12 ohms, after which functionality was completely lost.

Exposed to UV, heat and humidity

Figures 91 and 92 demonstrate the static stretch resistance of devices after production and in case the specific device was still functional at this point, after 1000 cycles. Figure 91 shows device 2 and 4 from batch 1, which reached their equilibrium stretched resistance after 50 and 100 minutes, respectively.

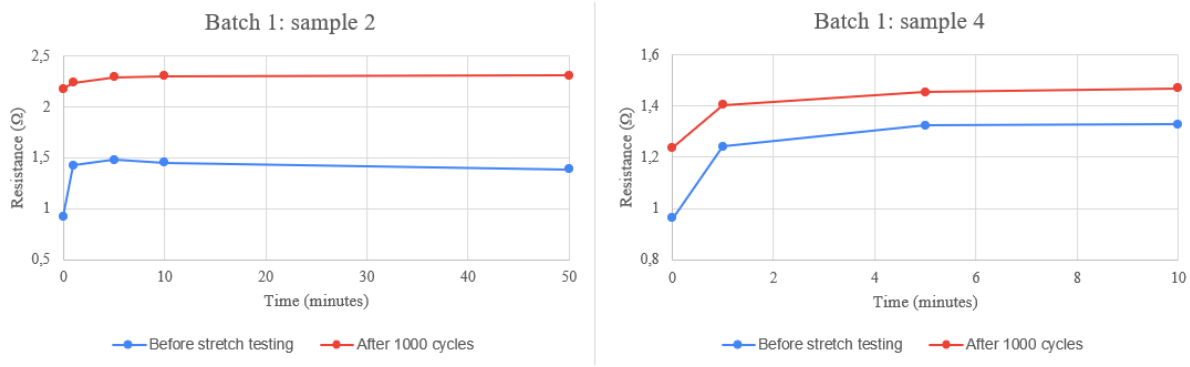

Figure 91: Devices from batch 1 which were exposed to UV, heat and humidity

Static stretch resistances of devices from batch 2, which were exposed in the QUV chamber, are shown in Figure 110. All devices reached their resistance equilibrium after 50 minutes, with the exception of device 8. After 1000 cycles, all devices except for device 10 lost functionality and were thus not able to being static stretch tested again.

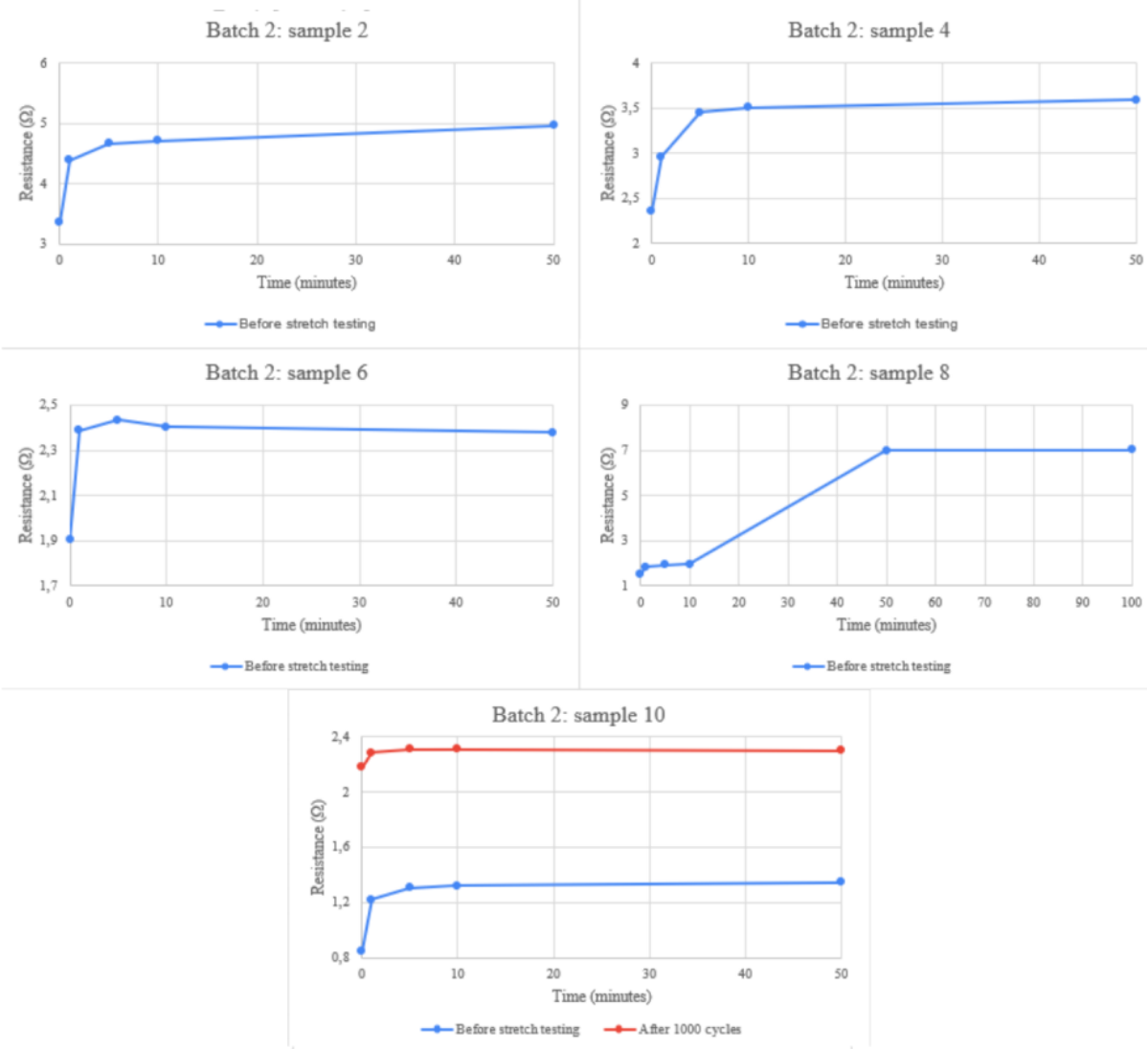

Figure 92: Devices from batch 2 which were exposed to UV, heat and humidity

7.2.5 Stretch testing results

All devices were stretch tested, during which their resistances were monitored. In this way, their functionality or lack of it, could be determined. All devices, except for device 3 from batch 3, lost their functionality at some point. It has to be noted that in the scope of the paragraphs under 7.2.5, loss of functionality was defined as a resistance increase of such proportions that the galistan trace did no longer conduct and function as a stretchable wire. Concretely, when resistance increases by more than 1000%, a loss of functionality will be presumed. Depending on the specific application which the devices are possibly meant for, this definition could potentially be different. However, this would not change the conclusions drawn in the following paragraphs from a general perspective.

Batch 1

Figure 93 shows the resistances of devices from batch 1 throughout their lifetime up until the moment of functionality failure. During cyclic testing, both the resistance in the relaxed and in the stretched state were monitored. Both resistances exhibit a similar curvature in every device, however, values in the curvature of the stretched resistance are, as expected, higher. The higher resistance corresponds to the thinning of the liquid metal trace within the device as it is stretched.

For device 4, at approximately 4100 cycles, it ruptured, and before this point a relatively short period of significant resistance increase was observed. The relaxed resistance remained measurable slightly longer, as relaxing the device reconnected parts of the party ruptured trace at that point in time. Devices 2 and 3 retained functionality to approximately 20 000 cycles.

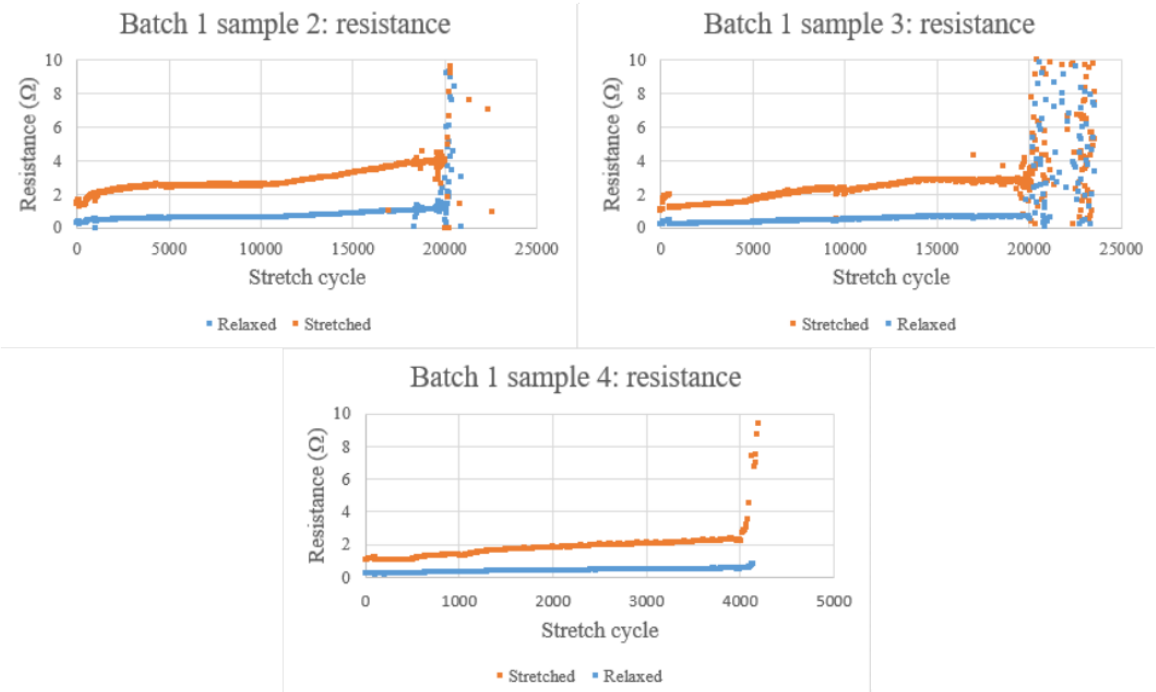

Figure 93: Resistance during cyclic testing of devices from batch 1

Batch 2

Figures 94 and 95 show the resistances of devices from batch 2 during cyclic testing. All devices exhibit a, slight or otherwise, drop in resistance approximately every 100 cycles. This drop correlates with the pausing of the cycletester setup to acquire an image, which typically lasts 8 to 10 seconds. It must be noted that some graph values, such as those of device 1, device 2, device 4 and device 10, appear to be missing. This is caused by measurements being invalid, presumably due to poor contact somewhere in the measurement circuit. This could either be within the traces or flexconnector contacts within the device itself, or in the wiring of the measurement equipment.

Furthermore, substantial increases or decreases in resistance values around 100, 500, 1000, or 5000 cycles, can be explained by taking the devices out of the cycletester setup for evaluation and or different measurements such as the static resistance measurements. When devices are taken out, the silicone is inevitably deformed, as merely holding a device impacts the shape of the device at that moment in some regard. This deformation of devices impacts the morphology of all traces within devices, causing their resistances to undergo changes. Also, as the adhesion between the flexconnector and the silicone degrades minor spacings form between them. These minor spaces can become filled with liquid metal, thereby decreasing the amount of liquid metal in the traces itself. By taking out the devices of the setup and performing evaluations and measurements on them, the process of the liquid metal flowing in these spacings can presumably be accelerated. Whether the changes in resistance are permanent resides upon the permanency of the changes to the traces and the liquid metal displacement.

Additionally, no valid measurements were taken for device 8 in the stretched state, meaning that the device was never functional in the stretched state.

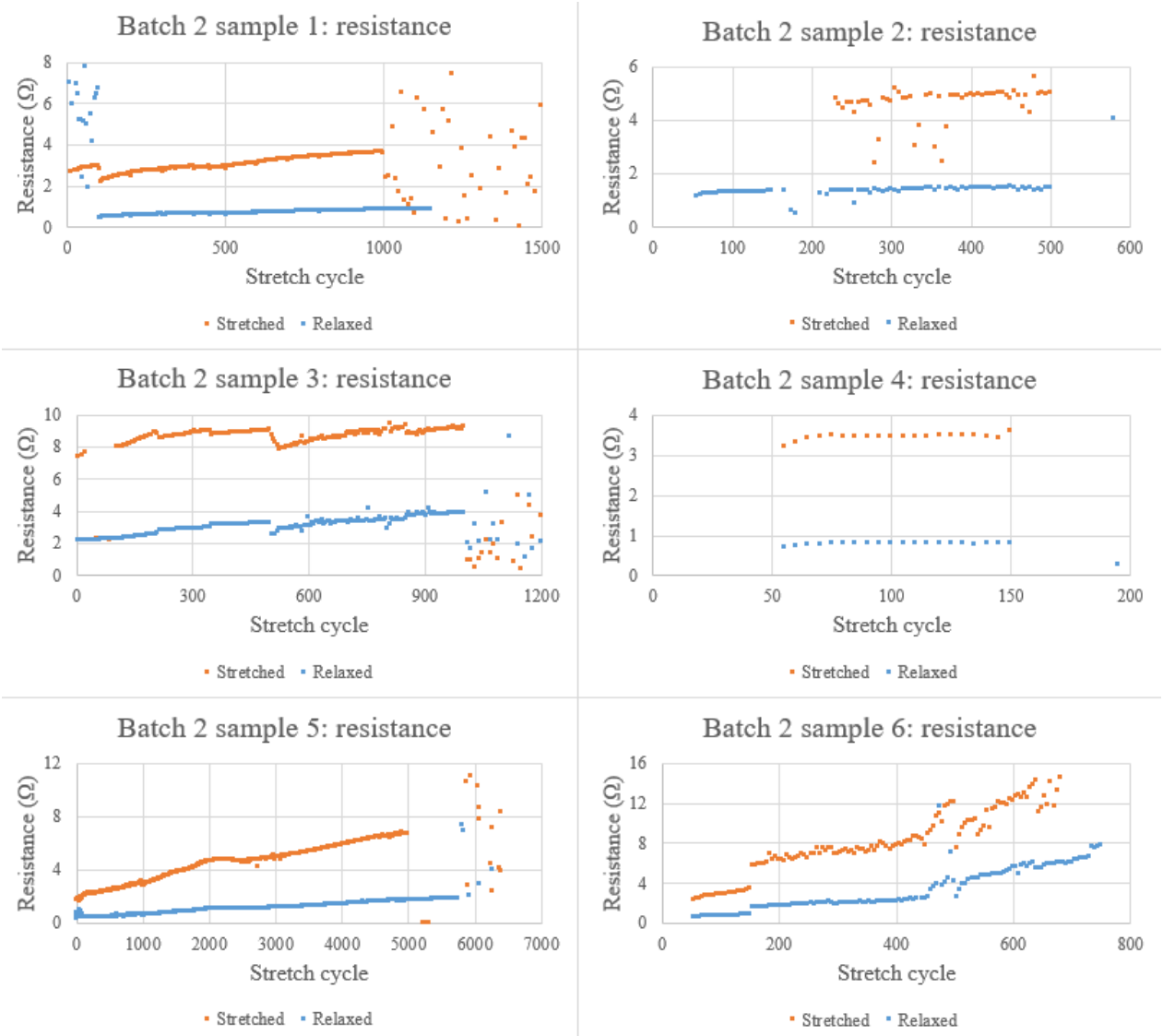

Figure 94: Resistance during cyclic testing of devices from batch 2 (sample 1, 3, 4, 5 and 6)

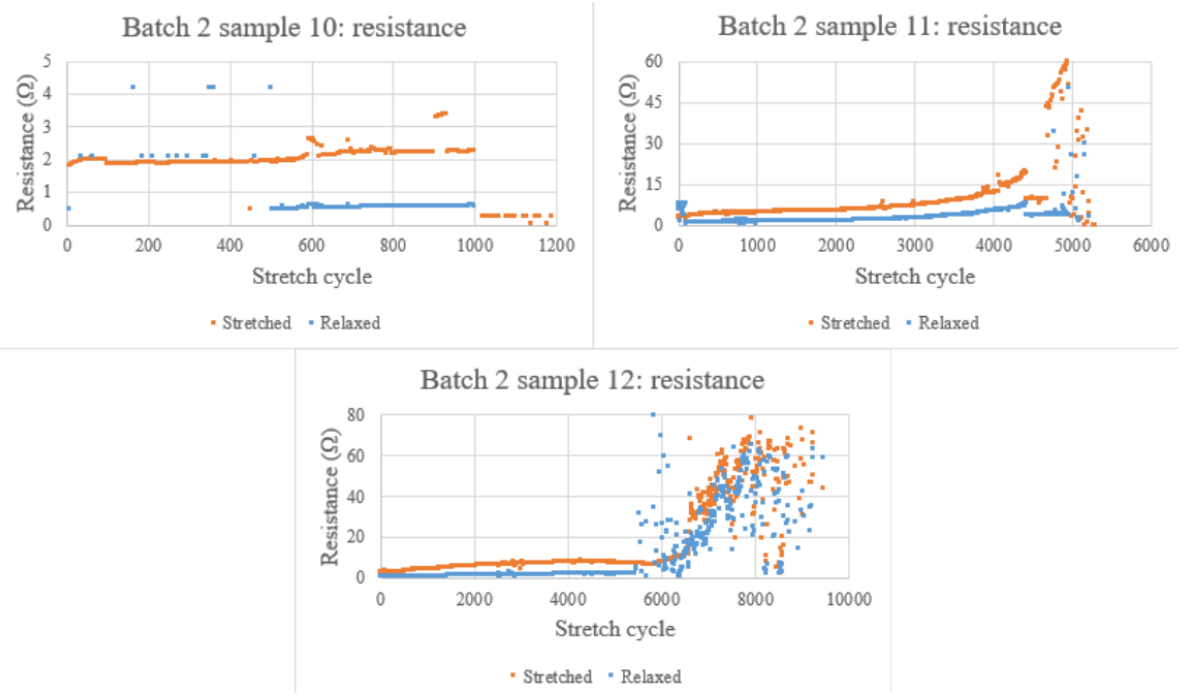

Figure 95: Resistance during cyclic testing of devices from batch 2 (sample 2, 11 and 12)

Batch 3

Resistance results of the devices in batch 3 during cyclic testing are shown in Figure 96. Analogous trends to the devices in batch 2 were observed, with major resistance changes at 100, 500, 1000, 5000, and 10 000 cycles, and minor inconsistencies in the curvatures every 100 cycles due to the imaging. Furthermore, none of the devices which underwent damp heat testing, with the exception of device 4 in the stretched state, were not able to function at any point in time during stretch testing.

Batch 3 device 3 exhibited resistance values varying between different specific values for the first 250 cycles in the relaxed state. Due to the resistance measurements being on plateaued values, presumably a measurement error lied at the basis, indicating a fault in the cycletester setup cabling or the digital multimeter itself. Also, between 19 000 and 23 000 cycles, erratically varying resistance values were observed. At 20 000 and 22 500 cycles the devices were taken out of the setup due to cycletester failures, as the cycletester had to be replaced or had to have parts replaced. This could have affected the erratic values, however, they can not be appointed as the singular cause, as the values became erratic before the cycletester failures.

The resistance of Batch 3 device 12 is shown in Figure 96 on a logarithmic scale, as it appeared on a regular scale the resistance dropped to 0 at certain points, which is not the case. However, a major decrease in stretched resistance can be observed between 1000 and 5000 cycles. Furthermore, the stretched resistance took on different values in this interval. Presumably, this was due to the movement of the flexconnector within the silicone, as explained in paragraphs 7.2.5 in detail. This is confirmed by the disappearance of this phenomenon after 5000 cycles, a point at which it was taken out of the clamps of the cycletester and put back in. This could have affected the forces present on the flexconnectors of the device, due to small variations in the position of the device in the clamps.

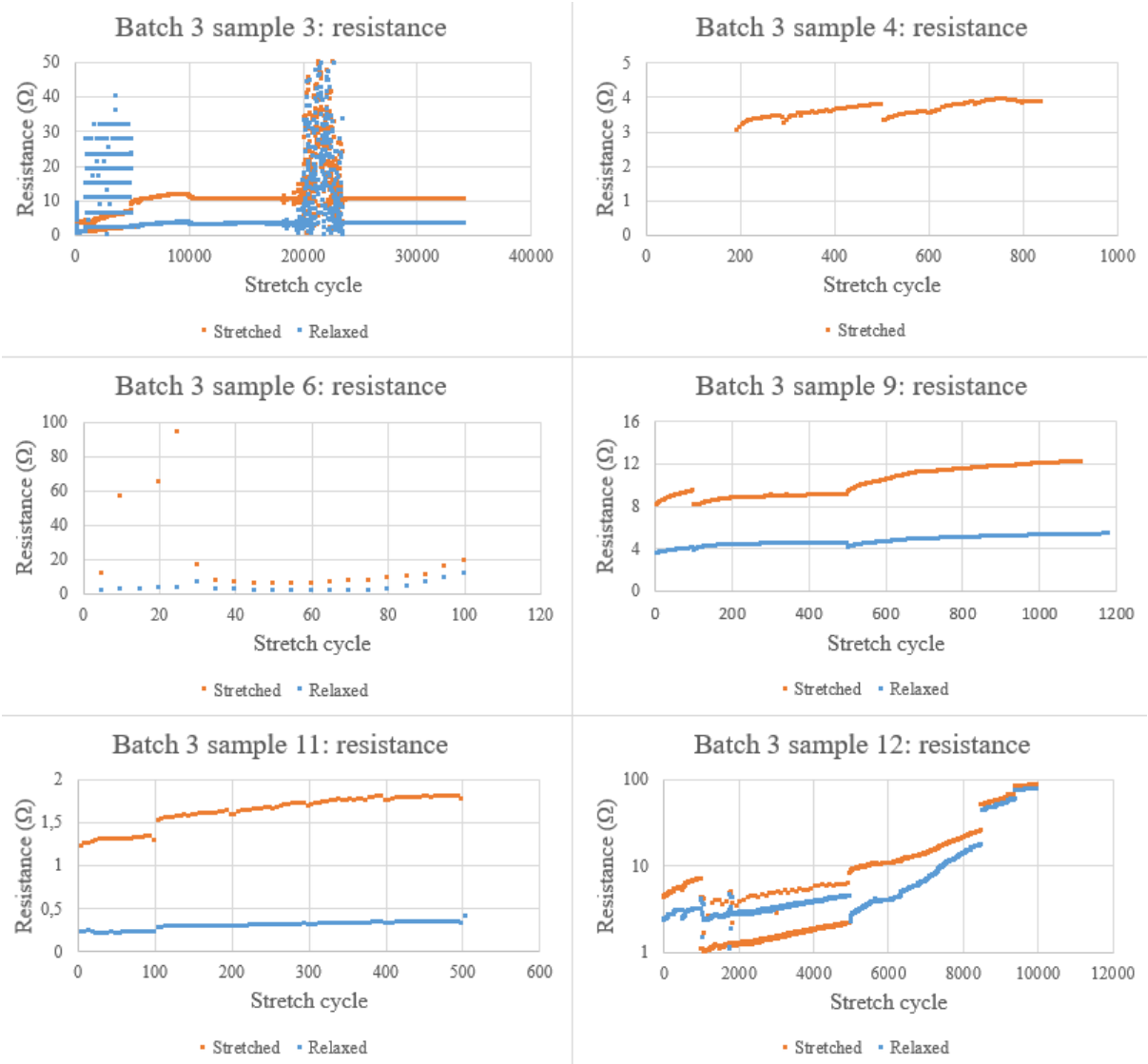

Figure 96: Resistance during cyclic testing of devices from batch 3

7.2.7 Failure mechanisms

Rupture

During cyclic testing, devices are continually brought from their relaxed state, to being stretched to three times their original length, stressing the silicone significantly. Prototype testing established that the corners of the stretched area of the design are the weakest points. Although the corners were rounded in the final design, as can be seen on Figure 97, they still proved to be the weakest part in the altered design.

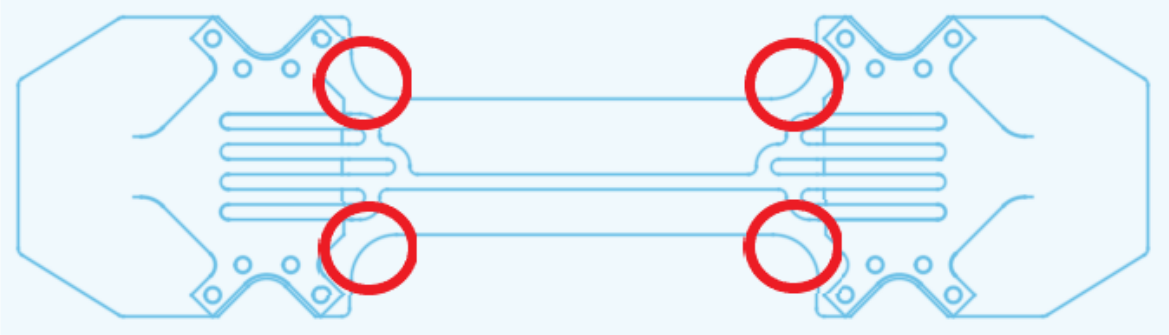

Figure 97: Weakest silicone parts of the stretchable wire design encircled in red

The device that failed due to ruptures in the weak spots depicted in Figure 97, was device 4 of batch 1. Figure 98 shows the device after rupture, with two red circles indicating where the rupture started.

Figure 98: Batch 4 device 1, after rupture occurred at a weak point in the silicone device shape

Figure 99 shows the images taken by the cycletest setup around the period that the rupture occurred. The different stages of the rupture are visible, starting at Figure 99a where the rupture is only visible in the form of a small anomaly at the bottom right corner of the stretched area, and ending at Figure 99e where the rupture is complete and the device is broken. These images correspond to the resistance measurements taken during cyclic testing, where the resistance started increasing significantly after approximately 4000 cycles. Contrary to expectations drawn from the testing of the prototypes, device 4 from batch 1 was the only device to rupture during cyclic testing.

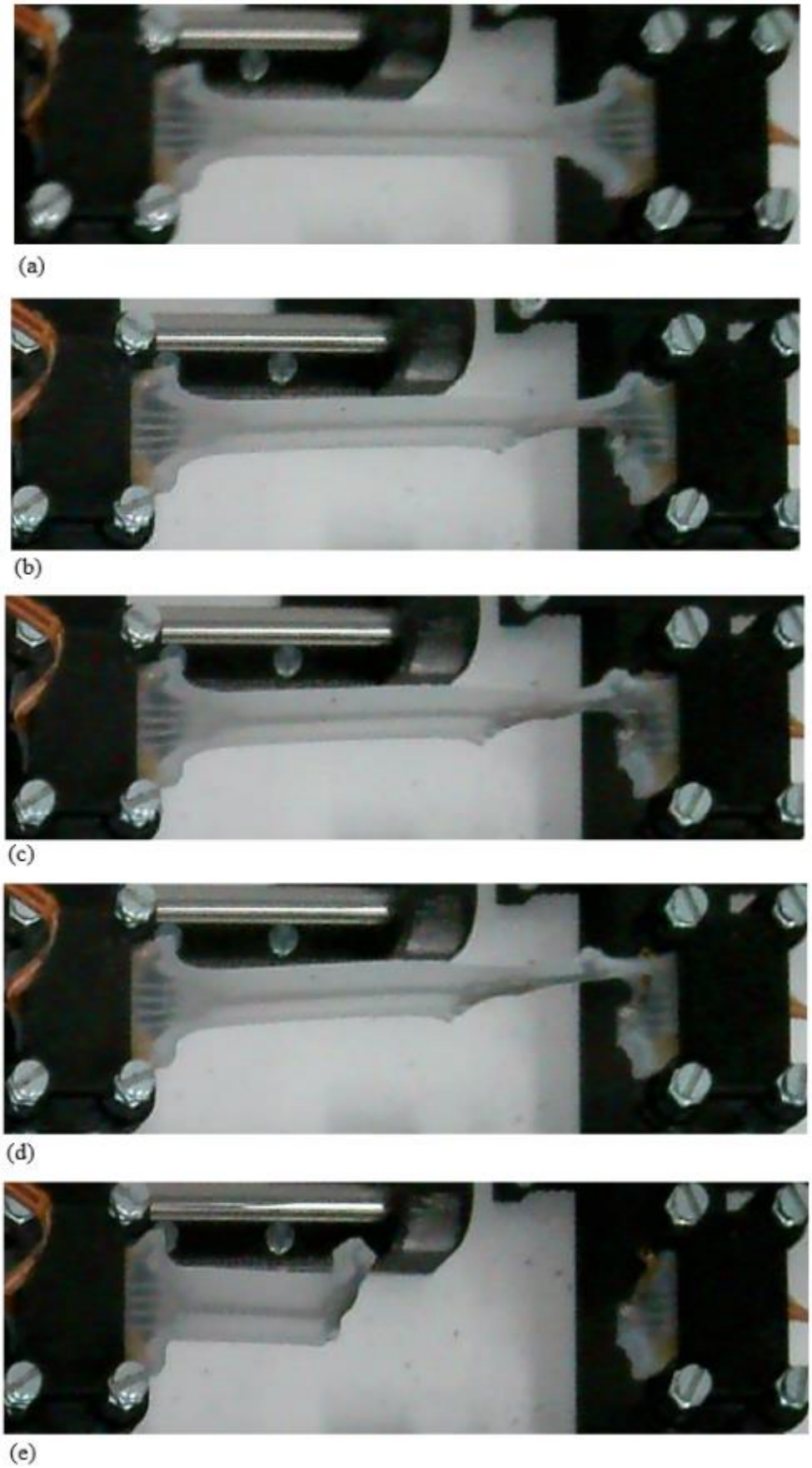

Figure 99: Batch 1 device 4 in its stretched state at 4000 (a), 4100 (b), 4200 (c), 4300 (d), and 4400 (e) cycles

Loss of adhesion between flexconnector and silicone

In an effort to reduce the deformation to the traces caused by the clamping of the devices, devices were designed in such a way that they could be clamped in the cycletesters using an area without metal traces. On Figure 100, the areas used to clamp the devices in the cycletester are indicated with red. This approach showed significant improvement in resistance measurements. Contrary to devices produced previously to the research described in this thesis, the new device design successfully stabilized resistance measurements, reducing the effect of clamping the devices. Older designs, where the entire area of the flexconnector is clamped, instead of an area laying largely to its side as shown in Figure 100, saw their resistance increase to a multitude of its original resistance when clamped. The novel designs described in this thesis, reduced this effect to a maximum of approximately 20%. Furthermore, for most devices the increasing effect disappeared completely, and was replaced with an effect of decreasing resistance when the devices were clamped. While being clamped the resistance of the novel device designs decreased in resistance, with 15% being the approximate maximal decrease observed.

However, although the novel device design successfully mitigated the problem previous designs exhibited in the clamping procedure, a secondary negative effect was discovered. This negative effect arose during cyclic testing itself. As the device was stretched, the silicone around the part of the flexconnector which was not clamped experienced significant stretching forces as well. This in turn put significant stress on the primer which function was to ensure adhesion between the flexconnector and the silicone.

Figure 100: Stretchable wire device, with areas used to clamp devices in red

During cyclic testing it was observed that after a certain number of cycles, the primer failed and the flexconnector lost connection with the silicone, thus causing the silicone to partly slide over the flexconnector. The flexconnector itself stayed rigid and did not move due to its rear end being clamped tight in the cycletester clamps. Confirmation of this movement of the flexconnector can be seen in Figure 101 and 102, black marks (consisting of oxidized liquid metal) which run in the stretch direction are noticeable on the flexconnectors.

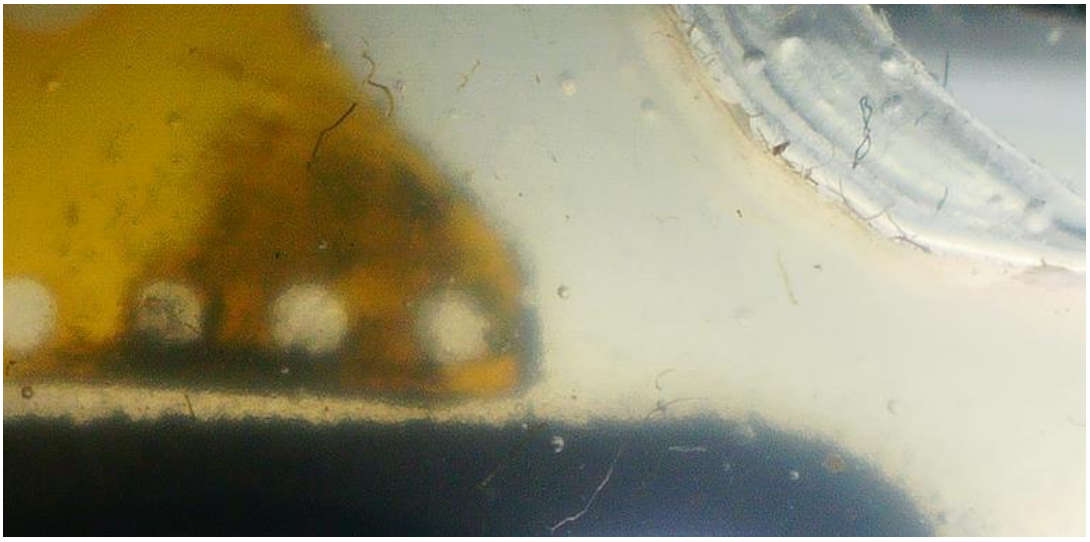

Figure 101: Batch 1 device 2, galistan marks on flexconnector after stretching

Figure 102 also shows that part of the flexconnector is no longer enclosed in silicone, as the silicone has been pulled off it during stretching. This causes the exposure of part of the flexconnector to the outside environment, presumably connecting the spacings between the flexconnector and silicone that was created to the outside environment. This in turn, could have further accelerated the oxidation of liquid metal. Furthermore, the partial vacuum that would theoretically exist in the spacings and hold the silicone and flexconnector through outside pressure, can no longer exist under such circumstances. This could yet be another factor which accelerates the whole process of loss of adhesion between the flexconnector and the silicone.

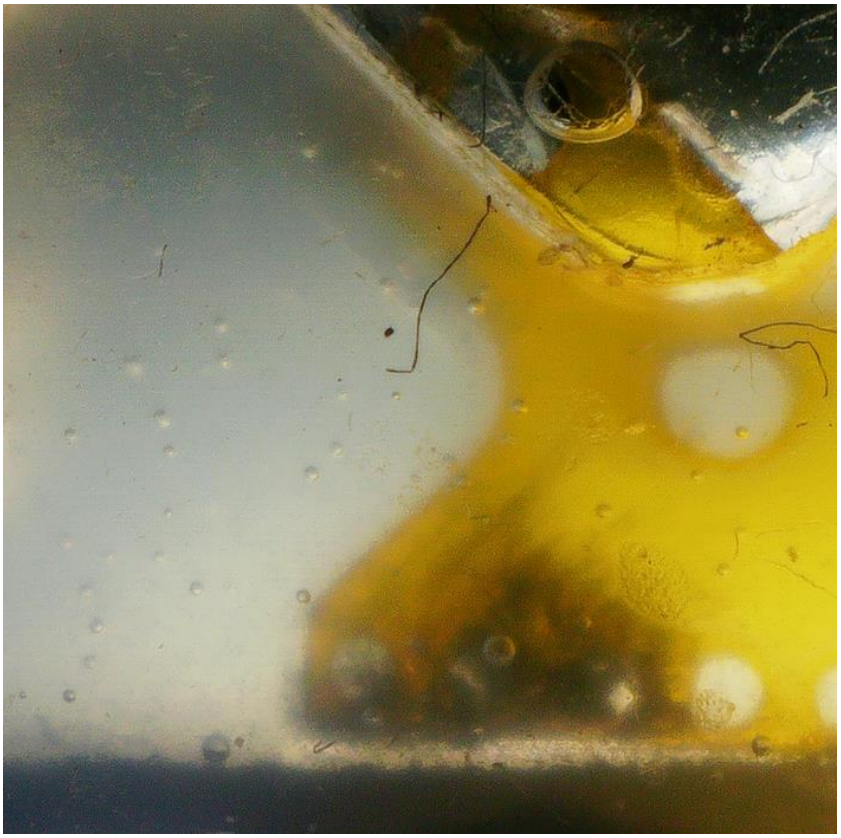

Figure 102: Batch 2 device 5, oxidated galistan on flexconnector after stretching, flexconnector partly outside silicone

The loss of adhesion between the flexconnector and the silicone inevitably creates minor spacings between them. This allows galistan to move from the traces into these spacings. Depending on the severity of the loss of adhesion, severe cases such as depicted in Figures 103 and 104 can arise, or less severe cases where only a small amount of galistan was displaced such as depicted in Figure 105. All devices that were stretch tested exhibited this migration of galistan, as is confirmed by Figure 106, which shows a reference device that was not stretch tested and thus exhibited no movement of galistan. However, one of the reference devices did exhibit a minor amount of galistan migration without stretch testing, as shown in Figure 107. This indicates that the effect of galistan migration onto the flexconnector is inherent to the devices, and furthermore greatly magnified by stretch testing.

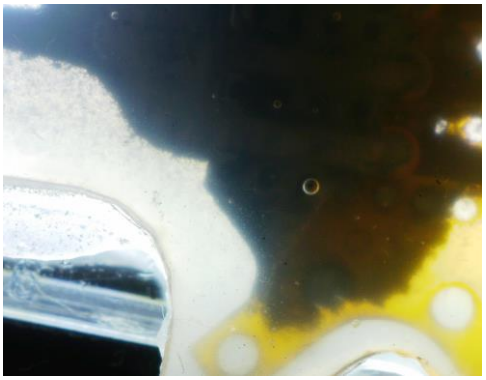

Figure 103: Batch 2 device 11, galistan migration to spacing between flexconnector and silicone

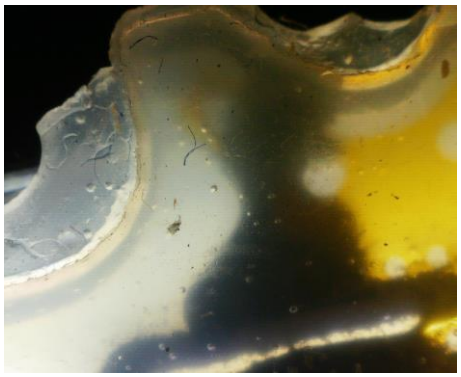

Figure 104: Batch 2 device 5, galistan migration to spacing between flexconnector and silicone

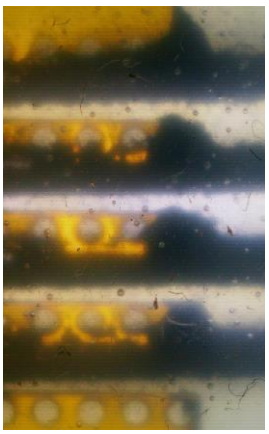

Figure 105: Batch 1 device 3, galistan migration to spacing between flexconnector and silicone

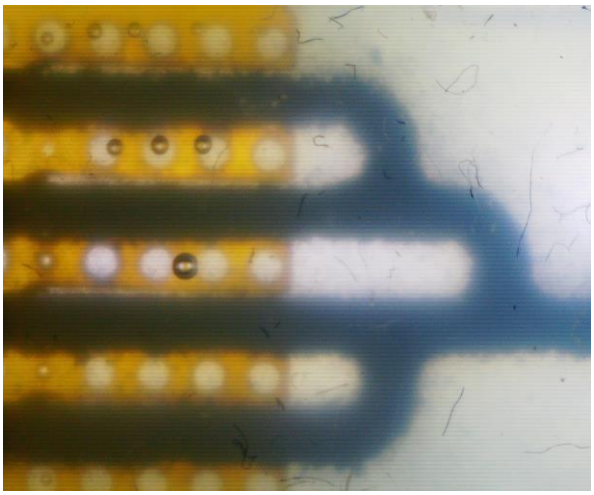

Figure 106: Batch 3 device 5, no galistan migration in reference device

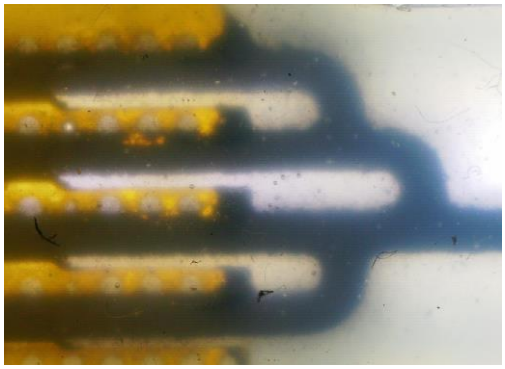

Figure 107: Batch 1 device 1, minor galistan migration in reference device

Figure 108 shows batch 3 device 12 after 5000 stretches, where a significant amount of galistan leaked into the spacing between the flexconnector and silicone. This causes possible connections between all the traces or, if sufficient galistan is displaced, the loss of connection of some contacts of the flexconnector.

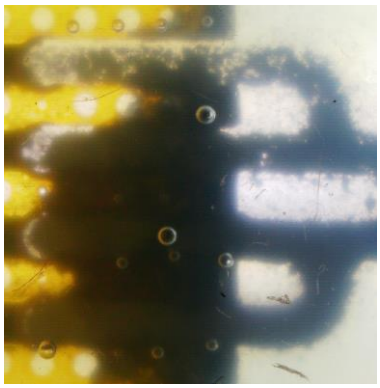

Figure 108: Batch 3 device 12, formed inter-trace connection due to galistan movement

Effect of environmental stress factors

Batch 2 devices 2, 4, 6, 8 and 10 were exposed to stress factors in the QUV tester. All those devices lost functionality before reaching 1000 cycles, as opposed to other devices from the same batch. QUV exposure proved to exhibit negative effects on the lifetime of the devices. As can be seen on Figure 109, all devices show signs of severe galistan movement, degrading the galistan tracks and presumably causing failing device functionality. The images were taken after 1000 stretching cycles had been reached and all devices had failed.

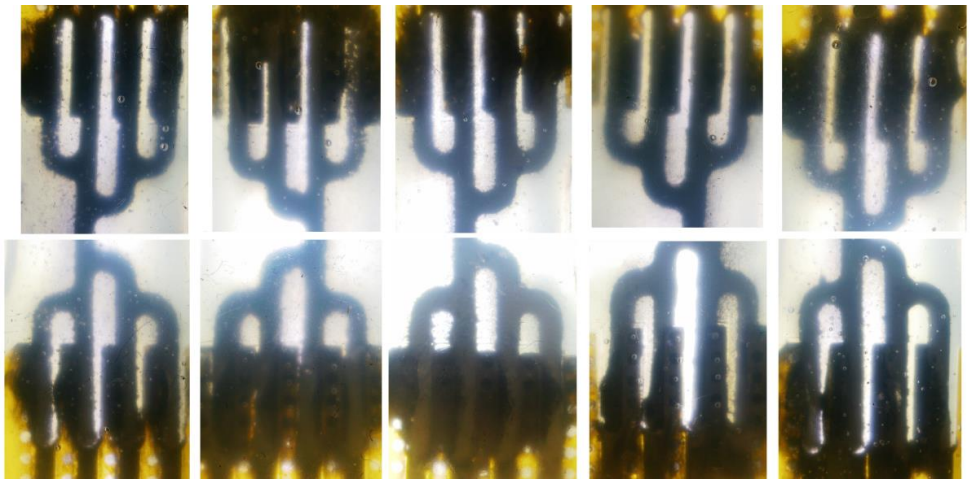

Figure 109: QUV exposed and stretched devices (1000 cycles). Flexconnectors depicted in a vertical arrangement. The flexconnectors shown represent devices from left to right: 2, 4, 6, 8, 10

In Figure 110, devices from batch 2 which were not exposed in the QUV chamber are shown. The devices were stretched 1000 cycles, after which devices 1 and 3 failed. Devices 5, 11 and 12 retained functionality for several thousand cycles. Although galistan movement is also observed for these devices, the amount that is displayed is presumably less. This is presumed due to the lesser amount of blackening of the flexconnectors on average, when compared to the QUV exposed devices after 1000 cycles.

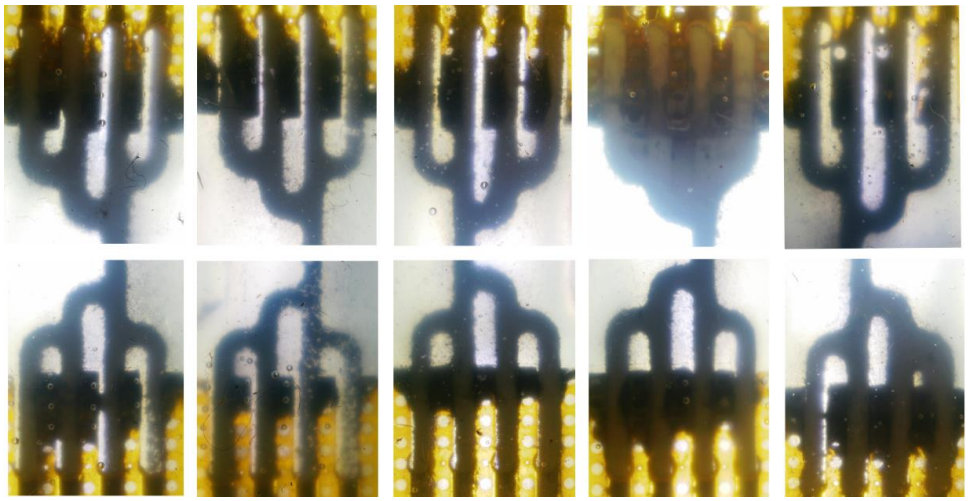

Figure 110Stretched devices (1000 cycles). Flexconnectors depicted in a vertical arrangement. The flexconnectors shown represent devices from left to right: 1, 3, 5, 11, 12

Figure 111 shows close ups of devices from batch 3 which were exposed in the damp heat chamber after 500 cycles of cyclic testing. Compared with devices from batch 3 after 500 cycles which were not exposed in the damp heat chamber, shown in Figure 112, there appears to be more oxidation forming on the flexconnectors. This implies that the heat and/or humidity in the damp heat chamber, affected the primer and therefore caused accelerated loss of adhesion between the flexconnectors and the silicone.

With the exception of the rupture, all failures are, presumably and at least in part, due to the loss of adhesion between the flexconnectors and the silicone which occurred during stretch testing and was accelerated by exposing devices to environmental factors.

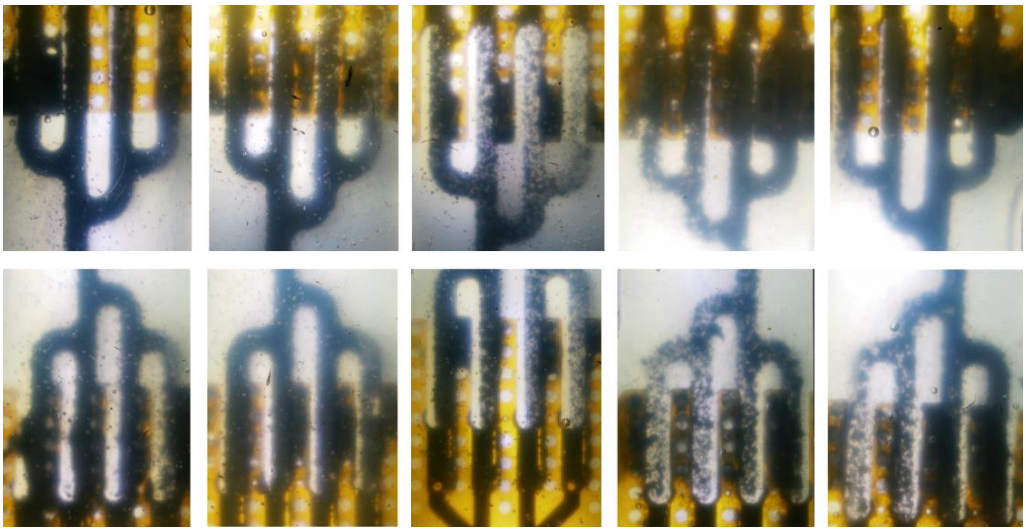

Figure 111: Stretched devices (500 cycles). Flexconnectors depicted in a vertical arrangement. The flexconnectors shown represent devices from left to right: 2, 4, 7, 8, 10

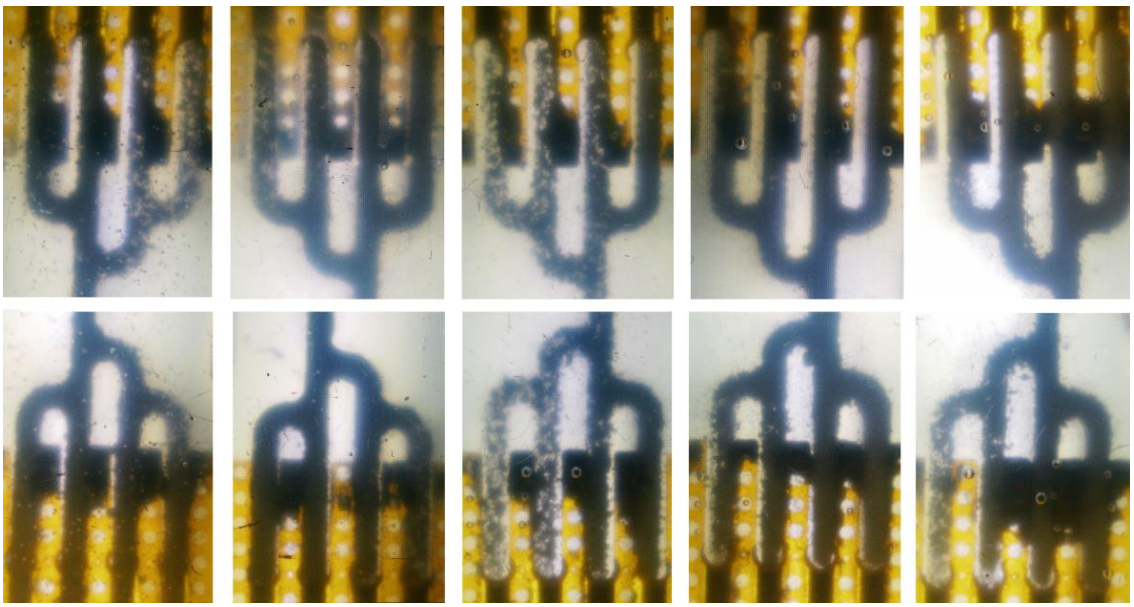

Figure 112: Stretched devices (500 cycles). Flexconnectors depicted in a vertical arrangement. The flexconnectors shown represent devices from left to right: 3, 6, 9, 11, 12

8 Conclusion

The investigation of the stretchable LED strips revealed that their failure primarily resulted from the detachment between the silicone and the LEDs. This allowed the galinstan to lose contact with the copper contacts of the LEDs. Furthermore, the stretchable LED strips had significantly lower stretch capability compared to the stretchable wires. Upon subjecting these devices to the damp heat test, the oxidation process of the galinstan traces was accelerated. Consequently, the devices became incapable of sustaining stretch, presumably due to the presence of an oxide layer that reduced the adhesion between the traces and the copper LED contacts. However, further investigation is required to better understand the influence of the oxide layer.

Contrary to expectations, the QUV test appeared to extend the lifetime of these devices. This unexpected outcome can be attributed to the increased stiffness of the silicone, which reduced deformation around the LEDs. Furthermore, this study revealed that unlike stretchable wires, the stretchable LED strips failed to function when stretched to 150%. Moreover, conducting stretch tests at 150% stretch revealed that UV radiation had a significantly greater influence on the silicone than increased temperature and humidity.

All stretchable wire devices exhibited an overall upward trend in their measured resistances during their lifetime. However, when devices were taken out of the cycletester setup for a certain period of time to perform other observations, the trend seen was that resistance partly decreased again. The exceptions, where devices increased in resistance after being taken out, are most likely anomalies caused by the uneven distribution of forces during clamping in the cycletest setup or during the intermediate observations.

Concerning the static stretch resistance, all stretchable wire devices exhibited an increasing resistance during a certain period of being held in a stretched state. The most significant rise in resistance occurred during the first 10 minutes, after which most devices reached an equilibrium. There were some anomalies where resistance rose for a longer duration of time, however these were likely caused by the inadequate mounting of the devices in the clamps of the cycletesters. Inadequate clamping occurred when the four bolts used in the clamping mechanism did not exercise an equal amount of force on the respective side of the device. This unequal amount of force arose due to the slightly varying thickness of devices throughout their length.

Ruptures can occur at the corners of the stretched area, even though they were rounded in the final design. Loss of adhesion between the flexconnector and silicone resulted in galistan migration to the flexconnectors, which caused potential unintended connections between traces and loss of connection for others. Furthermore, exposure to environmental stress factors, such as in the QUV tester and damp heat chamber, accelerated the failure process by degrading the primer and thus the adhesion between components and silicone. Overall, most devices failed due to the loss of adhesion between the flexconnectors and silicone, accompanied by galistan displacement. This study highlights the importance of addressing these failure mechanisms to improve the reliability and lifetime of the devices.

The test results indicate significant differences among devices from the same batch, highlighting the need for further research to improve the production process and reduce failure rates. Specific areas for optimization include the manual spraying of primer on flexconnectors, alignment techniques for flexconnectors and rigid components, mold alignment under the spraycoater, and prevention of air

bubbles formation in the silicone. Additionally, bend or twist tests to examine the impact of bending and twisting on the devices must still be performed. Furthermore, the influence of vibration on the devices in combination with cycletests, bend tests, or twist tests can be researched. Regarding the encapsulation of rigid components, research should be conducted to evaluate the effect of stress factors on different types of contacts. Finally, more research into the formed oxide layer is needed. Currently, not much is known about the exact influence of the oxide layer on the lifetime of the devices. Furthermore, the influence of the formed oxide layer on the adhesion with the copper contacts must be investigated. Hereafter, additional research can be done on methods to mitigate the formation of the oxide layer.

References

[1] J. A. Rogers, T. Someya, and Y. Huang, “Materials and Mechanics for Stretchable Electronics,” Science, vol. 327, nr. 5973, pp. 1603-1607, 2010.

[2] Y. Zhao, A. Kim, G. Wan, and B. C. K. Tee, „Design and applications of stretchable and self-healable conductors for soft electronics,” Nano Convergence, vol. 6, 2019.

[3] Y. Liu, M. Pharr, and G. A. Salvatore, „Lab-on-Skin: A Review of Flexible and Stretchable Electronics for Wearable Health Monitoring,” ACS Nano, vol. 11, pp. 9614-9635, 2017.

[4] Y. J. Hong, H. Jeong, K. W. Cho, N. Lu, and D.-H. Kim, "Wearable and Implantable Devices for Cardiovascular Healthcare: from Monitoring to Therapy Based on Flexible and Stretchable Electronics," Advanced Functional Materials, vol. 29, nr. 19, 2019.

[5] T. Vervust, G. Buyle, F. Bossuyt and J. Vanfleteren, „Integration of stretchable and washable electronic modules for smart textile applications,” The Journal of The Textile Institute, vol. 103, pp. 1127-1138, 2012.

[6] C. Heylands, Integratie van een sensoroplossing in rekbare elektronica om de functionaliteit van een zachte grijper uit te breiden [master's thesis], Diepenbeek: Gezamenlijke opleiding Industriële Ingenieurswetenschappen UHasselt & KU Leuven, 2022.

[7] T. Q. Trung and N.-E. Lee, "Materials and devices for transparent stretchable electronics," Journal of Materials Chemistry C, vol. 5, nr. 19, pp. 2202-2222, 2017.

[8] S. Nagels, R. Ramakers, K. Luyten, and W. Deferme, “Silicone devices: A scalable diy approach for fabricating self-contained multi-layered soft circuits using microfluidics,” presented at the 2018 CHI Conference on Human Factors in Computing Systems, Montreal QC, Canada, Apr. 2018, pp. 1–13.

[9] J.-H. Ahn and J. H. Je, "Stretchable electronics: materials, architectures and integrations," Journal of Physics D: Applied Physics, vol. 45, nr. 10, 2012.

[10] Smooth-On, "Dragon Skin Series," Jul. 2022.

[11] Smooth-On, "Dragon Skin™ FX-Pro™," Jul. 2022.

[12] T. Liu, P. Sen, and C.-J. Kim, “Characterization of Nontoxic Liquid-Metal Alloy Galinstan for Applications in Microdevices,” Journal of Microelectromechanical Systems, vol. 21, nr. 2, pp. 443-450, 2012.

[13] Y. Lin, J. Genzer, and M. D. Dickey, "Attributes, Fabrication, and Applications of Gallium-Based Liquid Metal Particles," Advanced Science, vol. 7, nr. 12, 2020.

[14] C. Majidi, „Mechanics of fluid-elastomer systems in soft robotics,” Robotic Systems and Autonomous Platforms, pp. 425-448, 2019.

[15] S. Vandervoort, Analyse van het temperatuursverloop van galinstan door variërende weerstand in zachte en rekbare elektronica [master's thesis], Diepenbeek, Gezamenlijke opleiding Industriële Ingenieurswetenschappen UHasselt & KU Leuven, 2022.

[16] Secure Systems & Technologies, "MIL-STD-810." [Online]. Available: https://www.google.com/url?sa=t&rct=j&q=&esrc=s&source=web&cd=&ved=2ahUKEwjh2rzD7fT8AhVLgv0HHUhdDQgQFnoECDUQAQ&url=https%3A%2F%2Fwww.apitech.com%2Fglobalassets%2Fdocuments%2Fproducts%2Fsecure-systems--information-assurance%2Fsst%2Fmil-std-810-overview-iss-5.pdf&usg=AOvVaw0PCzE9b6eRVTA2DkxjddgG. [Consulted 10 April 2023].

[17] B. Pitterman (Telcordia Technologies), "Telcordia Technologies: The Journey to High Maturity."

[18] W. D. van Driel and M. Y. Mehr, Reliability of Organic Compounds in Microelectronics and Optoelectronics. 2022.

[19] T. Kaneko, S. Ito, T. Minakawa, N. Hirai, and Y. Ohki, "Degradation mechanisms of silicone rubber under different aging conditions," 2019.

[20] F. B. Albuquerque and H. Shea, "Influence of humidity, temperature and prestretch on the dielectric breakdown strength of silicone elastomer membranes for DEAs," 2020.

[21] R. Saleh, M. Barth, W. Eberhardt, and A. Zimmermann, "Bending Setup for Reliability Investigation of Flexible Electronics," 2021.

[22] J. H. Chow, J. Meth, and S. K. Sitaraman, „Twist Testing for Flexible Electronics," in Electronic Components and Technology Conference (ECTC), 2019.

[23] K. D. Harris, A. L. Elias, and H.-J. Chung, "Flexible electronics under strain: a review of mechanical characterization and durability enhancement strategies," 2015.

[24] INVT, „Overview of the Damp Heat Test," 2020. [Online]. Available: https://www.invt.com/news/overview-of-the-damp-heat-test-75. [Consulted 23 March 2023].

[25] Q-Lab, "QUV Accelerated Weathering Tester," [Online]. Available: https://www.q-lab.com/en-gb/products/quv-weathering-tester/quv. [Consulted 16 April 2023].

[26] Q-Lab, "Test Standards for the QUV Accelerated Weathering Tester," [Online]. Available: https://www.q-lab.com/en-gb/resources/standards/category/quv-weathering-tester. [Consulted 16 April 2023].

[27] ISO, "ISO 4892-3:2016(en) Plastics — Methods of exposure to laboratory light sources — Part 3: Fluorescent UV lamps," 2016. [Online]. Available: https://www.iso.org/obp/ui/#iso:std:iso:4892:-3:ed-4:v1:en. [Consulted 16 April 2023].

[28] TinyTronics B.V., "WS2812B Digital 5050 RGB LED - separate," 2023. [Online]. Available: https://www.tinytronics.nl/shop/en/components/leds/leds/ws2812b-digital-5050-rgb-led-separate. [Consulted 13 May 2023].

[29] “Trotec Laser Speedy 100R 30W Co2 laser engraver laser cutter,” GEHT Marketplace, [Online]. Available: https://gehtmarketplace.com/category/laser-systems-by-application-areas/material-processing-and-industrial-laser-systems/marking-and-engraving/listing/2ec4cbb55f6a6ac20a56a0e4e4c72392. [Consulted 16 April 2023].

[30] WorldSemi, „WS2812B Ver. No.: V5 Intelligent control LED integrated light source”.

Appendix A: Production process

1 Materials

The following materials are needed for the production of a batch:

- lab coat,
- latex gloves,
- paper,
- tape,
- Fusion 360 software,
- Inkscape software,
- plexi sheets,
- vinyl,
- laser cutter (Trotec speedy 100R),
- 24 flexconnectors,
- 12 LEDs,
- pipette,
- measuring cup,
- petri dish,
- cotton swabs,
- water,
- 1M HCl with liquid metal,
- oven,
- primer,
- airbrush,
- fume hood,
- silicone (Dragon Skin),
- cup,
- scale,
- silicone mixer,
- automatic spray coater and syringe pump with liquid metal,
- metal stencil,
- isopropanol.

2 Method

The method described in this chapter will be the method used to produce the stretchable LED strips. The method for producing the stretchable wire is similar with the exception of the steps involving the LED component.

2.1 Designing and production of the molds

The first step of the production process is to design the devices and molds in a software program. A suitable program to design these in is Fusion 360. Other programs with the same functionality can also be used.

1. Design the device outlines, liquid metal traces outlines and the components outlines.

2. Add the shape of the molds to the design. This design will be further referred to as the ‘full design’.

3. Copy this design and remove all lines until only the outline of the mold with the screw holes remains. This design will be further referred to as the ‘base plate design’. Figure A.1.a shows this design.

4. Copy the ‘full design’ and remove the traces and components outlines from the design. The result is the design for the bottom and top mold. This design will be further referred to as the ‘mold design’. Figure A.1.b shows this design.

5. Copy the ‘full design’ and remove the outlines of the devices, and screw holes. This design will be further referred to as the ‘engraving design’. Figure A.2.a shows the design.

6. Copy the ‘full design ‘ and remove the devices outlines and components outlines. The result is the stencil design and will be further referred to as the ‘stencil design’. Figure A.2.b shows this design.

7. Export the ‘base plate design’, ‘mold design’, and ‘engraving design’ to Inkscape and remove possible double lines from the drawings.

8. Send the ‘base plate design’ to the laser cutter.

9. Choose the thickness of the plexi plate and cut out the base plate. The thickness of the base plate does not influence the final height of the devices. However, the base plate should be thick enough to not bend.

10. Send the ‘mold design’ to the laser cutter.

11. The molds should be cut out twice since a top and bottom mold are needed. The thickness of the bottom and top mold can vary depending on the design of the device.

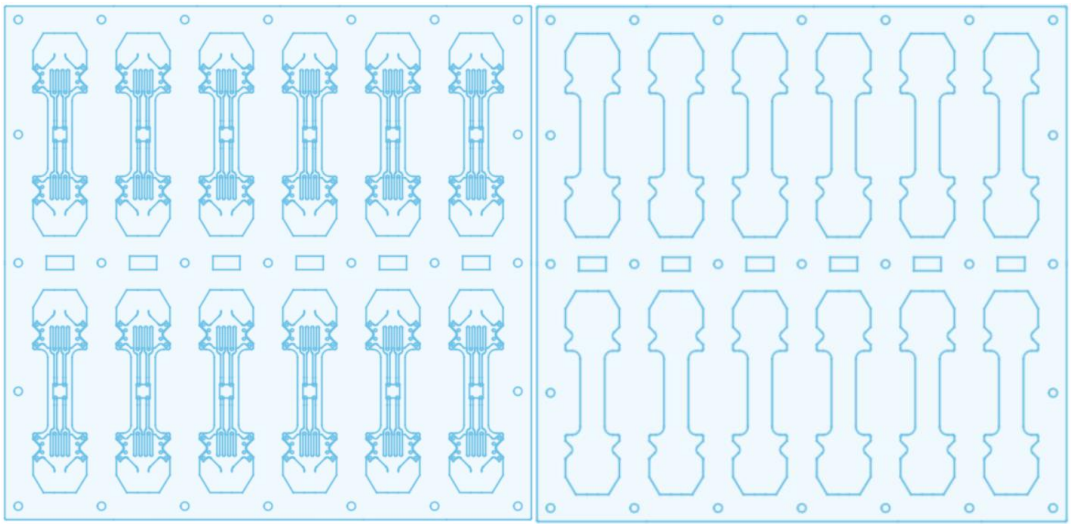

Figure A.1.a: full design, Figure A.1.b: mold design

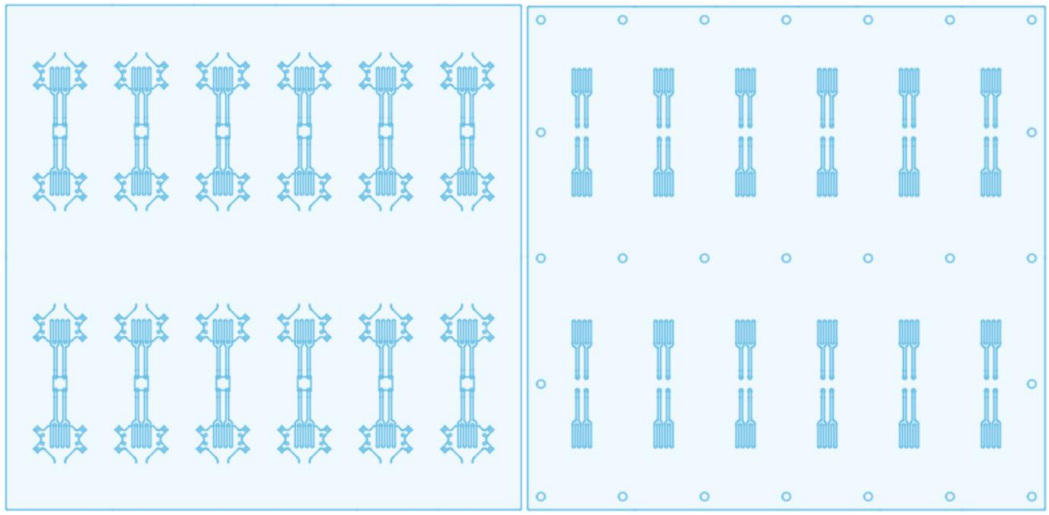

Figure A.2.a: engraving design, Figure A.2.b: stencil design

2.2 Engraving

To ensure that the components are placed on the correct positions, vinyl will be placed in the ground plate and engraved.

1. Cut out vinyl of the same size as the base plate.

2. Tape this vinyl with the sticky side upwards on the base plate.

3. Send the ‘engraving design’ to the laser cutter and engrave the vinyl. The outlines of the mold should not be engraved but can be used to align the base plate in the laser cutter with the drawing on the PC. Figure A.3.a shows the laser cutter. Figure A.3.b shows the base plate with the vinyl positioned in the laser cutter.

Figure A.3.a: Trotec speedy 100R, Figure A.3.b: base plate with vinyl in the laser cutter

2.3 Prewetting

To achieve optimal adhesion between the liquid metal and the components, a prewetting procedure needs to be conducted.

1. Put on a lab coat and latex gloves.

2. Set the oven to 60°C.

3. Cover the tabletop of the fume hood with paper.

4. Fill the petri dish with 1M HCl and use the pipette to transport the liquid metal from the bottle to the petri dish.

5. Fill a measuring cup with water.

6. Submerge the width part of the flexconnectors into the HCl and use the pipette to suck up the liquid metal and release it on the copper contacts of the flexconnector. HCl is an acid that will remove the possible oxide layer on the copper contacts and will prevent the liquid metal from oxidizing. Figure A.4 shows the bottle with the liquid metal inside the HCl. Repeat this until there is liquid metal on all contacts.

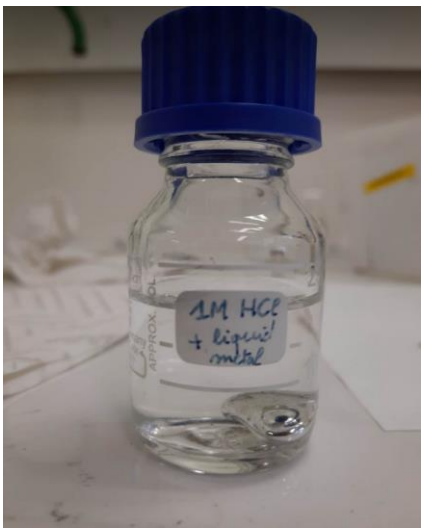

Figure A.4: bottle with 1M HCl and liquid metal

7. Use a cotton swab to remove the excess amount of liquid metal from the contacts. A thin flat layer of liquid metal on the contacts is sufficient.

8. Submerge the flexconnectors into the water to remove the HCl.

9. Place the flexconnector in the oven. Let them stay in the oven for a minimum of 10 minutes.

Keep repeating steps 5, 6, 7, and 8 until all flexconnectors are prewetted. Repeat these steps for all the other components that will be added to the devices. HCl is an acid that can damage some components, be careful not to damage the used components. Figure A.5 shows an LED being prewetted. Figure A.6.a shows a flexconnector before the prewetting process and figure A.6.b shows the same flexconnector after the prewetting process. Note that the four copper contacts on the width part of the connectors have a silver-looking liquid metal layer on top of them after the prewetting process.

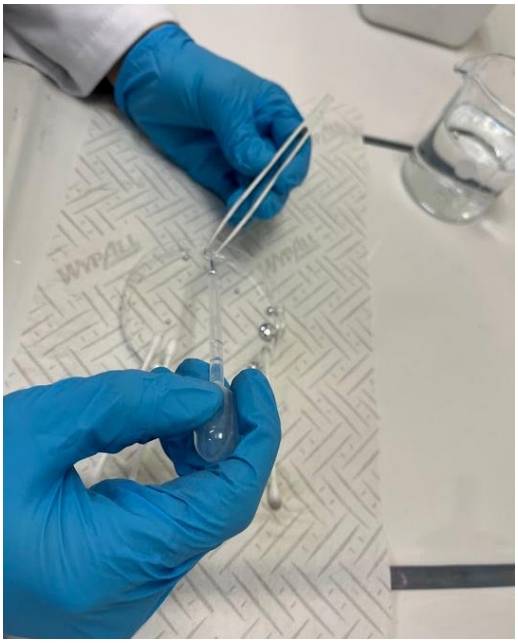

Figure A.5: LED being prewetted

Figure A.6.a: flexconnector before the prewetting process,
Figure A.6.b: flexconnector after the prewetting process

2.4 Primer spraying

The next step is to spray primer on the components to ensure that the silicone will attach to the components.

1. Put on a lab coat and latex gloves.

2. Tape the tails of the flexconnectors to a clean sheet of paper. The side with the prewetted contacts should face downwards. Figure A.7 shows the flexconnectors taped to the paper sheet. Figure A.8 shows the LEDs being positioned to be sprayed with primer.

Figure A.7: flexconnectors positioned to apply primer

Figure A.8: LEDs positioned to apply primer

3. Cover the tabletop of the fume hood with paper.

4. Connect the bottle with primer to the airbrush. Figure A.9 shows the bottle with primer. Put a pressure of 5 bar on the airbrush.

Figure A.9: bottle with primer

5. Spray the primer two times horizontally over the components under the fume hood.

6. Let it dry for one hour.

2.5 Placement of the components

The next step is to place the components on the engraved vinyl.

1. Put on a lab coat and latex gloves.

2. Remove the tape from the flexconnecotors.

3. Place the components with the side with the contacts downwards on the vinyl. It is important to place them as precisely as possible otherwise the devices may not function due to the misalignment of the components with the traces. Figure A.10 shows the result.

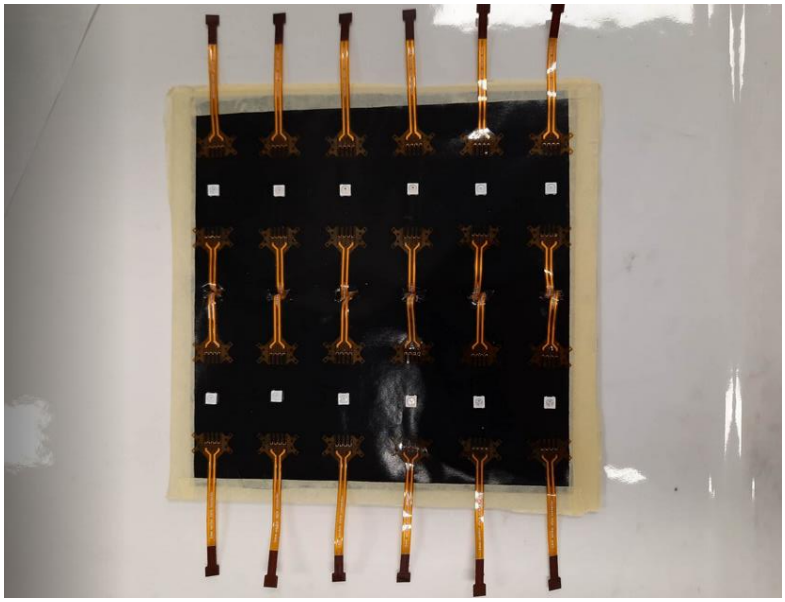

Figure A.10: components placed on the vinyl

2.6 Silicone pouring (first layer)

1. Cover the lab table with paper.

2. Place the top mold on the baseplate with the vinyl. Make sure that the top mold can not move during the silicone pouring process. To ensure that this is the case, the mold can be taped or screwed via the screw holes in the mold and baseplate to each other. Figure A.11 shows the result of this step.

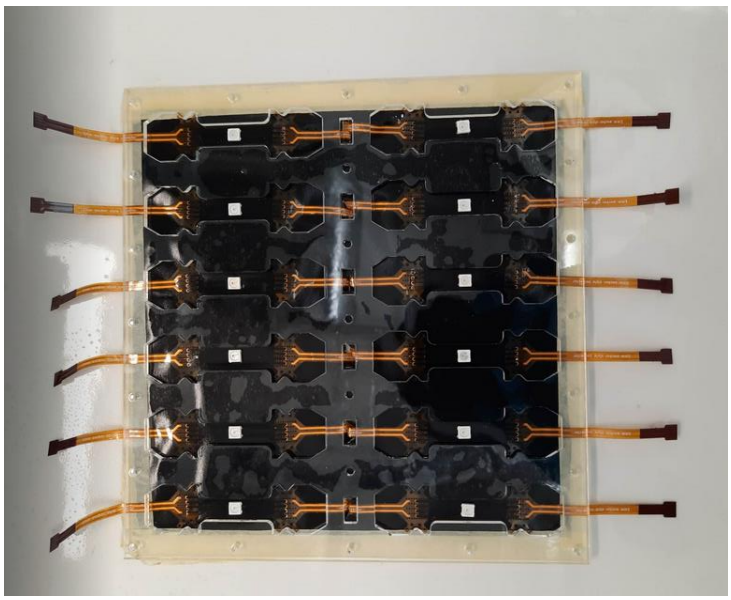

Figure A.11: top mold placed on the baseplate

3. Dragon Skin silicone consists of two liquids, liquid A and B, that need to be combined. Place a cup on the scale, stir liquid A in its bottle and pour 31 g of it in the cup. Next, stir liquid B and pour 31 g of it into the cup which already contains liquid A.

4. Place the cup in the mixer and mix the cup. Use as settings: 2000 rpm and 60 second. Figure A.12 shows the speed mixer.

Figure A.12: speed mixer

5. Pour the mixed silicone onto the vinyl.

6. Use a long cotton swab or plexi plate to remove the excess amount of silicone from the mold. Do this slowly otherwise silicone will be pulled out of the molds which will result in a thinner silicone layer. Furthermore, possible formed air bubbles can be removed with the tip of the scalpel. However this must be done before the silicone becomes too viscous.

7. Let the silicone cure.

2.7 Liquid metal spraying

1. Put on a lab coat and latex gloves. It is important to replace the gloves once they are contaminated.

2. Cover the fume hood in paper to keep it clean.

3. Carefully remove the baseplate and the vinyl sheet. The devices should stay in the mold.

4. Place the stencil on the mold and attach them to the mold with tape or screws. Figure A.13 shows the stencil taped to the mold. Make sure that the tails of the flexconnectors are also covered.

Figure A.13: stencil taped to the mold

5. Connect the syringe pump with the automatic spray coater. Connect the automatic spray coater with the N_2 gas supply. Figure A.14 shows the spray coater with the syringe pump attached to it.

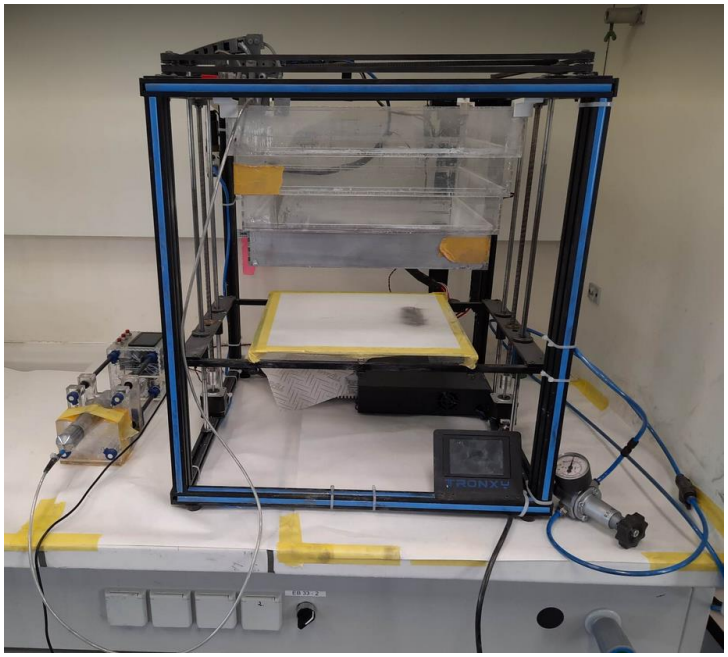

Figure A.14: spray coater with syringe pump

6. To properly position the plate on the platform, lower the pressure to 0 bar and press ‘stop’ in the menu of the syringe pump.

7. Place the mold with the devices and stencil on the platform of the spray coater.

8. Move the platform up until the final 2 plastic casings remain via the menu of the spray coater.

9. Make sure that there is more than 10 ml galinstan in the syringe. Execute the G-code that contains the path via the menu of the spray coater. Appendix B contains the G-code.

10. The sprayer can stutter in the beginning. Position the mold so that the first sprayed column is not on the mold.

11. Once the mold is properly positioned, make sure that the pressure is set to 3.5 bar and press ‘start’ in the syringe menu.

12. Execute the code via the spray coater menu. Figure A.15: shows the result of the spraying process.

Figure A.15: result spraying process

13. Remove the stencil from the mold under the fume hood . Clean the liquid metal metal from the stencil with isopropanol so that it can be reused.

14. Possible created shorts can be removed. Figure A.16 shows a possible short circuit between the traces. The excess amount of liquid metal can be removed with the tools shown in figure A.17.

15. Clean the workspace. Use isopropanol to remove possible liquid metal contamination.

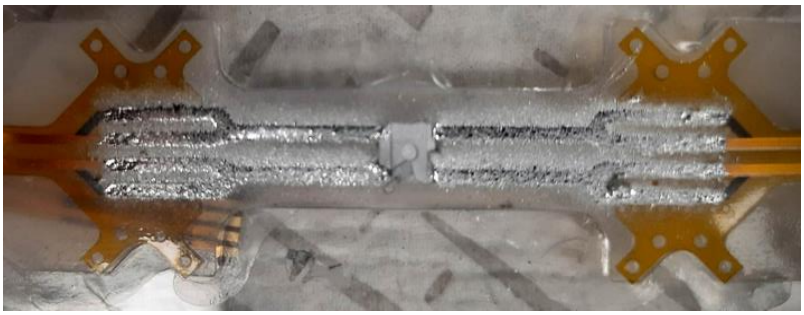

Figure A.16: possible short circuits between the traces

Figure A.17: tools that can be used to remove unwanted liquid metal

2.8 Silicone pouring (second layer)

1. Place the bottom mold on the top mold. Make sure that the molds can not move during the silicone pouring process. To ensure that this is the case, the molds can be taped or screwed via the screw holes to each other.

2. Place a cup on the scale, stir liquid A and pour 31 g of it into the cup. Next, stir liquid B and pour 31 g of it into the cup which contains liquid A.

3. Place the cup in the mixer and mix the cup. Use 2000 rpm and 60 seconds as settings.

4. Pour the mixed silicone onto the first silicone layer of the devices.

5. Use a long cotton swab or plexi plate to remove the excess amount of silicone from the mold. Do this slowly otherwise silicone will be pulled out of the molds which will result in a thinner silicone layer. Furthermore, possible formed air bubbles can be removed with the tip of the scalpel. However this must be done before the silicone becomes too viscous.

6. Let the silicone cure.

7. Once the silicone is cured, remove the devices from the molds and cut away the excess amount of silicone from the devices.

8. Clean the workspace.

Appendix B: G-code spray coater

```
FLAVOR:Marlin
M82 ;absolute extrusion mode
G28 X0 Y0 ;home on the X and Y axes
G92 E0
G1 F1500 E-6.5 ;set speed
M204 S10000 ;set acceleration
G1 X30 Y50 ;get cleared from the edges
M106 P1 S255 ;open the valve and start syringe pump
G4 P4000;

G1 X50 Y60;
G1 X50 Y220;
G1 X81 Y220;
G1 X81 Y60;
G1 X112 Y60;
G1 X112 Y220;
G1 X143 Y220;
G1 X143 Y60;
G1 X174 Y60;
G1 X174 Y220;
G1 X205 Y220;
G1 X205 Y60;
G1 X236 Y60;
G1 X236 Y220;

M107 P1 ;close the valve and stop syringe pump
M204 S4000 ;reset the acceleration
G28 X0 Y0 ;home on the X and Y axis
M82 ;absolute extrusion mode
```

Appendix C: Arduino code for the LED

```
#include <FastLED.h>
#define LED_PIN1 8
#define LED_PIN2 9
#define LED_PIN3 10
#define LED_PIN4 11
#define NUM_LEDS 1

CRGB device1[NUM_LEDS];
CRGB device2[NUM_LEDS];
CRGB device3[NUM_LEDS];
CRGB device4[NUM_LEDS];

void setup() {
  FastLED.addLeds<WS2812B, LED_PIN1, GRB>(device1, NUM_LEDS);
  FastLED.addLeds<WS2812B, LED_PIN2, GRB>(device2, NUM_LEDS);
  FastLED.addLeds<WS2812B, LED_PIN3, GRB>(device3, NUM_LEDS);
  FastLED.addLeds<WS2812B, LED_PIN4, GRB>(device4, NUM_LEDS);

  Serial.begin(9600);
}

void loop() {
  device1[0] = CRGB::White;
  FastLED.show();
  device2[0] = CRGB::White;
  FastLED.show();
  device3[0] = CRGB::White;
  FastLED.show();
  device4[0] = CRGB::White;
  FastLED.show();
}
```

Appendix D: Arduino code for the cycletesters (stretchable LED strips)

```
#include <AccelStepper.h>
//Define stepper motor DRV8825
#define dirPin 2
#define stepPin 3
#define motorInterfaceType 1
AccelStepper stepper(motorInterfaceType, stepPin, dirPin);
#define M2 4
#define M1 5
#define M0 6
#define stepperMaxSpeed 150 // determines max speed of stepper motor
#define stepperSpeed 150// determines actual speed of stepper motor, decrease to increase torque
#define microStep 1
String inString = "";

void setup() {
  pinMode(M0, OUTPUT);
  pinMode(M1, OUTPUT);
  pinMode(M2, OUTPUT);

  digitalWrite(M0, LOW);
  digitalWrite(M1, LOW);
  digitalWrite(M2, LOW);

  Serial.begin(9600);

  stepper.setMaxSpeed(stepperMaxSpeed*microStep);
  stepper.setAcceleration(2000*microStep);
}

void loop() {
  while(Serial.available() > 0){
    char inChar = Serial.read();
    inString += inChar;
    if (inChar == '\n') {
      int value = inString.toInt();
      if(value ==0){
        Serial.print("FIN\r\n");
      }
      if( value == 1){
        stepper.moveTo(20*microStep);
        stepper.runToPosition();
        Serial.print("FIN\r\n");
      }
      else if( value == 2){
```

```
      stepper.moveTo(0);
      stepper.runToPosition();
      Serial.print("FIN\r\n");
    }
    else{
      int cycles = value/20;
      for (int i =0; i<cycles; i++){
        stepper.moveTo(20*microStep);
        stepper.runToPosition();
        stepper.moveTo(0);
        stepper.runToPosition();
      }
      stepper.setCurrentPosition(0);
      Serial.print("FIN\r\n");
    }
    inString = "";  //reset inString
  }
 }
}
```

Appendix E: Labview code (stretchable LED strip)

Figure E.1 shows the front panel of the Cycletester_synchronous.vi. The port of the digital multimeter must be selected in the “DMM port” input, the port of the multiplexer must be selected in the “Multiplexer port” input, and the ports of all the used cycletesters must be selected in the “Cycletester ports”. Furthermore, in the “Function” input, the preferred measurement unit can be selected and the path to the text file where the measurements will be stored can be selected. Finally, the number of cycles between each measurement, the number of cycles between images, and the maximal number of cycles that will be executed can be selected.

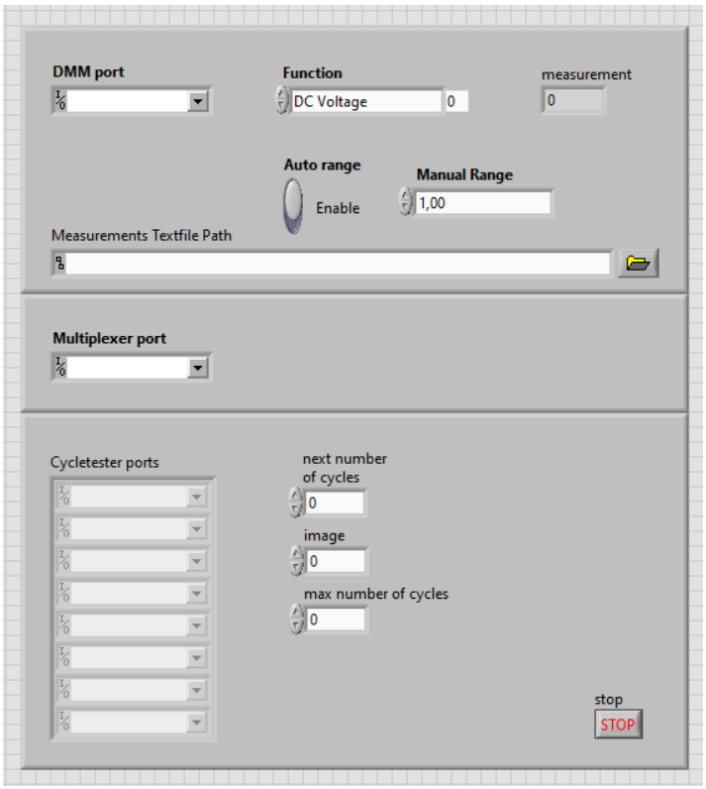

Figure E.1: Cycletester_synchronous vi

The Cycletester_synchronous vi consists of a while loop that contains a case structure in it. The case structure has three cases: “INIT”, “ACQ”, and “FIN”. The purpose of the “INIT” case is to initialize the multimeter and to send the required amount of steps to the arduino of the cycletesters. Figure E.2 shows the block diagram with the “INIT” case visible. The “INIT” case will only be executed at the start of the program.

Figure E.3 illustrates the block diagram with the “ACQ” case visible. In this case the read_measure subvi will be executed in a for loop. The for loop will be executed for each connected cycletester. Furthermore, depending on the state of the stop button and the current cycle number the next case will be “ACQ” again or will be “FIN”. Finally, figure E.4 shows the block diagram with the “FIN” case visible. This case will only be executed when the stop button on the front panel is pressed.

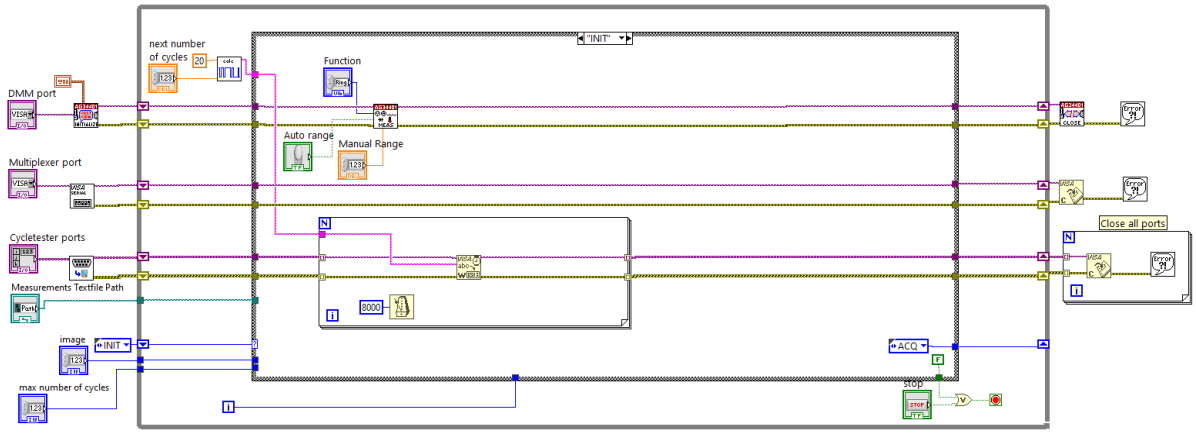

Figure E.2: block diagram of the Cycletester_synchronous vi with the “INIT” case visible

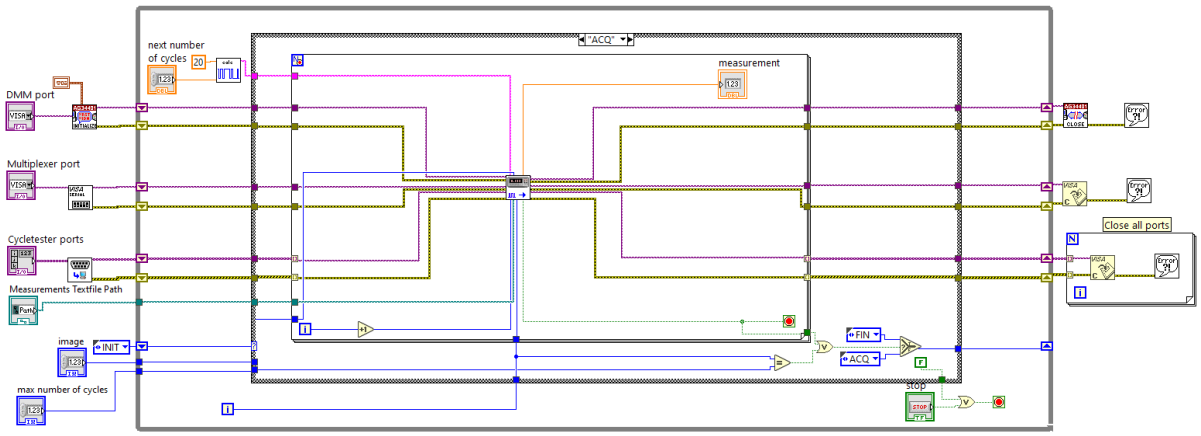

Figure E.3: block diagram of the Cycletester_synchronous vi with the “ACQ” case visible

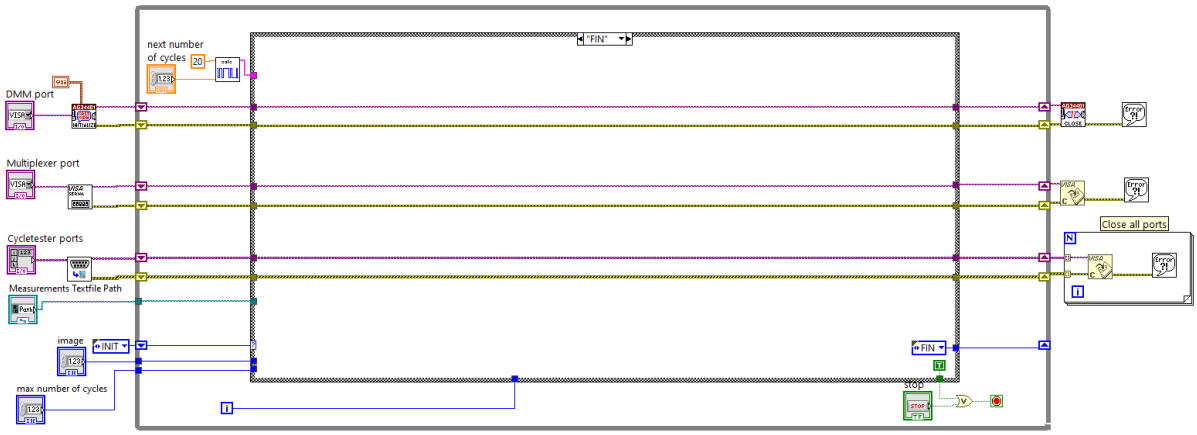

Figure E.4: block diagram of the Cycletester_synchronous vi with the “FIN” case visible

Figure E.5 illustrates the block diagram from the calculate_steps.vi. Figure E.6 shows the block diagram of the configure_ports.vi where the USB ports of the cycletester’s Arduino will be configured.

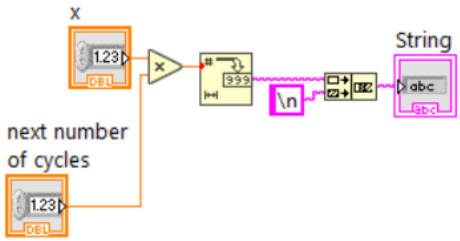

Figure E.5: block diagram of the calculate_steps vi

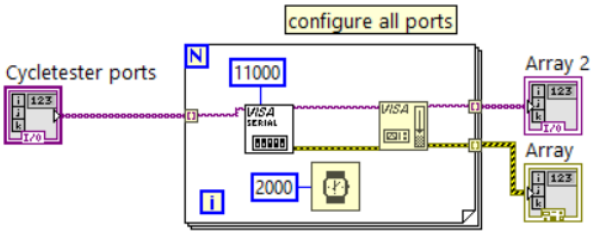

Figure E.6: block diagram of the configure_ports vi

Figures E.7 through 15 show different cases in the read_measure vi. The cases in order are:

1. SELECT,
2. READ,
3. MEASURE,
4. IMAGE,
5. STRETCH,
6. READ2
7. MEASURE STRETCHED
8. IMAGE STRETCHED,
9. RELAX,
10. READ3,
11. WRITE,
12. FIN,
13. and ERROR.

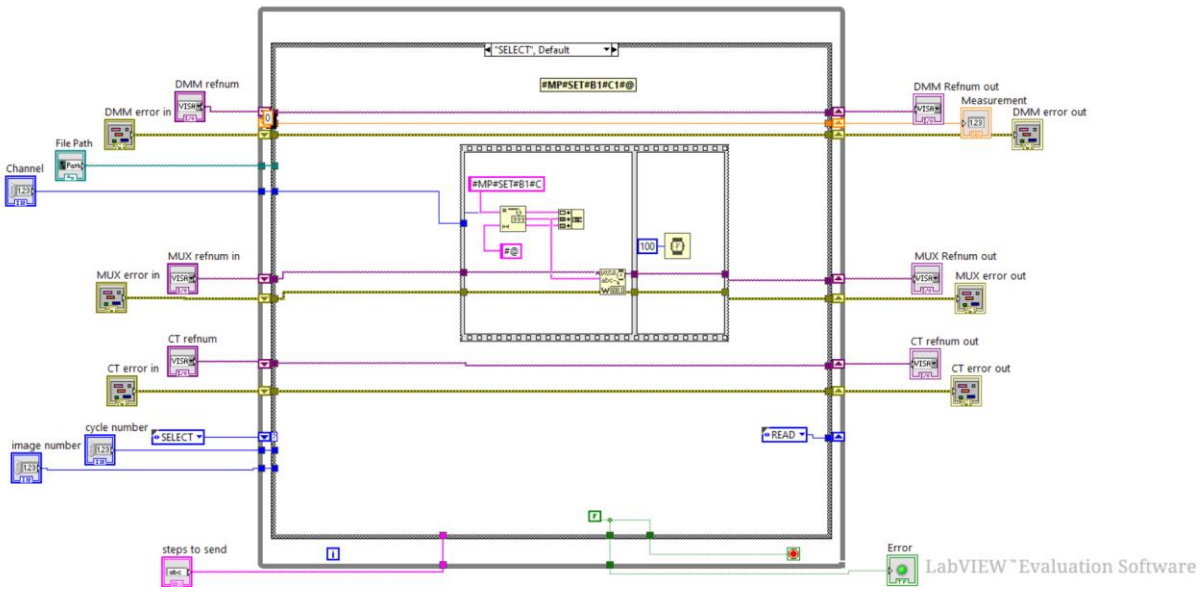

Figure E.7: block diagram of the read_measure_write vi showing the “SELECT” case

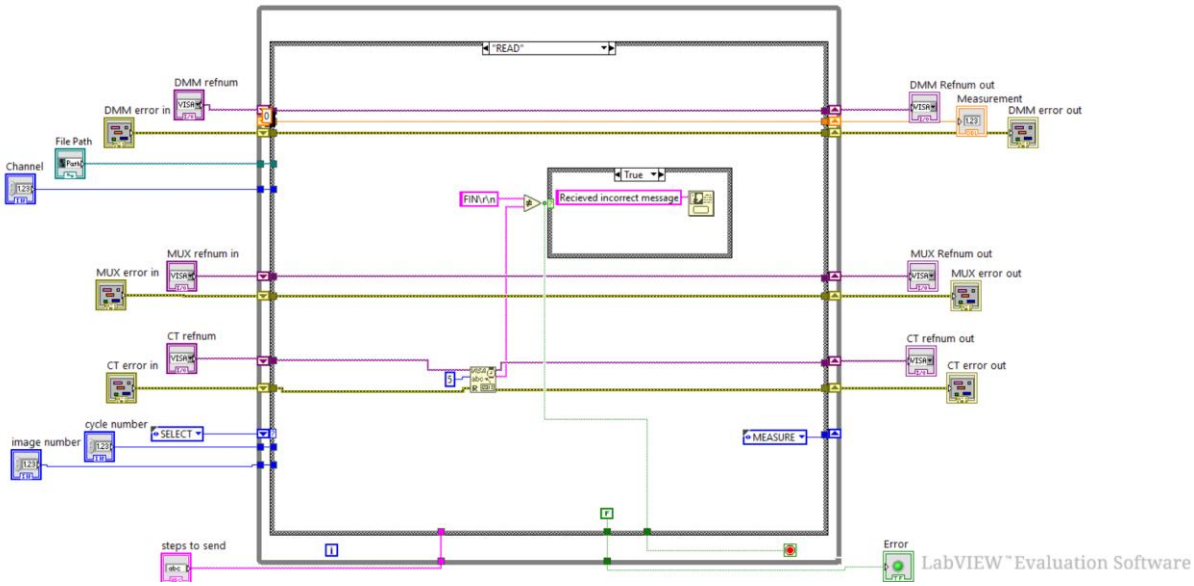

Figure E.8: block diagram of the read_measure_write vi showing the “READ” case

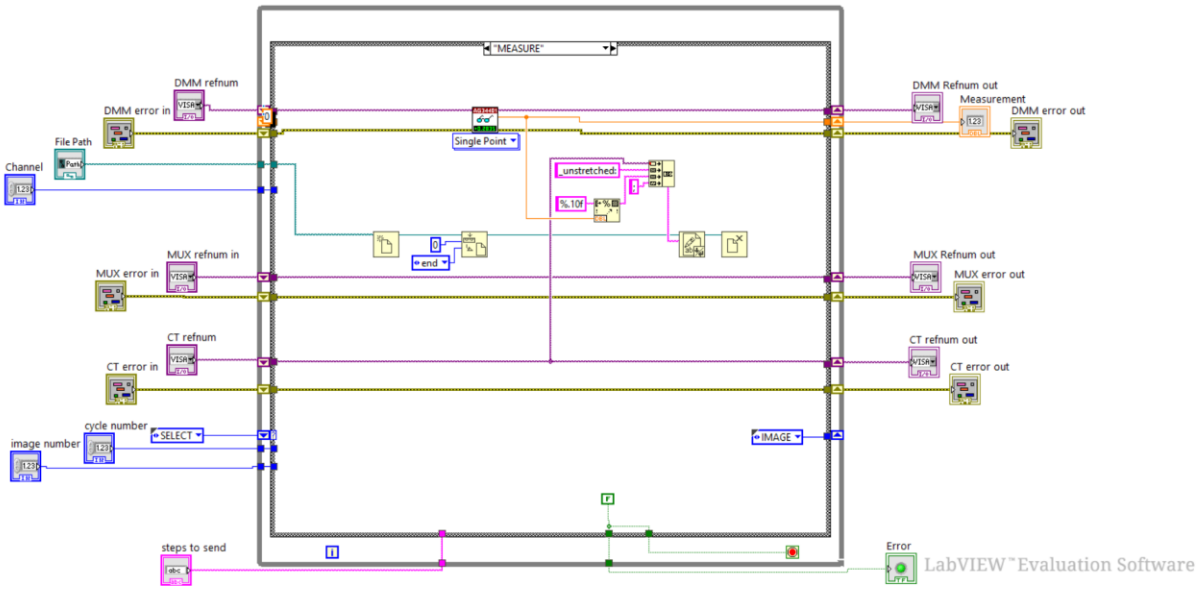

Figure E.9: block diagram of the read_measure_write vi showing the “MEASURE” case

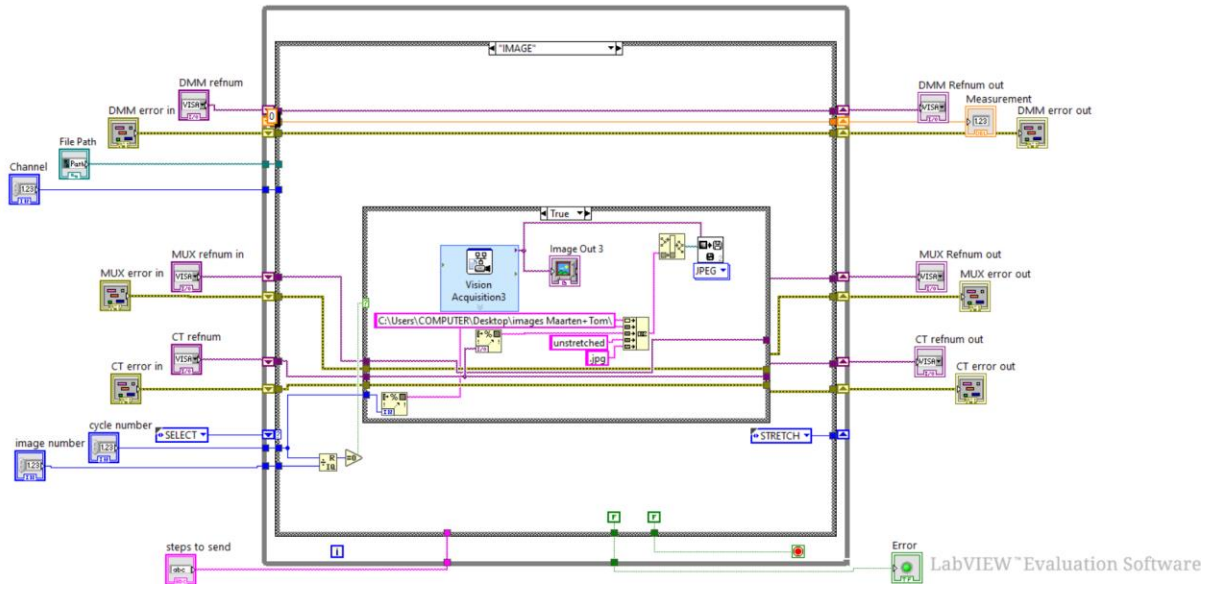

Figure E.10: block diagram of the read_measure_write vi showing the “IMAGE” case

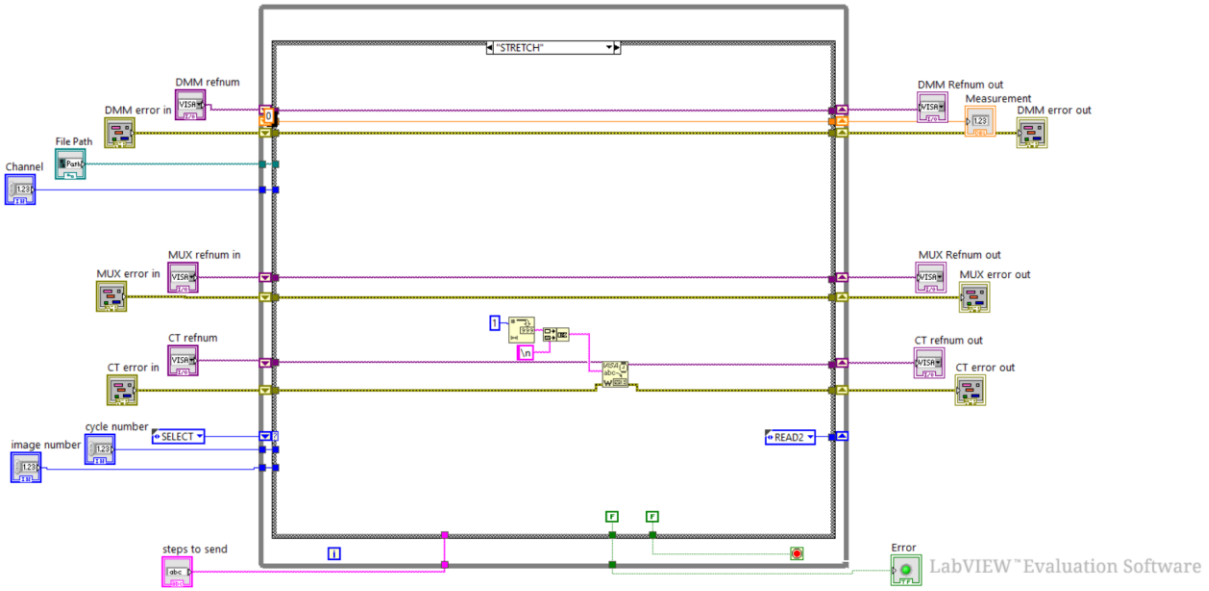

Figure E.11: block diagram of the read_measure_write vi showing the “STRETCH” case

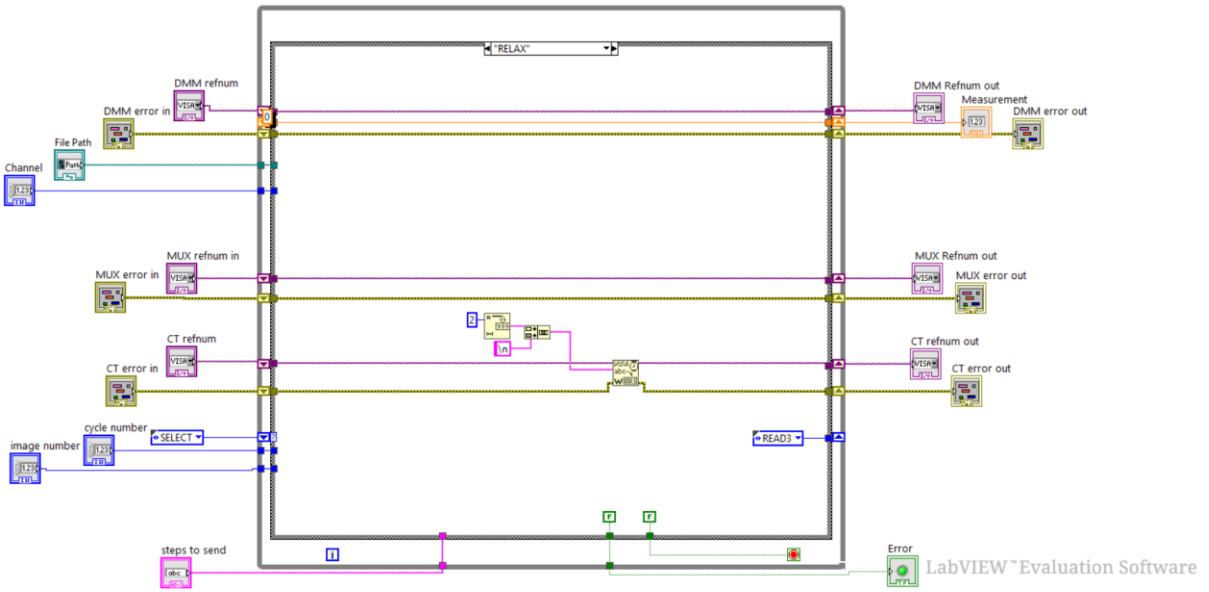

Figure E.12: block diagram of the read_measure_write vi showing the “RELAX” case

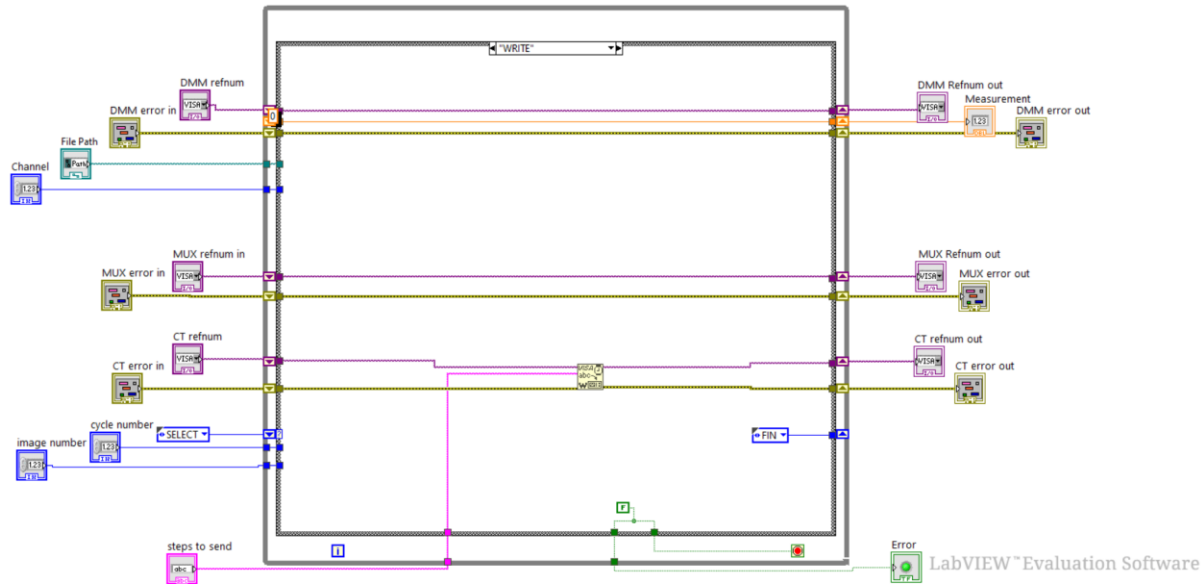

Figure E.13: block diagram of the read_measure_write vi showing the “WRITE” case

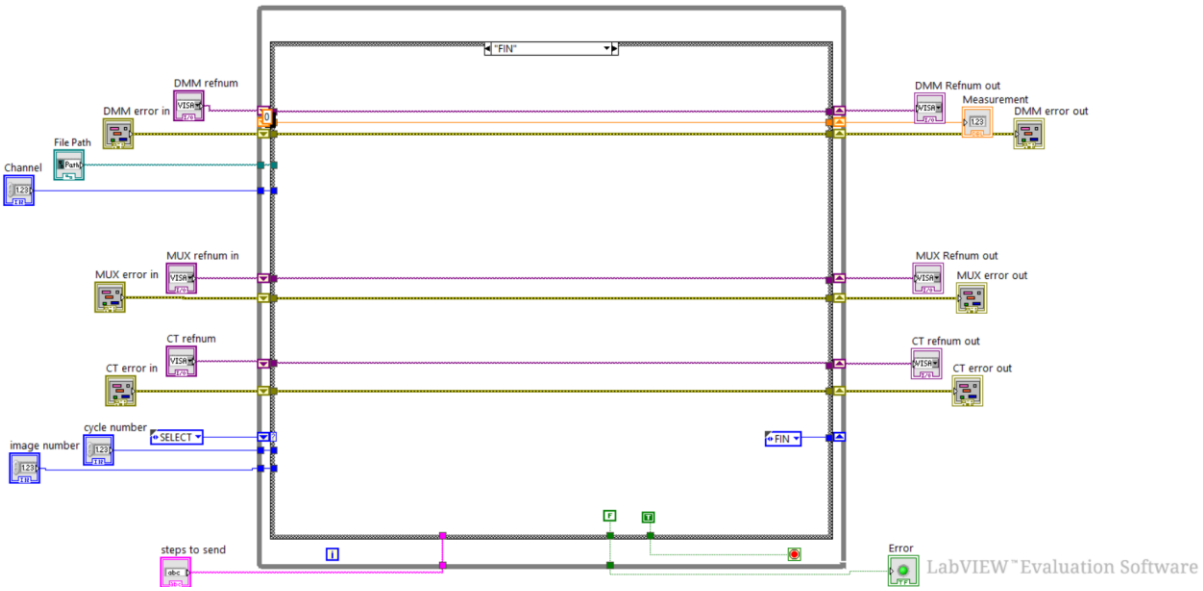

Figure E.14: block diagram of the read_measure_write vi showing the “FIN” case

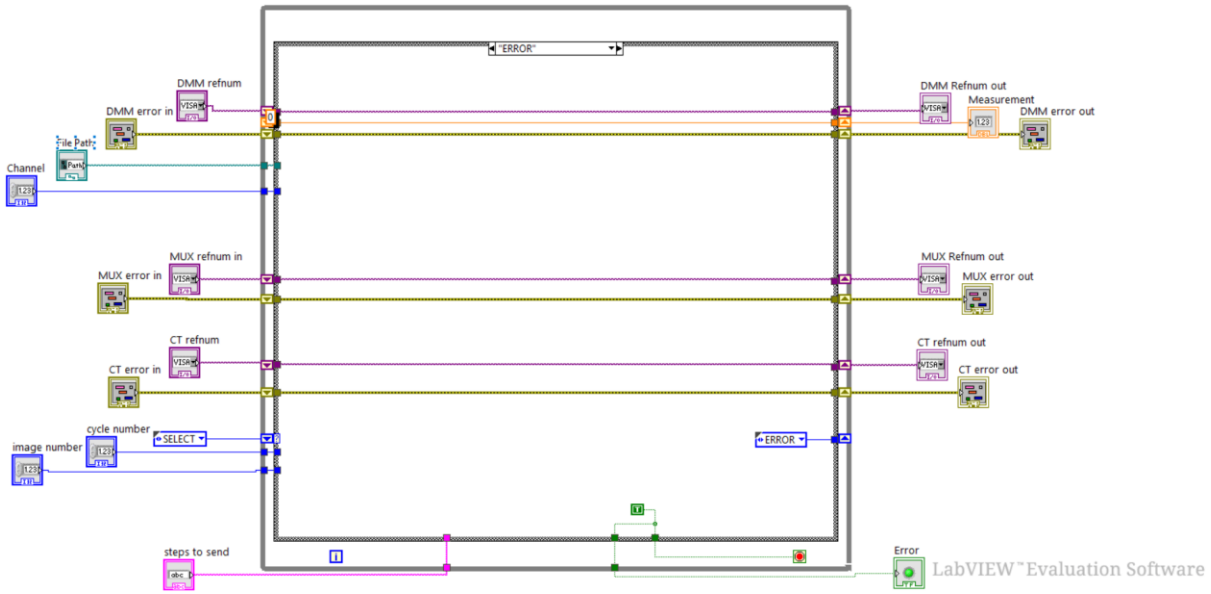

Figure E.15: block diagram of the read_measure_write vi showing the “ERROR” case

Appendix F: Arduino code for the cycletesters (stretchable devices)

```
#include <AccelStepper.h>

//Define stepper motor DRV8825
#define dirPin 2
#define stepPin 3
#define motorInterfaceType 1
AccelStepper stepper(motorInterfaceType, stepPin, dirPin);
#define M2 4
#define M1 5
#define M0 6
#define stepperMaxSpeed 100 // determines max speed of stepper motor
#define stepperSpeed 100// determines actual speed of stepper motor, decrease to increase torque
#define microStep 1

String inString = "";

void setup() {
  pinMode(M0, OUTPUT);
  pinMode(M1, OUTPUT);
  pinMode(M2, OUTPUT);
  digitalWrite(M0, LOW);
  digitalWrite(M1, LOW);
  digitalWrite(M2, LOW);

  Serial.begin(9600);

  stepper.setMaxSpeed(stepperMaxSpeed*microStep);
  stepper.setAcceleration(2000*microStep);
}

void loop() {
  while(Serial.available() > 0){
    char inChar = Serial.read();
    inString += inChar;
    if (inChar == '\n') {
      int value = inString.toInt();
```

```
      stepper.moveTo(value*microStep);
      stepper.runToPosition();
      stepper.setCurrentPosition(0);
      Serial.print("FIN\r\n");
      inString = "";  //reset inString
    }
  }
}
```

Appendix G: Labview code (stretchable wire devices)

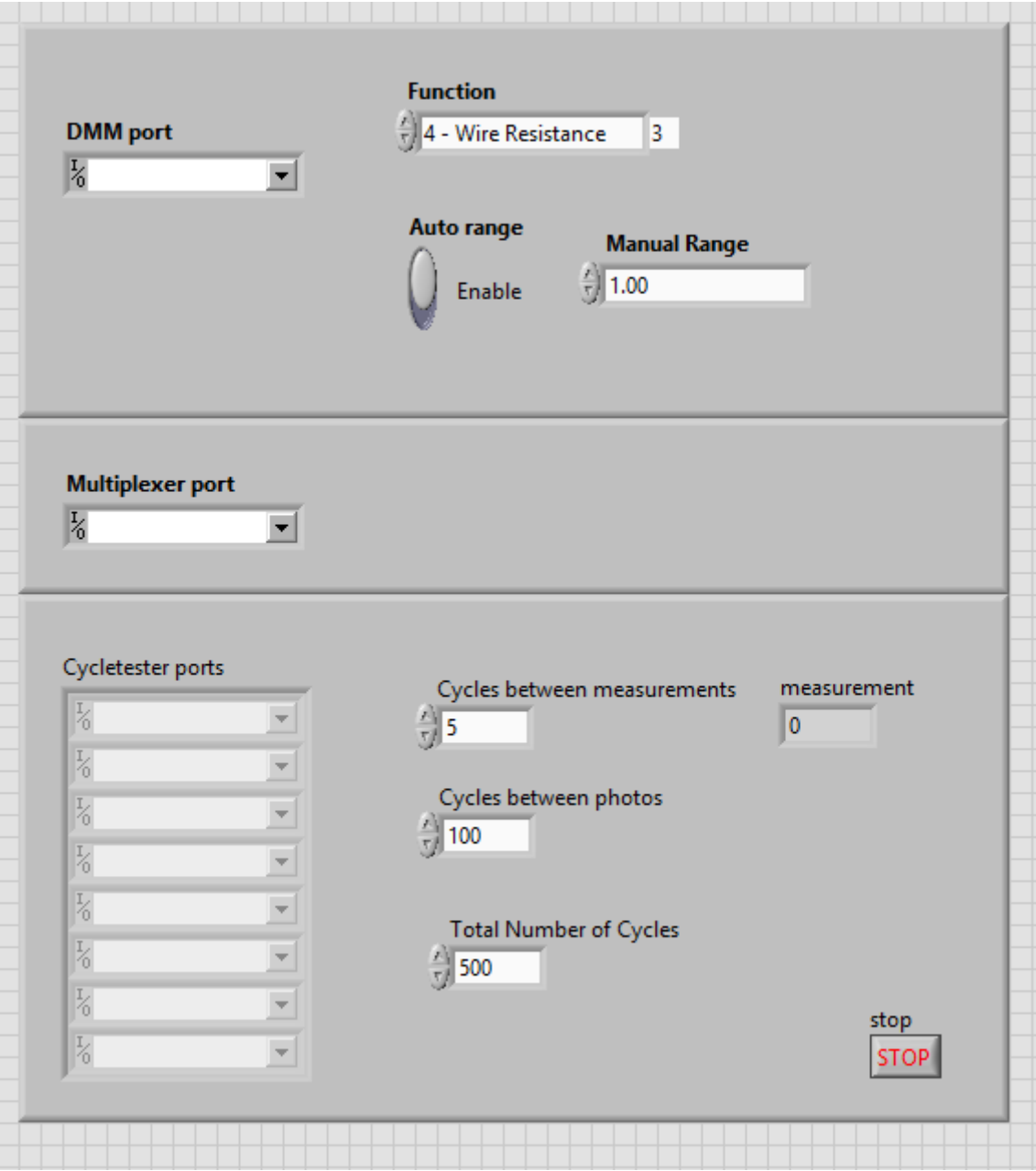

Figure G.1: front panel for stretchable wire program.

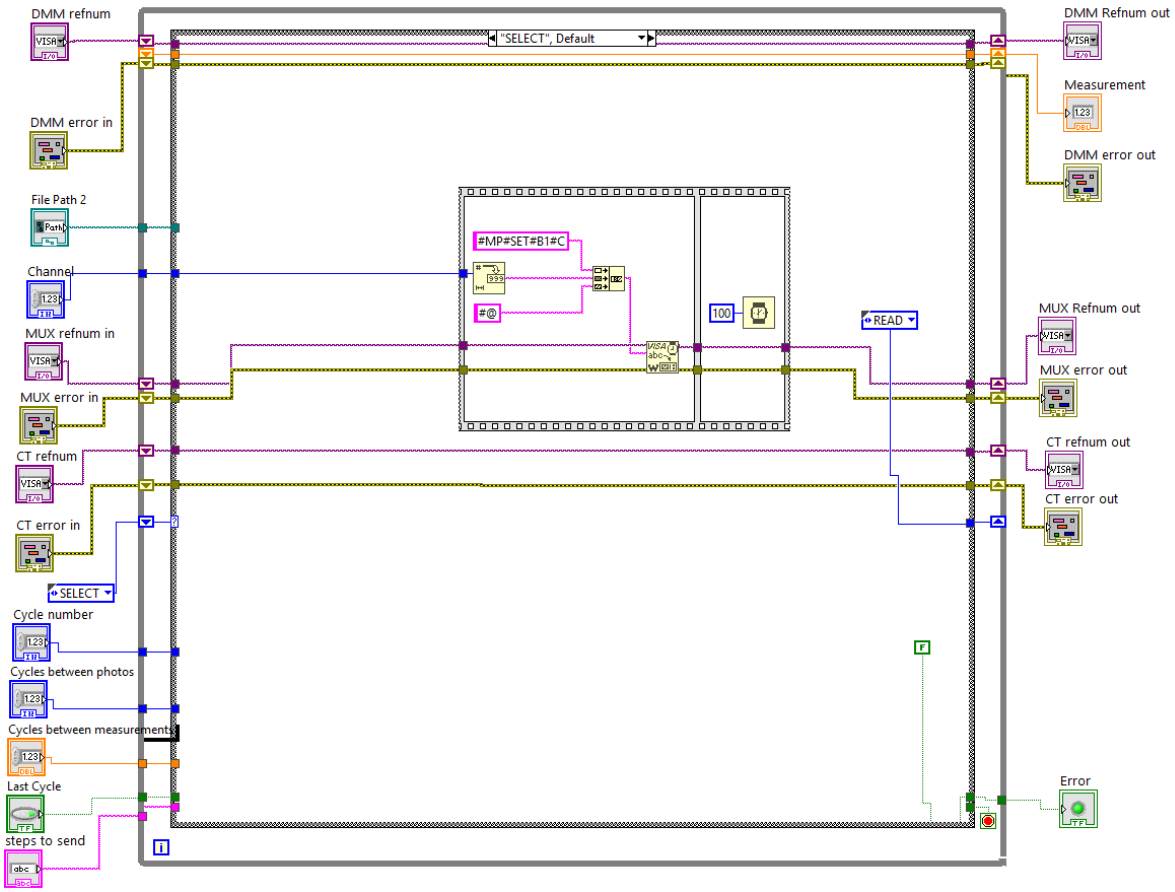

Figure G.2: SELECT (Default) case.

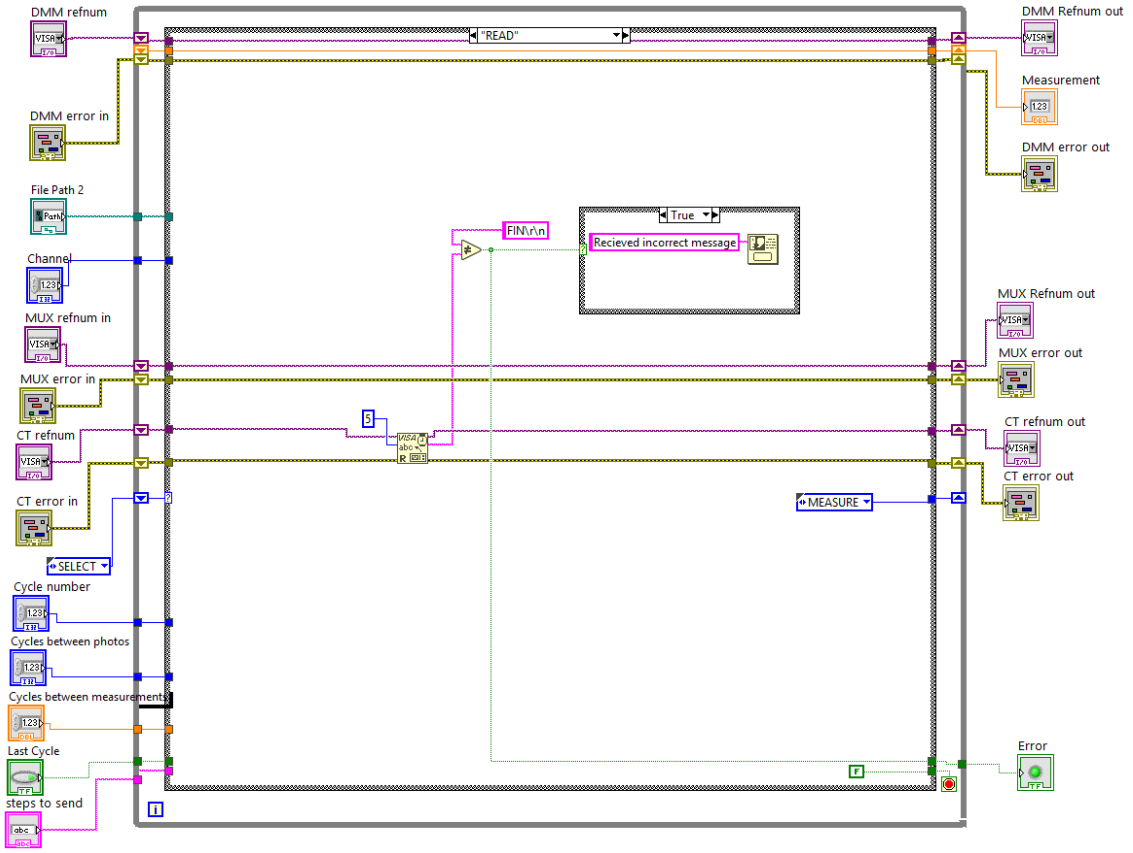

Figure G.3: READ case.

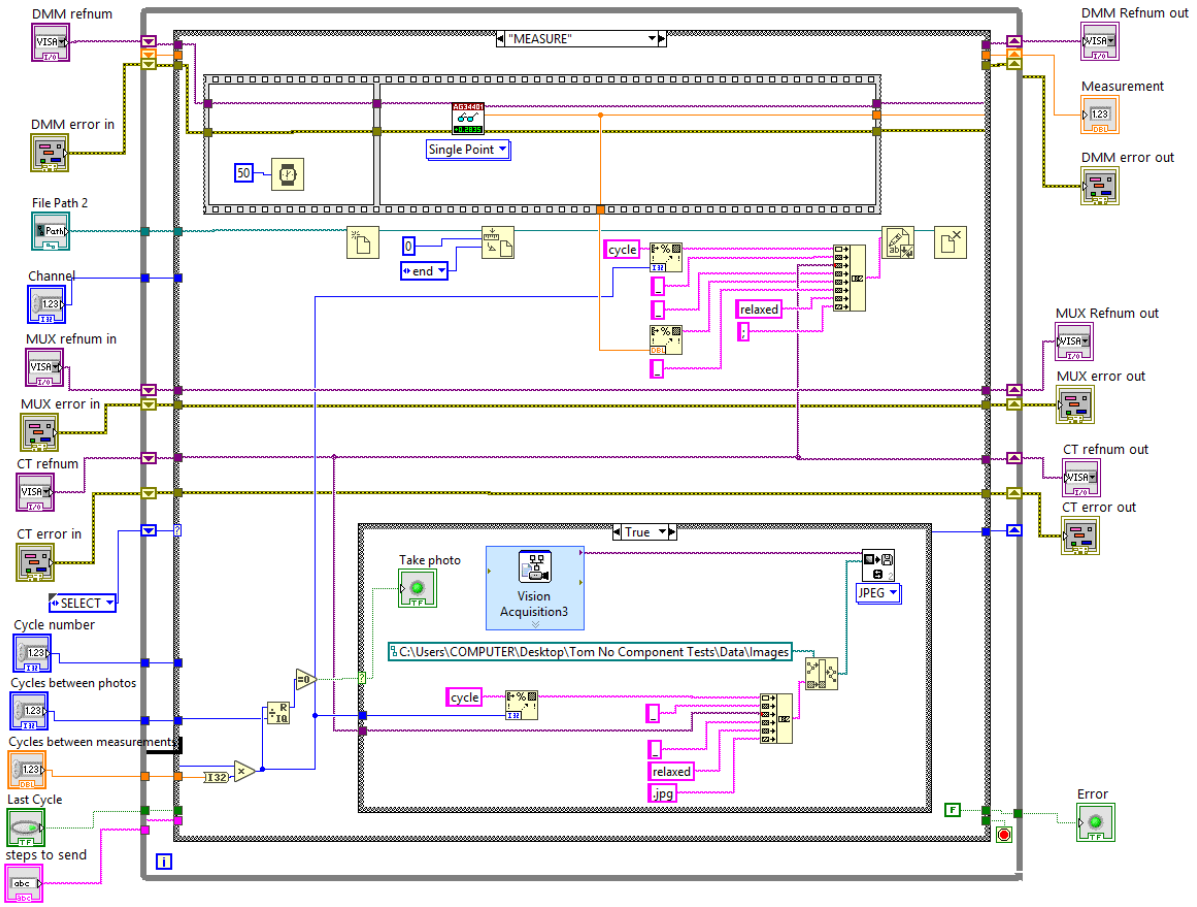

Figure G.4: MEASURE case.

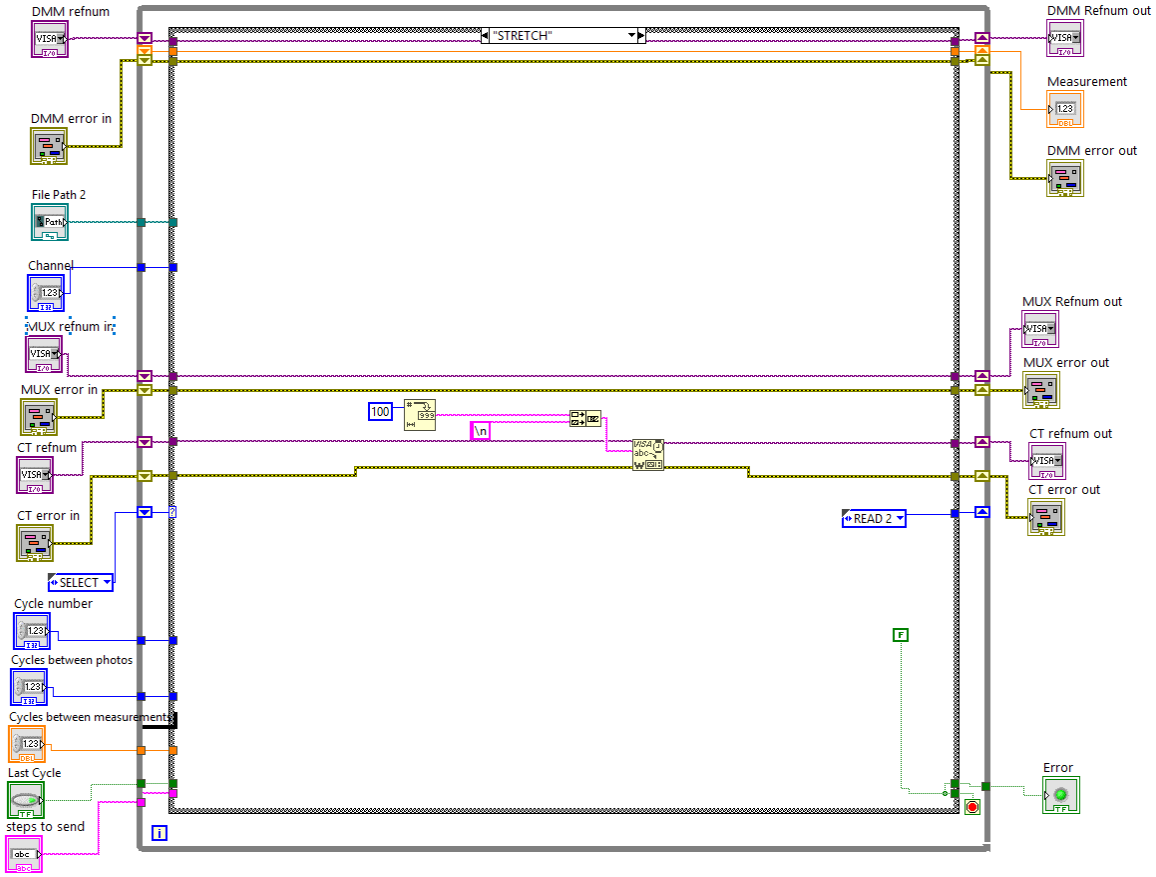

Figure G.5: STRETCH case.

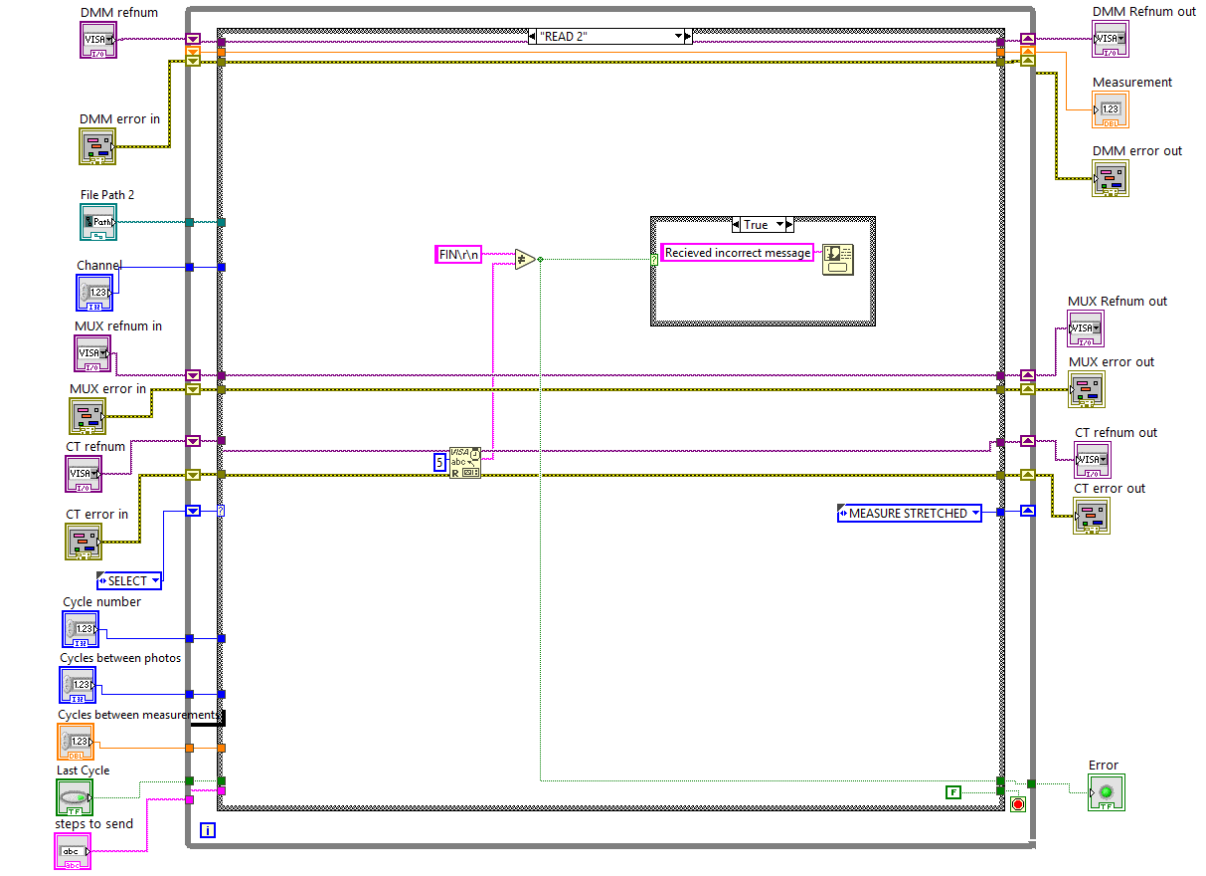

Figure G.6: READ 2 case.

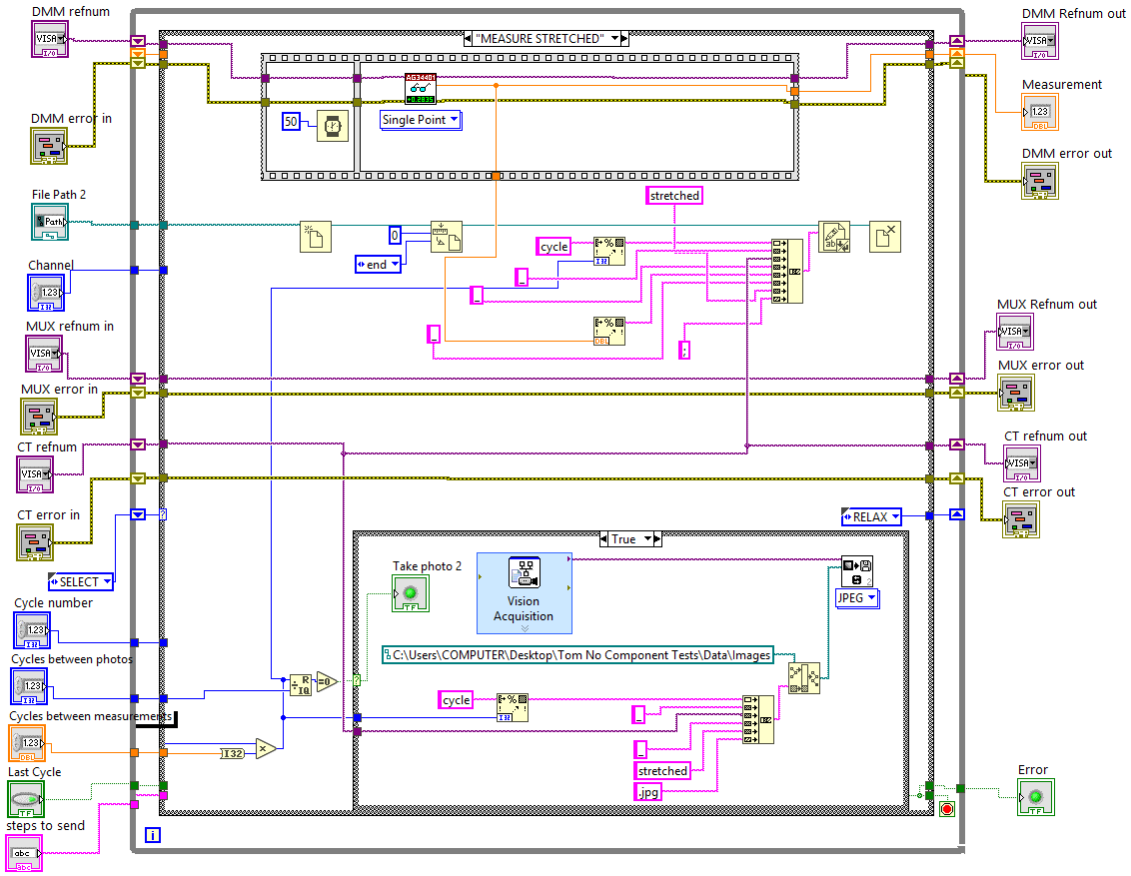

Figure G.7: MEASURED STRETCH case.

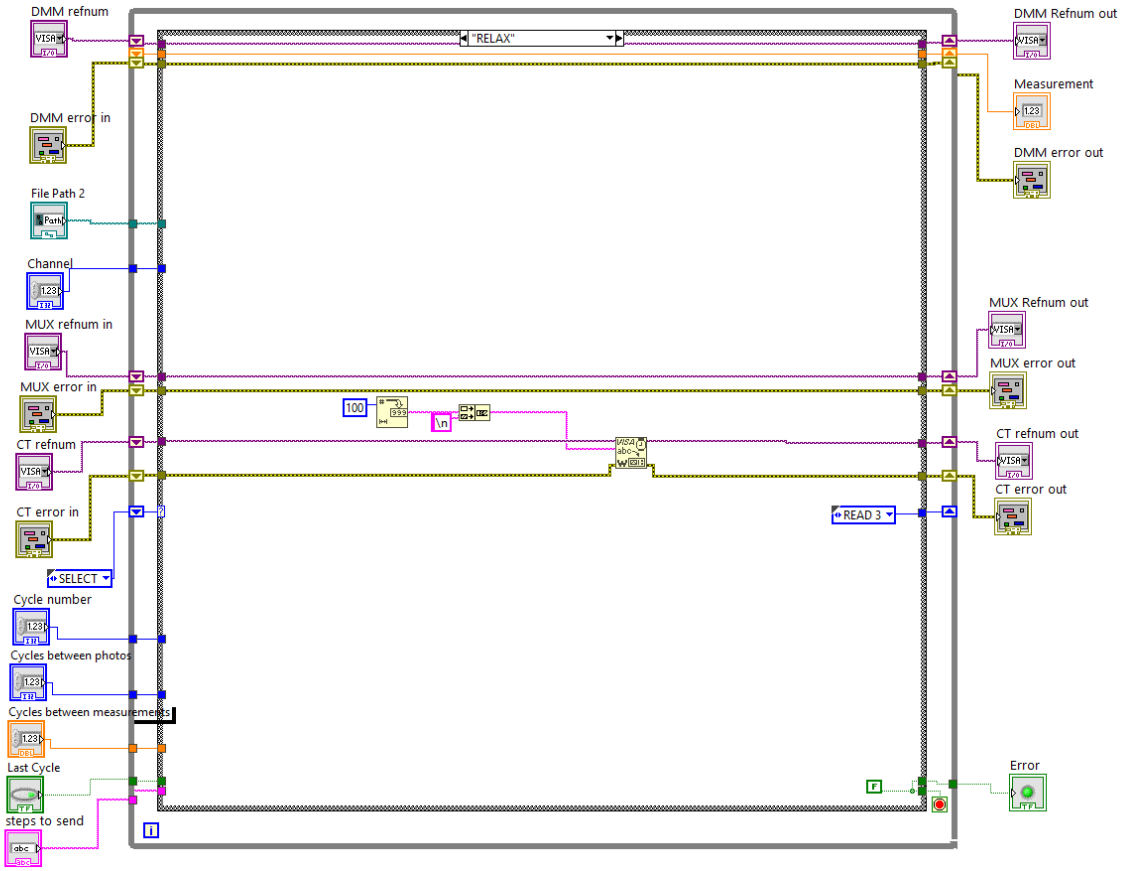

Figure G.8: RELAX case.

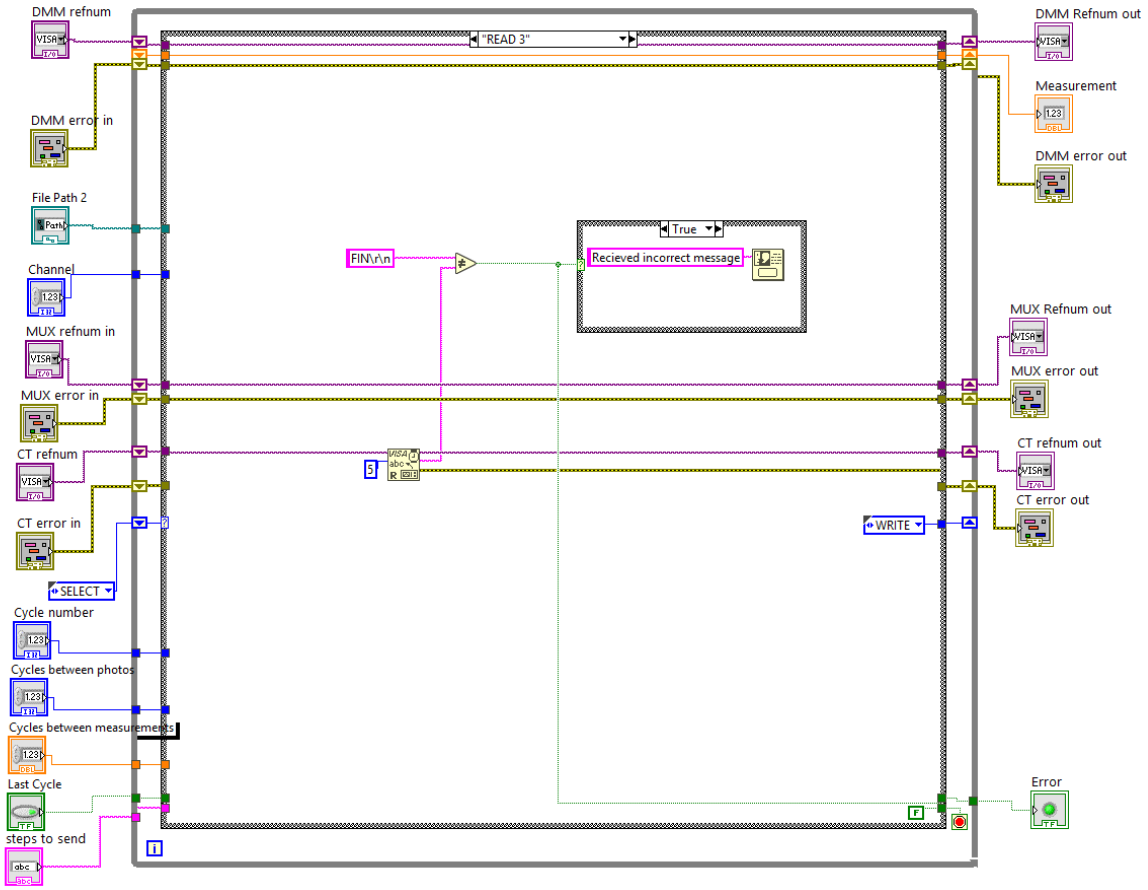

Figure G.9: READ 3 case.

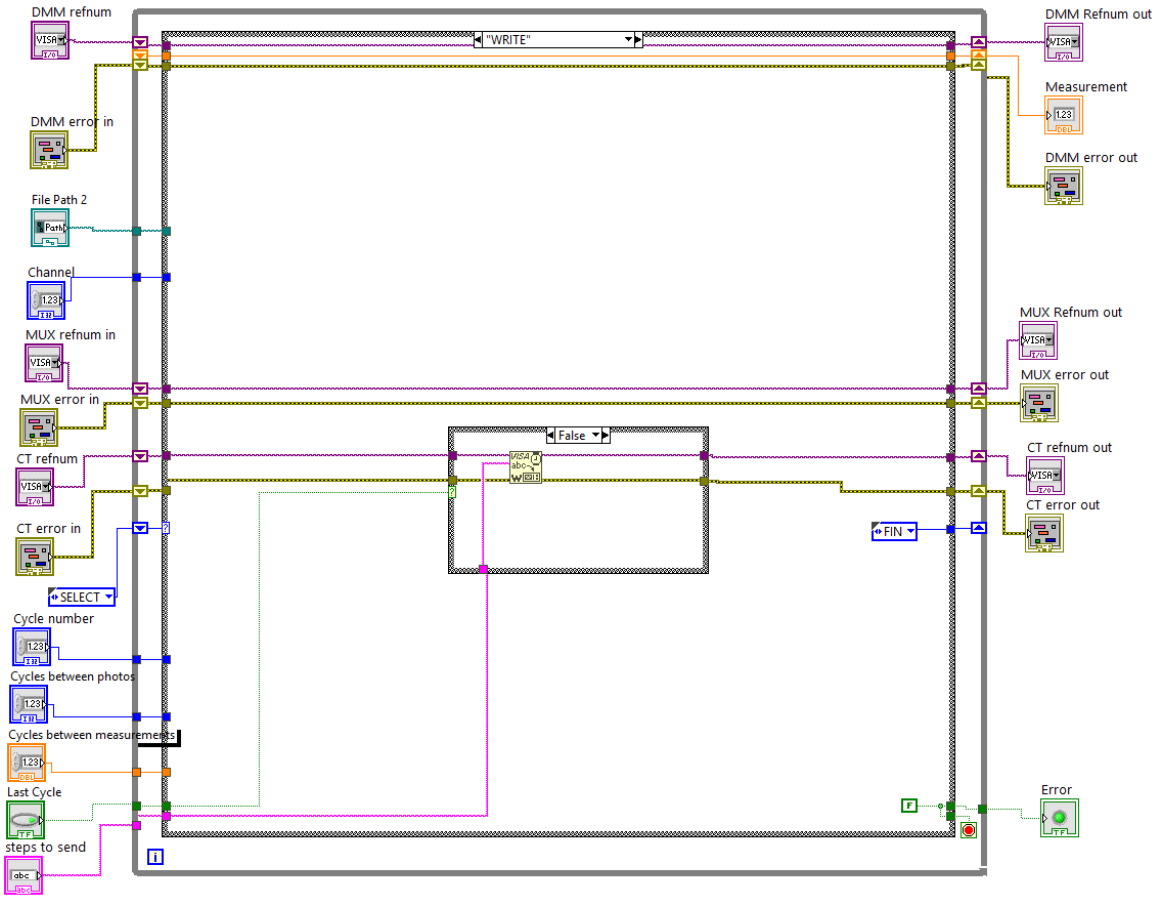

Figure G.10: WRITE case.

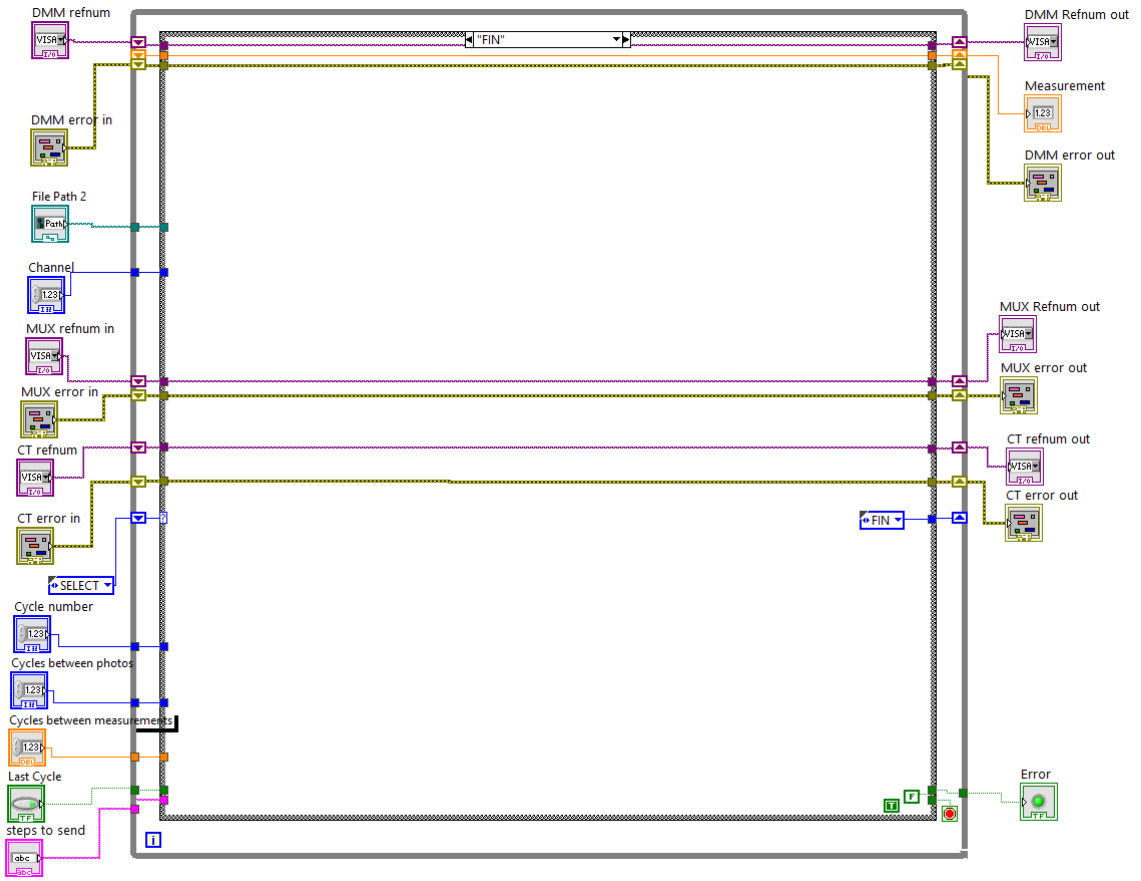

Figure G.11: FIN case.

Appendix H: Graphs stretch test stretchable LED strips

1 Not exposed to environmental stress factors

Figures H.1, H.2, H.3, H.4, H.5, and H.6 show the stretch test results for the devices that were not subjected to one of the environmental tests.

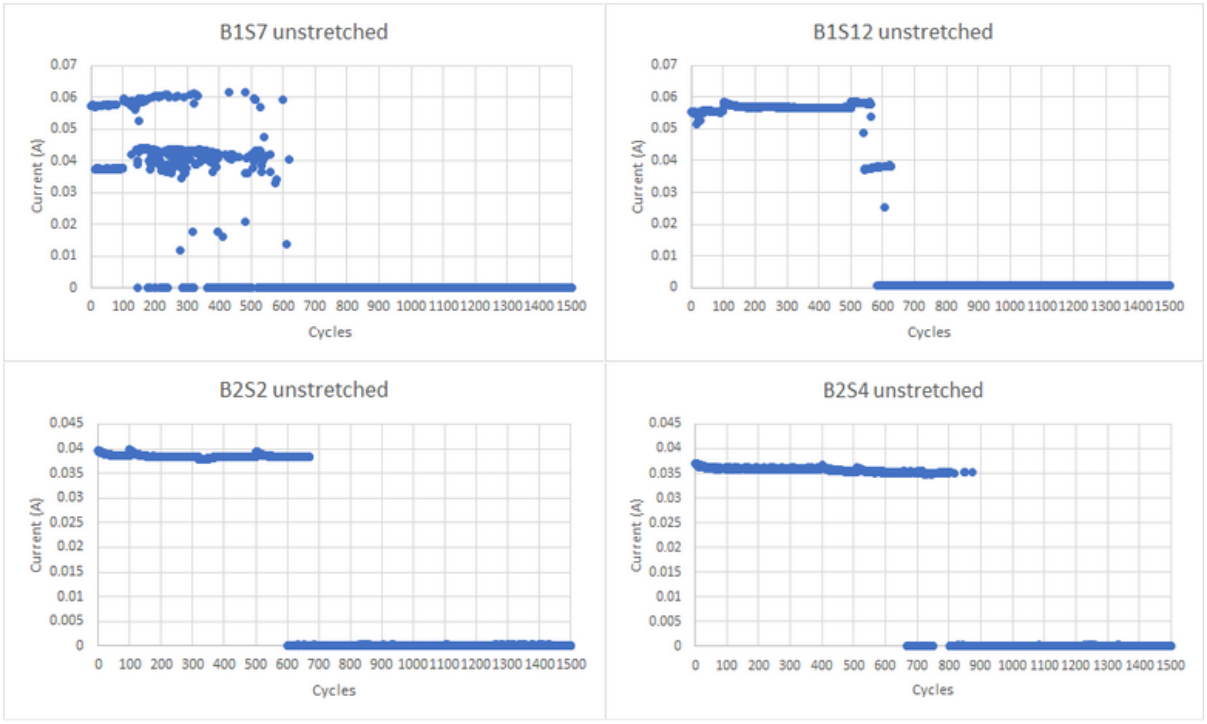

Figure H.1: current (unstretched) in function of the number of cycles for B1S7, B1S12, B2S2, and B2S4

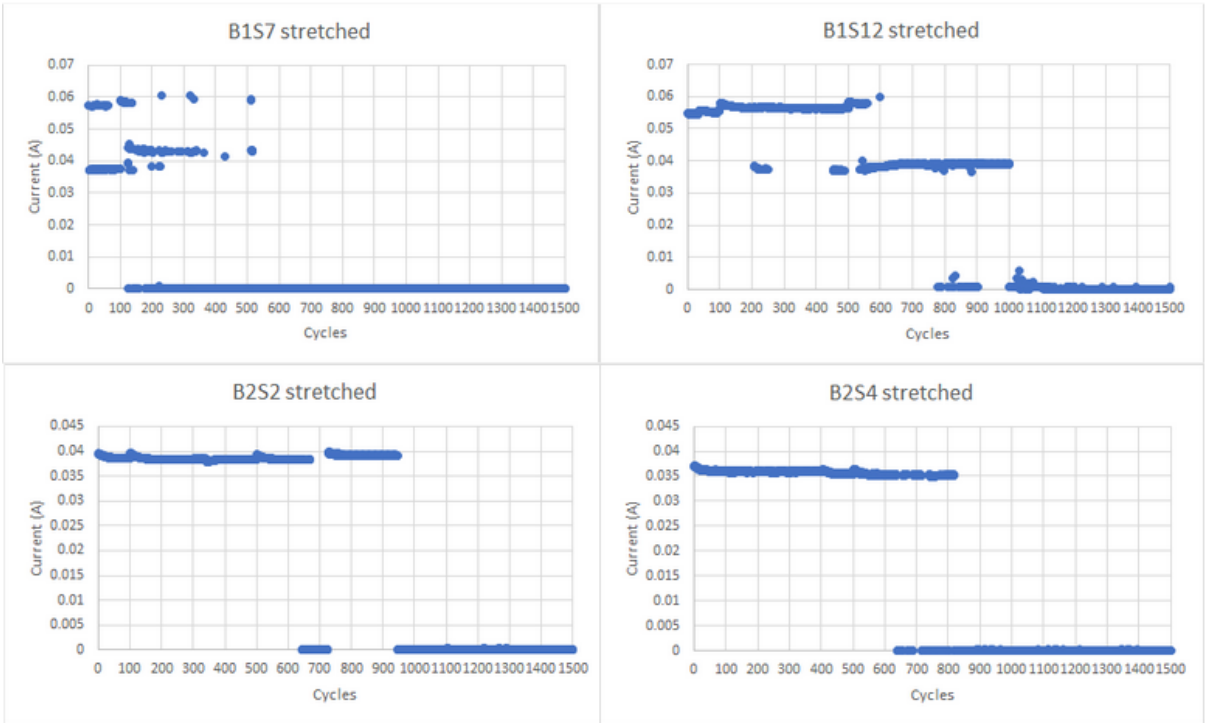

Figure H.2: current (stretched) in function of the number of cycles for B1S7, B1S12, B2S2, and B2S4

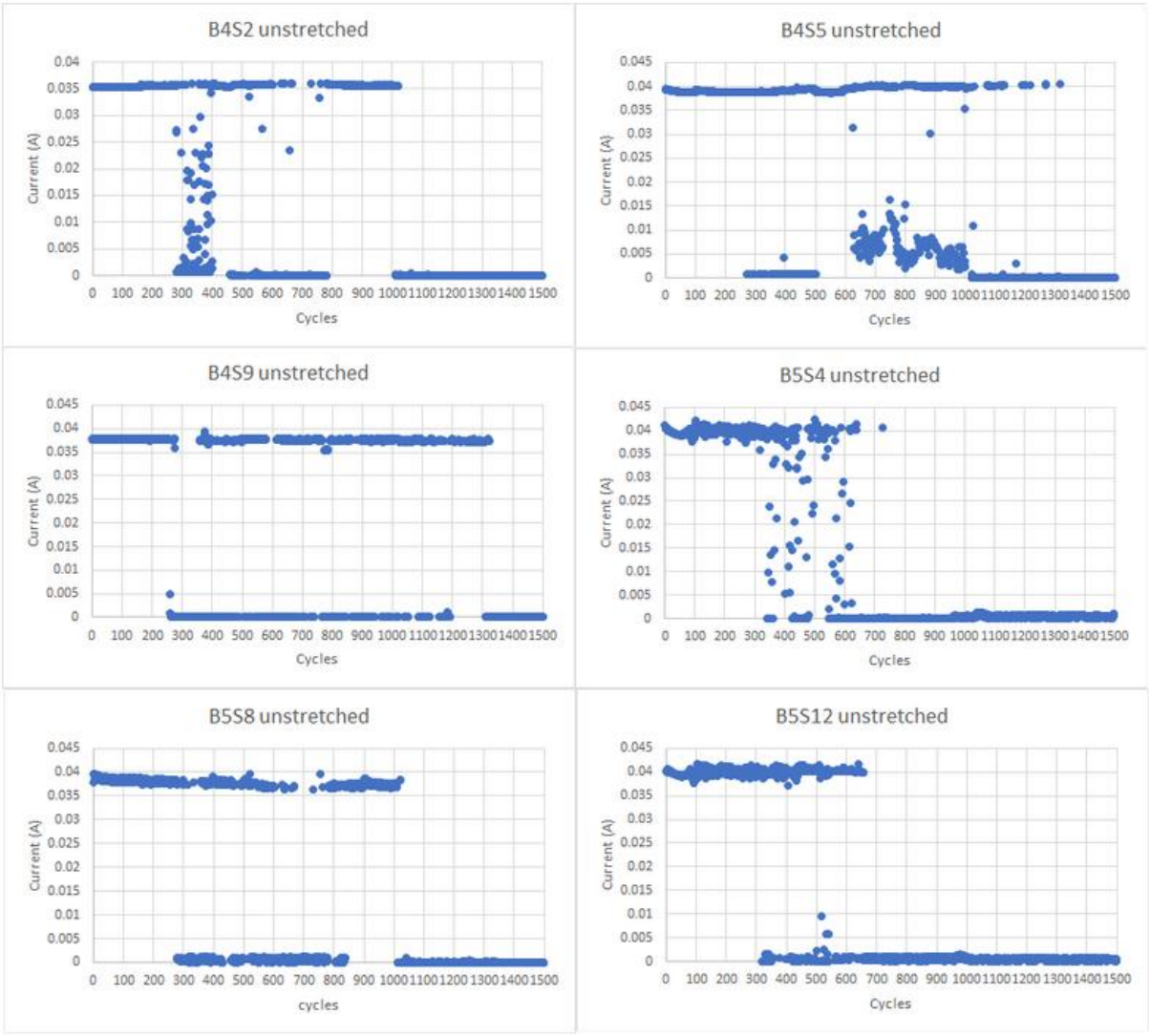

Figure H.3: current (unstretched) in function of the number of cycles for B4S2, B4S5, B4S9, B5S4, B5S8, and B5S12

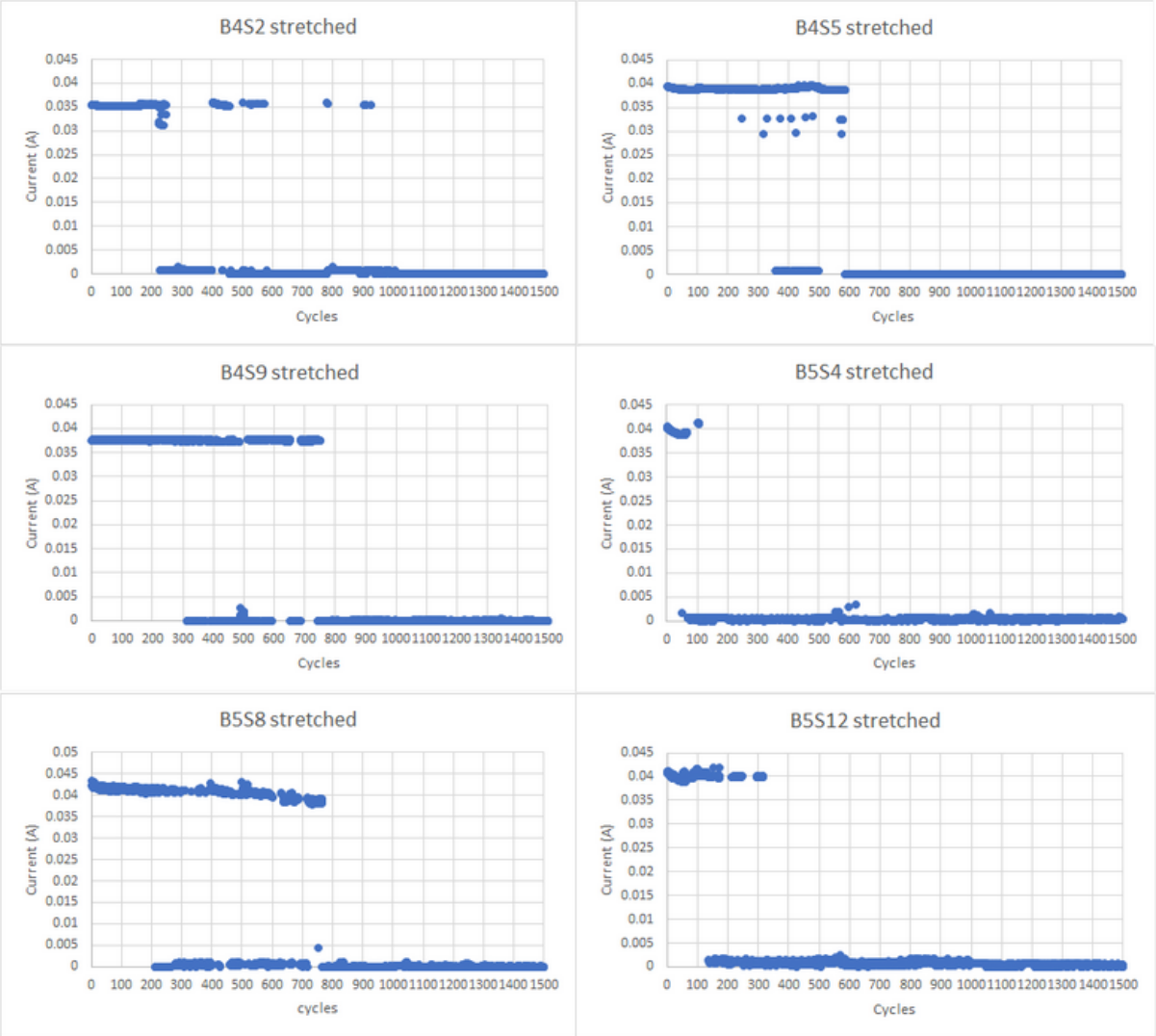

Figure H.4: current (stretched) in function of the number of cycles for B4S2, B4S5, B4S9, B5S4, B5S8, and B5S12

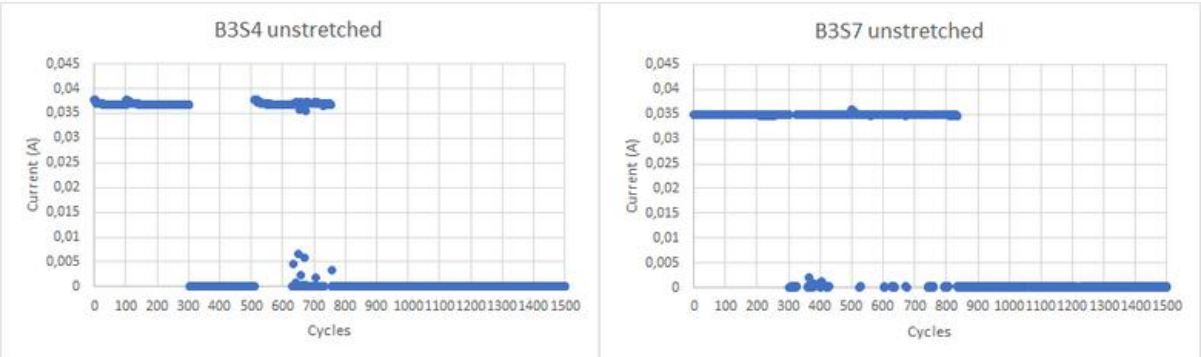

Figure H.5: current (unstretched) in function of the number of cycles for B3S4

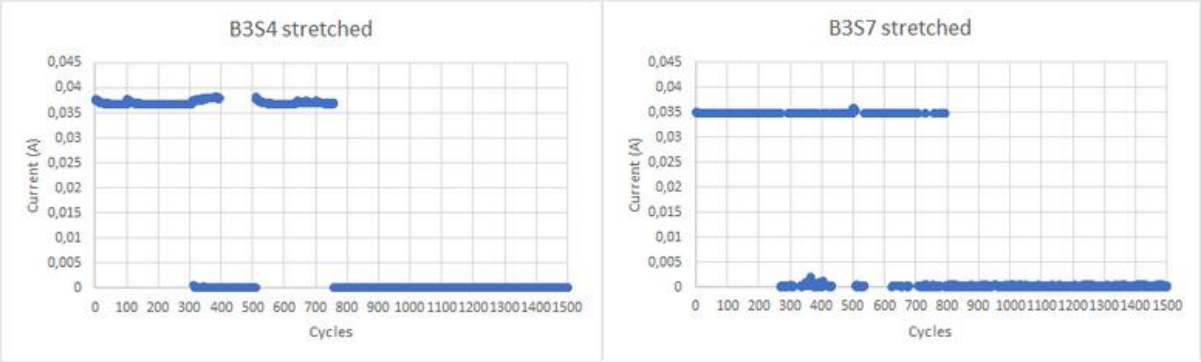

Figure H.6: current (stretched) in function of the number of cycles for B3S4

2 Exposed to UV

Figures H.7, H.8, H.9, H.10, H.11, and H.12 show the stretch test results for the devices that were subjected to the QUV test.

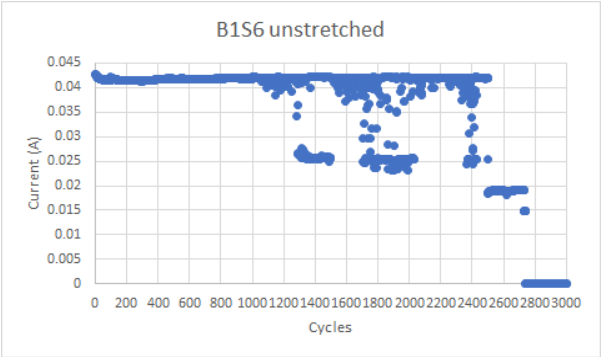

Figure H.7: current (unstretched) in function of the number of cycles for B1S6

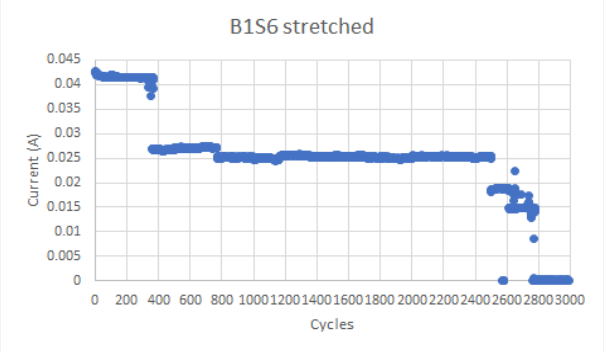

Figure H.8: current (stretched) in function of the number of cycles for B1S6

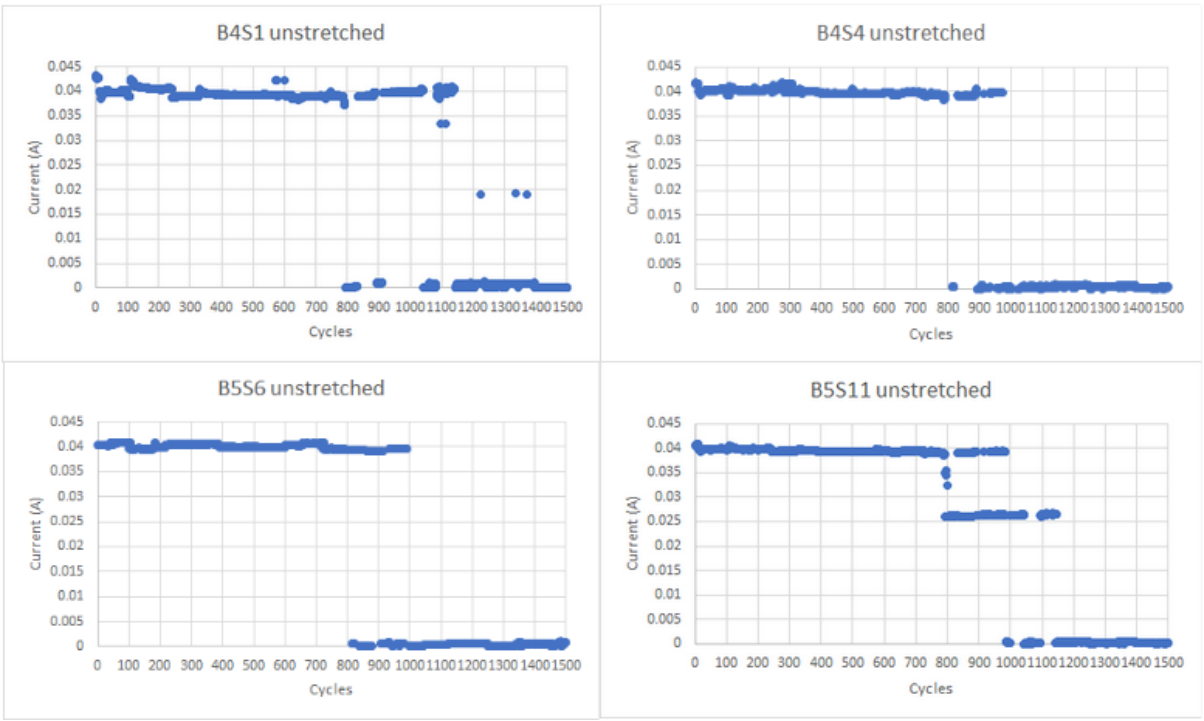

Figure H.9: current (unstretched) in function of the number of cycles for B4S1, B4S4, B5S6, B5S11

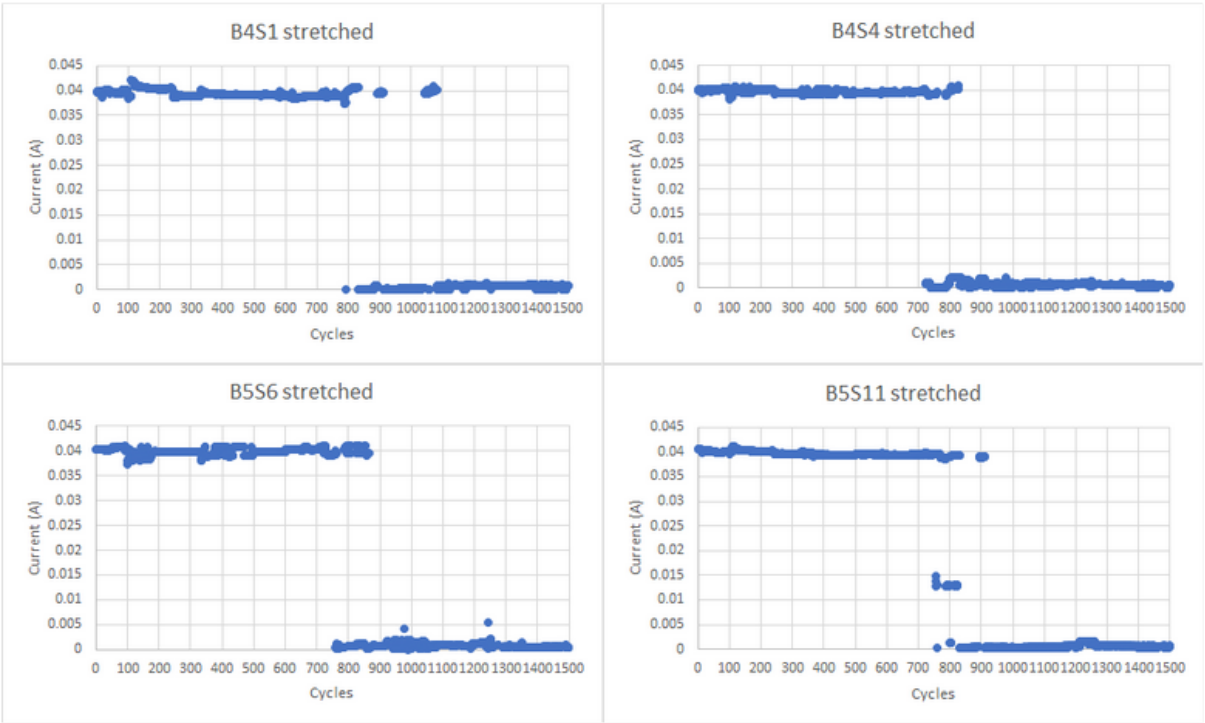

Figure H.10: current (stretched) in function of the number of cycles for B4S1, B4S4, B5S6, B5S11

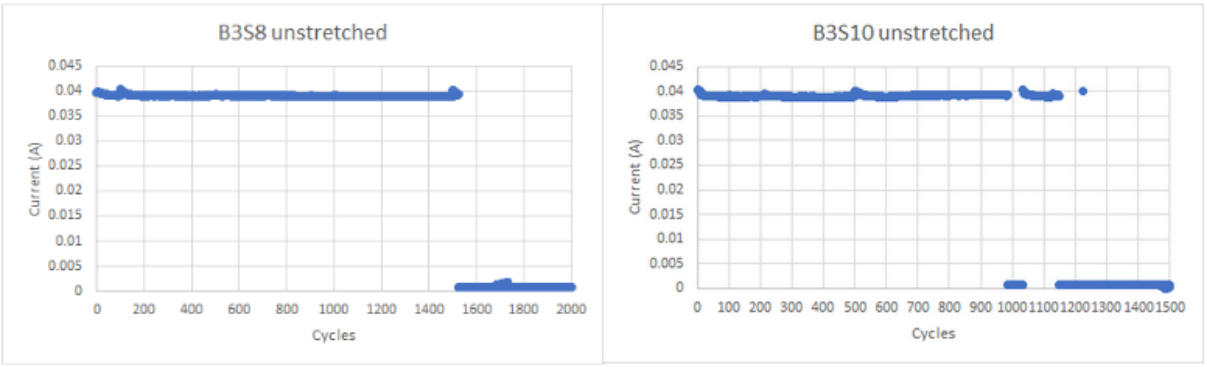

Figure H.11: current (unstretched) in function of the number of cycles for B3S10

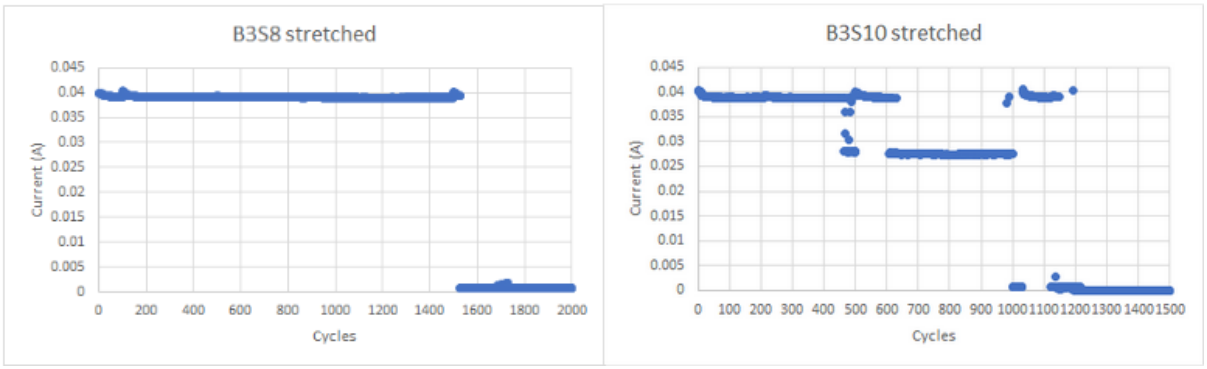

Figure H.12: current (stretched) in function of the number of cycles for B3S10